Structure of the San Bernardino Basin Along Two Seismic Transects: Rialto-Colton Fault to the San Andreas Fault and Along the I-215 Freeway (I-10 to SR30)

R.D. Catchings[1], M.J. Rymer[1], M.R. Goldman[1], G. Gandhok[1], and C.E. Steedman[1]

Open-File Report 2008-1197

2008

U.S. Department of the Interior
U.S. Geological Survey

[1] Menlo Park, Calif.

U.S. Department of the Interior
DIRK KEMPTHORNE, Secretary

U.S. Geological Survey
Mark D. Myers, Director

U.S. Geological Survey, Reston, Virginia 2008

For product and ordering information:
World Wide Web: http://www.usgs.gov/pubprod
Telephone: 1-888-ASK-USGS

For more information on the USGS—the Federal source for science about the Earth, its natural and living resources, natural hazards, and the environment:
World Wide Web: http://www.usgs.gov
Telephone: 1-888-ASK-USGS

Suggested citation:
Catchings, R.D., Rymer, M.J., Goldman, M.R., Gandhok, and G., Steedman, C.E., 2008, Structure of the San Bernardino Basin along two seismic transects; Rialto-Colton fault to the San Andreas fault and along the I-215 freeway (I-10 to SR30): U.S. Geological Survey, Open-File Report 2008-1197 [http://pubs.usgs.gov/of/2008/1197/].

Summary

In this report, we present seismic data and acquisition parameters for two seismic profiles acquired in the San Bernardino, California area in May and October 2003. We refer to these seismic profiles as the San Bernardino Regional (SBR) and San Bernardino High-Resolution (SBHR) seismic profiles. We present both un-interpreted and interpreted seismic images so that the structure of the area can independently interpreted by others. We explain the rationale for our interpretations within the text of this report, and in addition, we provide a large body of supporting evidence.

The SBR seismic profile extended across the San Bernardino Basin approximately N30^{o}E from the town of Colton to the town of Highland. The data were acquired at night when the signal-to-noise ratios were reasonably good, and for the larger shots, seismic energy propagated across the ~20-km-long array. Tomographic velocity data are available to depths of about 4 km, and low-fold reflection data are available to depths in excess of 5 km. The SBR seismic data reveal an asymmetric, fault-bound basin to about 5 km depth.

The SBHR seismic profile trended along the I-215 freeway from its intersection with the Santa Ana River to approximately State Road 30 in San Bernardino. Seismic data acquired along the I-215 freeway provide detailed images, with CDP spacing of approximately 2.5 m along an approximately 8.2-km-long profile; shot and geophone spacing was 5 m. Walk-away noise tests showed that freeway noise levels were low enough during the night hours to propagate seismic signals fairly well. However, for logistical reasons, the high-resolution (SBHR) seismic data were acquired during daylight hours on the shoulder of the I-215 freeway and within 5 to 10 m of high-traffic volumes. The resulting signal-to-noise noise ratios for the SBHR seismic survey were low, and although we increased out shot sizes to help compensate for the high-noise levels, the resulting seismic data contain significant noise in the reflection images. Due to the limited offset at which refracted first-arrivals could be measured along the SBHR seismic profile, tomographic refraction velocities are limited to relatively shallow (< 150 m) depths. The SBHR reflection data reveal a basin with complex structural details within the upper kilometer.

The two seismic profiles show internal consistency and consistency with other existing geophysical data. Collectively, the data suggest that the I-215 freeway trends along the faulted edge of a pull-apart basin, within a zone where the principal slip of the San Jacinto Fault is transferred to the San Andreas Fault (see Figure 26-28). Because the I-215 freeway trends at low angles to these flower-structure faults, both primary and numerous secondary faults are apparent between the I-10 exchange and State Road-30, suggesting that much of the 8-km-long segment of the I-215 freeway could experience movement along primary or secondary faults.

Introduction

The San Bernardino Basin is located in the county of San Bernardino, approximately 100 km east of Los Angeles, California (Fig. 1). The basin is bounded on the northeast, northwest, southwest, and southeast by the San Bernardino Mountains, the San Gabriel Mountains, the San Timoteo Badlands, and the Crafton Hills, respectively. The area has a population of approximately 1.7 million people (2000 U. S. Census), distributed among several cities, including Colton, Grand Terrace, Fontana, Highland, Loma Linda, Redlands, Rialto, and San Bernardino. The city of San Bernardino is the largest city in the area, with a population of approximately 185,000 (2000 U. S. Census), and it encompasses the principal area of this study.

Two major interstate freeways, I-215 and I-10, trend through the city of San Bernardino, and both freeways are heavily traveled lifelines that connect cities to the east and west (including Los Angeles) and to the north and south (including San Diego). To relieve traffic congestion on the I-215 freeway in San Bernardino, the California Department of Transportation (Caltrans), in a joint venture with the San Bernardino Association of Governments (SANBAG), plans to widen a 6.6-mile section of the I-215 freeway between the I-10 and State Road-30 (SR-30) intersections. The effort includes widening of bridges and reconstruction of interchanges (Aragoan, 2004). Because the area is situated between at least two major fault zones, the San Jacinto fault zone (SJFZ) to the southwest and the San Andreas Fault zone (SAFZ) to the northeast, Caltrans is incorporating expected ground shaking and rupture into the design of the roadways and bridges along the section of the freeway to be widened. However, one of the principal factors that affect ground shaking and structural failure during an earthquake, the proximity of faults to the structures in question, is not known because the area is covered by alluvium (Morton and Miller, 2003).

The U.S. Geological Survey's (USGS) Earthquake Hazards Team (EHZ) is part of the National Earthquake Hazards Reduction Program (NHERP), which conducts research designed to reduce hazards associated with earthquakes. The USGS-EHZ program includes an active-source seismic imaging effort designed to locate details of faults and basin structure. To accomplish the common goals of the USGS and Caltrans, both organizations jointly conducted seismic imaging investigations in May 2003 and October 2003 across the San Bernardino Valley and along the I-215 freeway, respectively. The primary goals of these seismic investigations were to more accurately locate known and unknown (buried) fault strands relative to structures and major lifelines in the San Bernardino area. In addition, we evaluated seismic velocities, basin depth and geometry, and fault geometry, all of which affect ground-shaking resulting from earthquakes. This report presents results of the seismic imaging studies to Caltrans and is part of a more comprehensive report that details fault structures in the San Bernardino area (Catchings et al., in prep).

Tectonic Setting

The ~1300-km-long San Andreas fault (SAF) system, which extends from near the U.S.-Mexican border to Cape Mendocino, California, represents the boundary between two of the Earth's major tectonic plates, the Pacific Plate to the west and the North American Plate to the east. Deformation associated with the SAF system largely occurs along a zone that averages about 120 km in width, but most of the deformation is concentrated along a relatively narrow zone near the surface trace of San Andreas fault zone (Wallace, 1990). The City of San Bernardino is located near a particularly complex

area of the SAF system where the fault system splays into multiple strands and deviates from its largely N40°W orientation. At the latitude of the San Bernardino area, deformation is distributed among numerous faults from the Mojave Desert to the Pacific Ocean. Faults within this zone have a wide range of orientations and include strike-slip, reverse, and dip-slip components of motion. Although deformation is distributed over a wide zone, most of the deformation is concentrated along three principal fault zones, the San Andreas, San Jacinto, and Elsinore fault zones (Wallace, 1990). In the City of San Bernardino, the San Andreas and San Jacinto fault zones are less than 10 km apart, and the distance between the two fault zones decreases to less than 3 km in the northwestern part of the San Bernardino Basin (Fig. 1).

The San Jacinto fault zone (SJFZ) is a right-lateral, strike-slip fault zone that extends approximately 250 km from the northwestern Imperial Valley to Cajon Pass. It is by far the most seismically active fault zone in southern California for earthquakes less than M 7 (Vernon, 1989; Hill et al., 1990; Hauksson et al., 2003). The SJFZ has produced at least nine events registering M 6.0 or stronger since 1890 and four since 1932. The last three large (M6+) earthquakes on the SJFZ were the 1968 M 6.4 Borrego Mountain earthquake and the 1987 M 6.0 and M 6.6 Superstition Hills earthquakes (Hill et al., 1990). Although the principal motion in the fault zone is strike-slip, locally there is also a small vertical component of offset. The SJFZ does not have a continuous linear surface trace, rather it forms multiple sub-parallel surface strands along the zone (Sharp, 1972). Seismicity data indicate that the SJFZ is composed of discontinuous splays and strands in a zone that is up to 6 to 10 km wide (Hill et al., 1990; Hauksson et al., 2003). These sub-parallel surface strands vary in length from 30 to 70 km and form complicated substructures within the general linear trend of the fault zone, making identification of the near-surface active strand or strands difficult (Vernon, 1989).

The San Andreas fault zone (SAFZ) is an ~10-km-wide zone that includes numerous individual strands. Regionally, the SAFZ is separated into multiple branches, including the Banning fault zone, the Mill Creek fault zone, and many others (Matti and Morton, 1993; Yule and Sieh, 2002). However, for purposes of discussion in this report, we refer to the SAFZ as the several-kilometer-wide zone of faults near its mapped surface traces in the San Bernardino area (Morton and Miller, 2003). Much like the SJFZ, faults in the SAFZ have right-lateral, predominantly strike-slip components (Fig. 1). In the San Bernardino area, seismicity is most concentrated near the SJFZ, with relatively little seismicity near the surface trace of the SAF (Hauksson et al., 2003). However, farther south, the SAFZ generates a large amount of seismicity (Hill et al., 1990; Hauksson et al., 2003). Recent paleoseismological investigations show that some segments of the SAF have experienced at least 14 large-magnitude earthquakes in the past 1500 years and is now likely near failure again (Fumal et al., 2002).

Local Geology

The I-215 freeway is underlain by road construction materials at shallow depths (upper few meters), but the underlying, near-surface deposits consist of Quaternary sediments ranging in age from late Pleistocene to late Holocene (Morton and Miller, 2003). Specific deposits along the seismic profile consist of late Holocene wash deposits, late Holocene alluvial valley deposits, middle Holocene alluvial valley deposits, middle to early Pleistocene alluvial valley deposits, and Holocene to late Pleistocene eolian (sand dune) deposits (Miller and Morton, 2003). Water-well borings show that deposits at several hundred meters depth are Holocene alluvium (unconsolidated dune sand, river-channel deposits, and younger alluvium), late Pleistocene alluvium, Tertiary-to-

Quaternary partly consolidated to consolidated continental deposits, and pre-Tertiary basement complex (Dutcher and Garrett, 1963; Woolfenden and Kadhim, 1997; Izbicki et al., 1998). On the basis of driller's logs and water-level data from more than 800 wells, Dutcher and Garrett (1963) divided the valley fill sediments into upper, middle, and lower zones, where each zone includes a fine-grained, less-permeable hydrologic unit overlying a coarse-grained permeable hydrologic unit. The near-surface equivalent of these hydrologic units could be important for purposes of determining liquifaction potential along the I-215 freeway (T. Noce, Pers. Comm., 2004). The basement complex is composed of metamorphic and igneous rocks that crop out in the surrounding mountains and at various places within the valley (Dutcher and Garrett, 1963; Morton and Miller, 2003).

Sediment thickness or basement depth is poorly determined in the San Bernardino Valley and is particularly poorly known along the I-215 freeway between its intersection with I-10 and SR-30. Several 300-m-deep water wells along I-215 freeway did not encounter basement rocks (Izbicki et al. 1998), but a recent seismic reflection survey suggests that maximum depth to basement is about 1.7 km near the I-215/I-10 Interchange, with basement decreasing in depth toward the northwest (Stephenson et al., 2002).

Seismic Surveys

In 2003, the U.S. Geological Survey and Caltrans conducted two seismic surveys in the San Bernardino Basin (Fig. 1). The first survey was a regional-scale seismic survey that was acquired in May 2003 from the southern part of the City of Colton to the City of Highland, largely along the trend of the Santa Ana River. We refer to this seismic survey as the San Bernardino Regional (SBR) seismic survey (Fig. 2). The SBR seismic survey was principally designed to provide regional-scale velocity images and relatively low-fold reflection images of the upper few kilometers of the San Bernardino Basin. A second seismic survey was acquired in October 2003 along the northbound shoulder of the I-215 freeway between the I-215/I-10 Interchange and State Road-30 (SR-30) (Fig. 2). We refer to this survey as the San Bernardino High–Resolution (SBHR) seismic survey, which was designed to provide high-resolution reflection and velocity images of the upper ~2 km along the I-215 freeway. In this report, we first present acquisition and processing parameters and images for the SBR and SBHR surveys, followed by interpretations and discussions of the seismic images and fault structures.

SBR Seismic Data Acquisition

The SBR survey consisted of a N30^{o}E-trending seismic transect that extended ~20 km from Tropicana Ranch Road in Colton to slightly northeast of the San Andreas fault near Highland (Figs. 1 and 2). Seismic sources were generated by 15 explosions in ~5-m- to ~18-m-deep (15 to 60 ft) boreholes, with explosions ranging in size from 2 to 35 kg (5-75 lbs). The seismic sources were spaced approximately 1 km apart. Data were recorded with 456 "Texan"seismographs, borrowed from the Program for Array Seismic Studies of the Continental Lithosphere (PASSCAL), a division of the National Science Foundation. The Texan seismographs are small, stand-alone seismic recorders that are about 20 cm (8 in.) in height, 8 cm (3in.) in diameter, and weigh about 0.9 kg (2 lbs). We attached the Texan seismographs to vertical-component, single-element, Mark Products 1-10B, 4.5-Hz sensors (geophones). Individual Texan seismographs were spaced approximately 50 m apart along the profile, and they were programmed to turn on at specific times that correlated with planned shot times. The internal timing of the seismographs was checked

using Global Positioning System (GPS) clocks before and after deployment. Internal seismograph clock drift is typically less than 2 ms between deployment and pickup. The data were recorded and retrieved within a 24-hour period, whereby the seismographs were deployed during the day, the 15 shots were recorded during the night (12:00 A.M. to 5:00 A.M.), and the seismographs were retrieved and downloaded the following day. The seismic data were recorded at a 2-ms sampling rate. See Table 1 for principal acquisition parameters of the SBR profile.

Table 1. Acquisition Parameters for the SBR Profile. Distance is relative to the first geophone.

Profile	Orient.	Array Length	# of Seismographs	Shot Type	# of Shots	Shot Spacing	Geo. Spacing	Geo. Freq.	Record Length	Sample Rate
LR	NE-SW	~20 km	456	Explosion	15	~1 km	50 m	4.5 Hz	60 s	2 ms

SBR Array Geometry

To account for variations in geometry, each shot point and geophone location was surveyed using a Global Positioning System (GPS) with theoretical lateral accuracies of about 1 m. The geometry data for the SBR profile are presented in Appendix 1. Relief along the profile was about 275 m (Fig. 3a). The array of geophones varied from a best-fit line (linearity) by about 600 m along the length of the ~20 km-long array (Fig. 3b). Shot points varied in elevation by about 220 m (Fig. 3c), and the shot-point array varied in linearity by about 1 km (Fig. 3d). The deviations in the linearity of the shot-point and seismograph arrays were necessary because of limitations on shot-point and seismograph placement imposed by the highly urban setting.

SBR Seismic Data

We present shot gathers from each shot point along the SBR seismic profile (Fig. 4a-o). Although only 6 s of seismic data are presented in figure 4, 60-s-long records were recorded for each shot so that all angles of the wavefield could be recorded. We minimally processed the shot gathers presented in this report (Fig. 4a-o) by editing noisy or dead traces, applying automatic gain control (AGC Window = 4000 ms), and applying low bandpass (2-4-12-24 Hz) filtering. Compressional waves (P-waves), surface waves, air waves, and some shear waves are apparent in the shot gathers. Near-vertical and wide-angle reflections are also present on all shot gathers, which allow low-fold reflection images to be developed. Although the urban environment was noisy, seismic energy propagated across the entire seismic profile for most shots. However, small explosions (~2 kg) in shallow boreholes (5 m), used near residential property or in bedrock locations, did not propagate as well. The larger shots generally provided the strongest seismic signal at the greatest offsets. Propagation of the seismic signal was, in some cases, related to the structure of the Earth, whereby sharp-edged basin boundaries reflected much of the seismic energy. Also, in some cases, propagation was related to the shot location, whereby shots within the basin generally propagated well. Empirical observations elsewhere have shown that shots located within basins generally propagate seismic energy better than shots outside of basins.

Asymmetry in first-arrival travel times is apparent for shot point 2-7, with earlier arrivals to the south. This pattern reverses for shot point 8, and shot points 9-12 are not markedly asymmetric. At shot point 7, an appreciable delay in the first arrival at the shot gather is indicative of vertically offset (down to the northeast) shallow-depth strata immediately beneath the shot point (Fig. 4g). The overall variation in the symmetry of

first-arrival refractions is consistent with deepening of basement northward from shot points 2-7, shoaling from shot points 8-13, deepening from shot points 13 to 14, and shoaling from shot points 14 to 15 (Fig. 5).

SBR Seismic P-Wave Velocity Analysis and Image

To develop P-wave tomographic seismic-velocity models of the subsurface along the SBR seismic profile, we inverted first-arrival travel times from usable seismograms using a modified version of an algorithm by Hole (1992). The velocity inversion method uses 2- and 3-dimensional ray tracing to match observed and calculated travel times until a suitable fit is obtained for all arrivals from all shots. In parameterizing the model, we used 50-m by 50-m horizontal and vertical grid spacings and 2-D starting models derived from composite 1-D velocity models calculated from the shot gathers. When inverting the seismic data for velocity structure, we used multiple 2-D velocity starting models, given the asymmetry of shot gathers, as discussed above. Regardless of the starting model used, successive velocity inversions yielded similar 2-D final velocity models (Fig. 5a), suggesting that the velocity structure along the profile is well resolved. In general, the model is best resolved where we have the highest density of ray coverage (Fig. 5b). For the final velocity model, we applied a smoothing routine to the inversion that yielded an approximately 100- to 300-m vertically and horizontally smoothed model.

The minimum depth of velocity imaging is related to the shot (~1 km) and geophone (~50 m) spacings, the model grid spacing (~50 m), frequency of the data, and the amount of smoothing used in modeling. Therefore, velocities in the upper 100 m, for example, are a smoothed average of the velocities within those depth ranges. The maximum depth of velocity imaging was limited by the maximum distance that clear first-arrival refractions could be measured on the shot gathers (Fig. 4). Because of the noisy urban environment, clear first-arrival refractions were measurable to varying distances for each shot. However, propagation was greater than 10 km from the source for most shots, which allowed us to develop a P-wave velocity image to maximum depths of approximately 4 km (Fig 5a). Observed velocities are highly variable across the model but are generally highest (> 6 km/s) below depths of about 2 km along most of the seismic profile and near the surface on the southwestern end of the profile. Velocities are lowest (< 2 km/s) within the upper few hundred meters along most of the profile, but relatively low velocities (< 3 km/s) extend to depths as great as 1 km between meters 3000 and 7000 of the velocity model. These deep regions of low-velocity can be interpreted as a well-developed basin that is about 5 km wide at its deepest points (Fig. 5). The velocity image suggests that the basin gradually shoals to the northeast but is abruptly terminated on the southwest (Fig. 5a). A prominent feature of the velocity image is the high near-surface velocity (~6 km/s) that is underlain by relatively lower velocities (~4 km/s) on the south end (La Cadena Drive) of the profile. Such reversals in velocity are indicative of complex structures, such as thrust faults and variable geologic layering, because on crustal scales, lower-velocity rocks usually overlie higher-velocity rocks. Geologic interpretations of the velocity images are discussed in later sections of this report.

SBR Seismic Reflection Processing

In acquiring the seismic data, we used a “shoot-through” geometry, whereby shots were systematically fired through the stationary recording array. The combination of multiple sources and multiple receivers, which were spread over long distances, permitted both refraction and reflection data to be simultaneously acquired. This

geometrical setup enables recording of wide-angle reflections from steeply dipping structures, which can be migrated to their proper geographical locations (Hole et al., 2002).

In seismic reflection data processing, we used procedures similar to those outlined by Brouwer and Helbig (1998), but we adapted the procedures to accommodate the low fold of the SBR data. Processing steps for stacked images included geometry installation, independent trace editing, timing corrections, elevation static corrections, AGC, bandpass filtering, surgical muting, velocity analysis (from refractions, semblence, and hyperbolic moveout), NMO correction, stretch muting, common-depth-point stacking, post-stack AGC, post-stack bandpass filtering, and post-stack deconvolution. For migrated sections, we used Kirchoff pre-stack depth migration after velocity analysis. Principal parameters used in processing are listed in Table 2. In trace editing, noisy traces (due to cultural noises) or redundant traces (due to profile geometry) were removed from the shot gathers before stacking or migrating, leaving approximately 400 channels per shot gather. Elevation statics, migration, and velocity analyses were accomplished using the tomographic velocity model (Fig. 5a). For velocities at depths greater than those determined by the tomography velocity model, we used parabolic methods, and we inferred velocities based on laboratory-based velocity-depth (pressure) relations (Christensen, 1982; Carmichael, 1989) and refraction velocities from similar rocks in nearby terranes (Fuis et al., 2001).

Table 2. Reflection Processing Parameters for the SBR Profile

Maximum Fold	15
CDP Spacing	25 m
AGC Prestack Poststack	 1000 ms 1000 ms
Bandpass Filter Prestack Poststack Low	 1-2-10-20 Hz 2-4-50-100 Hz
Surgical Mute	Top (refraction) mute Bottom (surface- and air-wave) mute
Deconvolution	
Migration (max freq., aperture, emergence angle)	80 Hz, 8000 m, 30 degrees

SBR Low-fold Migrated Reflection Image

A migrated reflection image was developed for the SBR profile using low-fold reflections from the shot gathers (Fig. 6). Because of the design of the SBR survey and because the data were bandpass filtered with dominant frequencies between 1 and 20 Hz, reflectors are best resolved at the higher end of the frequency spectrum. Assuming velocities of 1500 and 6000 m/s, frequencies between 1 and 20 Hz, and the quarter-wavelength criteria for a reflection to be generated (Dobrin and Savit, 1988), only layers that are at least 20 m thick are likely to be imaged with the SBR data. However, most layers imaged in the upper few kilometers by these low-frequency data are likely to be about 40 m thick.

Strong, shallow-depth reflections are observed along most of the seismic profile, but most reflections below depths of about 200 m are less laterally continuous. Apparent

reflections from the basement dip southward for locations northward of meter 3000 of the seismic profile. Although apparent noise is observed on the seismic image, clear reflections are observed to several kilometers depth.

SBR Combined Velocity and Seismic Reflection Image

We superimposed the velocity model (Fig. 5a) onto the seismic reflection image (Fig. 6) so that direct comparisons between velocities and reflections could be made (Fig. 7). The combined images show that the strong shallow-depth reflectors correspond to strata with P-wave velocities less than about 3000 m/s and that these low-velocity reflectors are deepest (~1 km) beneath the I-215/I-10 Interchange and beneath the Tippecannoe Avenue area. The low-velocity reflectors largely dip southward between meters 19000 to 5000 (San Andreas fault to south of the I-215/I-10 Interchange), where they are abruptly offset to shallow (~200 m) depths on the south of meter 5000. Strong reflectors within basement rocks (> 4000 m/s) also dip southward (Fig. 7). A peculiarly thick low-velocity (<4000 m/s) basement (?) interval is seen between model coordinates 6500 and 9500, which we discuss below in the interpretative section.

SBHR (I-215) Data Acquisition

We acquired an approximately 8.2-km-long, high-resolution, combined reflection and refraction profile from the intersection of I-215 and Fairview Drive (Santa Ana River) to the intersection of I-215 and 28th Street (Fig. 8). The seismic profile, which we refer to as the San Bernardino High-Resolution (SBHR) profile, was acquired along the northbound shoulder of I-215. Acquisition parameters for the SBHR profile are shown in Table 3. Seismic sources were generated by a combination of ~1500 Betsy-Seisgun^{TM} blasts (400 grain) and ~0.9 kg (2 lb.) explosions in 3-m-deep boreholes. The data were recorded on an array of four Geometrics Strataview^{TM} RX60 seismographs, with a total of 240 active channels. The sensors were coupled to the ground via Mark Products L-40A ^{TM} single element 40-Hz geophones and 60-pair refraction cables. Both shots and geophones were spaced at 5-m intervals, with the geophones and shots laterally offset by 1 m. For seisgun blasts, shot timing was determined electronically at the seismic source when a hammer, used to trigger the seisgun, electrically closed contact with the BETSY Seisgun^{TM}, sending an electrical signal by radio to the seismograph. For downhole explosive blasts, the shooter's box simultaneously triggered the blast and a radio signal that turned on the seismographs. Three seconds of data for each seisgun blast and 5 s of data for each explosive blast were recorded in SEG-2 format on the hard drive of the seismographs during field acquisition. The data were later transferred to 4-mm tape in SEG-Y format for long-term storage.

Prior to acquiring the data, we surveyed geophone and shot locations using a measuring tape. After acquisition, more precise (several centimeters) geophone and shot locations were surveyed using a GPS receiver.

SBHR Array Geometry

In seismic reflection imaging, artifacts can be mistaken for structure if geophones and/or shot locations have significant elevation variations and non-linear alignments that are not included in processing the data. To properly account for such variations in geometry, each shot point and geophone location was surveyed using a Global Positioning System (GPS) with theoretical accuracies of a several centimeters. The geometry data for SBHR seismic profile are presented in Appendix 2.

Four RX-60 seismographs with 240 active channels were utilized to record the data. The geophone array was stationary while the first 180 shots were recorded. Afterward, 120 channels of the array were moved to the north end of the array, and 120 additional shots were recorded. This process was repeated until the end of the profile was reached. During field data acquisition, two channels of each 60-channel seismograph were overlapped as an additional constraint on timing between the seismographs. A total of 1505 shots were fired into the array, with 175 shot points not utilized due to cultural features.

Data were acquired from south to north, and the total length of the SBHR profile was 8332 m. Elevations of geophones along the profile varied by more than 67 m over a distance of about 8332 m (Fig. 9a), and the geophone alignment varied from a linear array by less than 283 m (Fig. 9b). Variations in shot-point elevation (Fig. 9c) and linearity (Fig. 9d) along SBHR profile are similar to those of the geophones.

Fold along the SBHR profile (Fig. 9e) was not smoothly varying because the recording array was not stationary for all shots. Maximum fold was about 173 near the ends of the SBHR profile, but fold of approximately 100 was obtained for most of the profile.

Table 3. Acquisition parameters for the SBHR seismic profile. Distance is relative to the first (southern-most) geophone (Channel).

Profile Name	Orientation	Geophone Array Length (m)	Shotpoint Array Length (m)	No. of Shots	No. of CDPs	Maximum Fold
SBHR (I-215)	S-N	8332.52	8246.32	1505 total shots 181 exp 1324 shotgun	1681	173

SBHR Seismic Data

Example shot gathers near the ends and middle of the SBHR seismic profile are shown in figure 10. The shot gathers have been minimally processed, whereby bandpass filtering (8-16-200-400 Hz) and AGC (300) were applied. Whereas the down-hole explosions provided lateral propagation to offsets of approximately 500 m, propagation from the shotgun blasts were limited to about 100 m lateral offset. Because of the relatively long recording array (240 channels or 1200 m), both reflection and refraction data were simultaneously acquired. We processed the seismic data as both shallow-depth velocity images and reflection images. Seismic data from both the shotgun blasts and the explosions were stacked at high fold (Fig. 9e) in an attempt to add the seismic signals and cancel random noises. Generally, the combined sources produced good images in the upper few hundred meters, but the deeper reflections contained appreciable noise due to the low-signal-to-noise ratios of the seisgun blasts. Generally, the explosions were energetic enough to provide good signals to depths in excess of 1500 m, but when the seisgun blasts and the explosive blasts were stacked together, the seisgun data significantly degraded the combined stack at depths in excess of a few hundred meters. However, the seisgun data significantly improved the stack at shallow (<100 m) depth. Thus, we present several reflection images, whereby some images include only explosive sources and other include both explosive and seisgun blasts.

The quality (resolution and depth) of the seismic data was degraded by the high level of traffic noise along the I-215 freeway during the daylight hours (see cover of this report). Prior to data acquisition, we conducted walk-away tests during the daylight and night-time hours, and we concluded that night-time data acquisition would be most

advantageous. We anticipated nighttime data acquisition in planning the seismic survey; however, logistical support needed to conduct nighttime data acquisition was not available. Thus, all of the seismic data were acquired during daylight hours when cultural and traffic noises were highest.

SBHR (I-215) Velocity Analysis and Image

To develop tomographic P-wave seismic velocity models of the subsurface along the SBHR seismic profile, we inverted first-arrival travel times from usable seismograms from the SBHR shot gathers in a similar manner as done for the SBR velocity image. In parameterizing the SBHR model, we used 5-m by 5-m horizontal and vertical grid spacings and 2-D starting models derived from composite 1-D velocity models, calculated from shot gathers. Multiple 2-D starting velocity models yielded consistently similar 2-D final velocity models (Fig. 11a), suggesting that the velocity structure along the profile is well resolved. Although only two reversing raypaths are required to obtain accurate velocities, the SBHR model is best resolved where we have the highest density of ray coverage (Fig. 11b). For the final velocity model, we applied a smoothing routine to the inversion that yielded an approximately 10- to 15-m vertically and horizontally smoothed model.

The minimum depth of velocity imaging is related to the shot (~5 m) and geophone (~5 m) spacing, the model grid spacing (~5 m), frequency of the data, and the amount of smoothing used in modeling. Therefore, velocities in the upper 10 m, for example, are a smoothed average of the velocities within those depth ranges. The maximum depth of velocity imaging was limited by the maximum distance that clear first-arrival refractions could be measured on the shot gathers (Fig. 10). For the SBHR profile, the high noise level limited the maximum distance to about 600 m for the explosions and only to about 100 m for the seisgun blasts. Typically, refractions penetrate to depths equal to about 25% of the maximum distance first arrivals can be measured, resulting in maximum imaging depths of about 100-150 m along much of the SBHR profile.

Along the SBHR (I-215) profile, P-wave velocities in the upper 150 m range between about 800 m/s and 2800 m/s (Fig. 11a). Low-velocity (< 1500 m/s) deposits thicken appreciably from south to north along the profile, with a maximum thickness of about 75 m on the north end of the profile. As discussed in the sections below, the 1500 m/s velocity contour largely coincides with the ground water table in unsaturated sediments (Schon, 1996; Catchings et al., 1999; 2000; Gandhok et al., 1999). Because of the importance of the ground-water table in delineating structures such as faults (Woolfenden and Kadhim, 1997; Izbicki et al. 1998), we highlight the 1500 m/s contour here in white (Fig. 11a). The apparent ground-water table (1500 m/s) (not including perched or thin ground-water aquifers) is offset by about 10 to 15 m at multiple locations along the profile. However, between meters 800 to 1200 of the SBHR profile, the 1500 m/s contour is vertically offset by about 25 m, with thicker low-velocity deposits to the southwest. Deposits with velocities above 2000 m/s also show appreciable vertical offset along the seismic profile. As discussed below, such vertical displacements in the saturated sediments (1500 m/s) can be indicative of fault zones (Catchings et al., 1999; 2000; Gandhok et al., 1999).

SBHR (I-215) Reflection Processing

As with the SBR profile, the combination of multiple sources and multiple receivers, which were spread over long distances, permitted both shallow refraction and

near-vertical reflection data to be simultaneously acquired along the SBHR profile. To process the seismic reflection data, we used procedures similar to those outlined by Brouwer and Helbig (1998). Processing steps for stacked images included geometry installation, independent trace editing, timing corrections elevation static corrections, AGC, bandpass filtering, surgical muting, velocity analysis (from refractions, semblence, and hyperbolic moveout), NMO correction, stretch muting, common-depth-point stacking, post-stack AGC, Post-stack bandpass filtering, and post-stack deconvolution. We removed noisy traces (due to highway noises) or redundant traces (due to line geometry) from the shot gathers before stacking, leaving approximately 232 channels per shot gather. Elevation statics and shallow depth conversion were accomplished using the SBHR tomographic velocity model (Fig. 11a). For velocities deeper than those determined by the SBHR tomography velocity model, we used parabolic methods, inferred velocities based borehole lithologies, and refraction velocities from the SBR profile.

We also used Kirchoff prestack depth migration to remove diffractions and properly account for dipping strata. For unmigrated stacks, we laterally combined every three traces to enhance the reflection signals. This effectively smoothed the image over three CDP's or about 7.5 m. For the migrated images, we chose not to laterally combine signals so that locations of specific structures could be more clearly determined.

SBHR Seismic Reflection Images

We developed depth images for the SBHR profile by either stacking (1) approximately 181 explosive blasts and/or (2) more than 1300 seisgun blasts, with approximately 232 channels per shot (Fig. 12). Fold (with all shot points) along the seismic profile was laterally varying but was generally between 100 and 175, except at the very ends of the seismic profile (Fig. 9e). Common-depth-point (CDP) spacing along the profile is 2.5 m, such that a seismic trace was produced every 2.5 m along the ~8250-m-long profile. The reflection images were processed to approximately 2000 milliseconds (2 seconds), which included a datum above the topography of the seismic profile; however, the signal-to-noise ratio is low for depths in excess of 1200 m (Fig. 12).

When only the explosive sources are stacked and every three traces are laterally summed, reflectors can be traced across most of the seismic transect, but most of the reflectors appear to be vertically offset at multiple locations (Fig. 12a). To visually enhance the reflectors, we highlighted (in yellow) the spaces between every other reflector to depths of about 900 m (Fig. 12b). The visually enhanced image suggests dipping and vertically offset layers across much of the seismic profile. We used the SBHR and SBR tomographic velocity models and other velocity analyses to develop a Kirchoff, pre-stack migrated depth image along the SBHR profile (Fig. 12c). The migration image shows many of the same features, as does the stack; however, as is typical of Kirchoff migration images, the resolution is lower than the stacked image. The migrated image shows multiple near-vertical zones along the seismic transect where strata are disrupted or truncated. We attempted to correlate these zones with variations in acquisition parameters (such as fold, missing shots, street crossings, etc.), but most of the zones do not correlate with changes in acquisition parameters. We also varied migration parameters and migrated the images multiple times, but the apparent disrupted zones were present on each migrated image. As discussed below, we conclude that these apparent disrupted zones are likely due to the subsurface structure and not to acquisition or processing parameters. The near-surface (upper 50 m) is not well imaged with only the explosive sources because the explosive sources were spaced at about 40 m. However,

by combining the seisgun sources, which were spaced at 5-m increments, details of the near-surface stratigraphy were better imaged (Fig. 12d).

We used relatively low bandpass filtering (15-30-60-120 or 20-40-80-160 Hz) in developing the seismic reflection images because the recorded signals were dominated by relative low-frequency energy. The relative low-frequency of the recorded seismic energy is probably due to either highly attenuating near-surface materials or to disrupted subsurface layering. At higher frequencies, poorly consolidated and laterally variable deposits that contain boulders, large rock fragments, or gravel generally do not image well with seismic reflection methods. These types of deposits are known to underlie parts of the SBHR profile at shallow depths (Dutcher and Garret, 1963; Morton and Miller, 2003; T. Noce, Pers. Comm., 2004). Furthermore, boulders, faults, and other sharp discontinuities tend to scatter and attenuate the seismic energy and produce numerous diffractions at higher frequencies. As a result, the best seismic images from the SBHR profile utilize relatively low-frequency energy, which is less scattered and attenuated. The resulting lower frequency images show larger scale features and thicker layer sequences. Assuming velocities between 1000 and 3000 m/s, frequencies between 15 and 60 Hz, and the quarter-wavelength criteria for a reflection to be generated (Dobrin and Savit, 1988), only reflectors that are at least 4 m thick are likely to be imaged in the near surface with the SBHR data. However, deeper reflectors imaged by the SBHR data are likely to be 10 m or more thick. Because of the Fresnel zone limitation (Dobrin and Savit, 1988), individual reflectors at 100 m depth must be radially continuous for at least 6 m to produce good reflections. At depths of 1 km, similar reflectors must be radially continuous for at least 55 m to generate good reflections with 20-Hz data. For deeper images, the Fresnel zone requirement became progressively more important because, in such a tectonically active area as San Bernardino, reflectors may be too disturbed over the distances needed to generate strong, continuous reflections.

Interpreted Images

Lithology (SBR Profile)

We broadly categorize the major lithologic units along the SBR profile as (1) unsaturated and unconsolidated alluvium, (2) saturated and unconsolidated alluvium, (3) consolidated to partially consolidated alluvium, (4) Pliocene and Pleistocene (old) alluvium, and (5) basement (metamorphic or crystalline). These broad categories are largely based on comparison of our measured seismic velocities with our reflection images and observations of deposits in nearby well borings (Izbicki et al., 1998). Reflection images are not particularly good at differentiating among the various rock types listed above because all can be reflective. However, broad categories of lithologic units, such as sediments and basement, can be inferred on the basis of reflectivity because sediments are likely to be more reflective and have lower velocities and densities than crystalline basement rocks (Fig. 13).

Within the sedimentary section, deposits with velocities less than 1500 m/s are not imaged on the SBR profile because these deposits are largely confined to the upper few tens of meters, and the SBR seismic data averages the velocities and reflectors in that depth range (Fig. 7). Deposits with average velocities between about 1500 m/s and 2200 m/s (upper few hundred meters) are probably saturated but are mostly composed of unconsolidated alluvium, as observed in well borings in the area (Izbicki et al, 1998). Deposits with velocities between about 2200 m/s and 3000 m/s (~300 m to 1000 m depth) are likely to be partially consolidated to consolidated (Brocher et al., 1997). Similar relations between the physical condition of sediments, their seismic velocities,

and depth of burial have been observed elsewhere in pre-Tertiary sedimentary basins in California (Catchings et al., 1999; in prep; Gandhok et al., 1999). Sediments with velocities between 3000 and 3800 m/s are likely to be older Pliocene to Pleistocene deposits, like those exposed on in the San Timoteo Badlands to the southeast of the seismic profiles (Morton and Miller, 2003). We observed these velocities only in the deeper parts of the San Bernardino Basin (Fig. 7). All of these sedimentary deposits are reflective in the seismic reflection images. Rocks with velocities greater than 4000 m/s are interpreted to be metamorphic (Pelona Schist) or crystalline (tonalite or granodiorite) rocks, similar to rocks that crop out in the hills within the San Bernardino Basin and within the surrounding mountains. These rocks are less reflective than the overlying sediments (Figs. 7 and 13).

Basin Structure (SBR Profile)

We use both the seismic velocities and the seismic reflection images to infer the depths and dimensions of the San Bernardino Basin. The reflection and velocity images suggest that basement is only a few hundred meters deep on the southwestern end of the SBR profile, but basement abruptly deepens along several faults to a depth of about 1200 m between meters 3000 and 8000 of the seismic profile (Fig. 13). The deepest part of the San Bernardino Basin along the SBR profile is about 5 km wide, but the base of the basin has considerable topography. Both basement and the overlying sediments also appear to be folded and uplifted in the central part of the basin. From about Tippecanoe Avenue (~meter 8000) to Highway SR-30 (meter 14000), we interpret basement to rise along a series of faults, with an average slope of about 7 degrees.

The basement rocks (~4000 to 6000 m/s) contain strong reflectors that dip predominantly southwestward. The basement reflectors are more prominent northeast of meter 3000, suggesting that basement rocks are probably not the same on both sides of the San Jacinto fault zone (near meter 3000). We suggest that basement rocks northeast of meter 3000 are probably composed of Pelona Schist for several reasons. First, Pelona Schist is observed in outcrop a few kilometers southeast of the northeastern end of the SBR profile, within the Crafton Hills, and to the northwest of the SBR profile, within the Shandin Hills (Morton and Miller, 2003). The basement topographic high observed between meters 12000 and 16000 of the SBR profile (Fig. 13) is probably part of a northwest-trending structure between the Crafton Hills, Perris Hills, and the Shandin Hills. Second, the upper basement rocks along the SBR profile have P-wave velocities of ~ 4000 to 5000 m/s (Fig. 7), which are similar to velocities observed by Fuis et al. (2001) for the Pelona Schist at shallow depths in the San Gabriel Mountains. Third, because the Pelona Schist is likely to be more reflective than crystalline igneous rocks, the more reflective rocks northeast of meter 3000 of the SBR profile are more consistent with Pelona Schist than crystalline igneous rocks. Fourth, although the sedimentary rocks to the northeast of the deep part of the basin are thinner than those near meter 3000, the Bouguer gravity anomaly remains relatively low to the northeast (Anderson et al., 1999), suggesting less dense basement rocks to the northeast (Fig. 13).

On the southwestern end of the profile, however, we interpret the underlying high-velocity (~ 6000 m/s) rocks to be crystalline (granodiorite and tonalite) basement rocks (Fig. 7) like those exposed in the nearby hills (Morton and Miller, 2003). The velocity reversal (~4000 m/s) below ~ 500 m, however, is somewhat curious; it may suggest that crystalline rocks have been thrust over lower-velocity rocks.

Fault Structures (SBR)

Due to the low-fold design of the SBR profile, interpretations of the seismic reflection images are non-unique. However, we use several criteria in interpreting faults along the SBR and SBHR seismic profiles. First, we interpret faults on the seismic reflection images where a series of reflectors are vertically offset over a range of depths. Second, because empirical studies have shown that seismic P-wave velocities within fault zones are typically 17 to 40% lower than that of the surrounding materials (Aki and Lee, 1976; Mooney and Luetgert, 1982; Catchings 1999; Catchings et al., 2002), we consider coincident low-velocity zones and layer offsets to be indicative of fault zones. Third, we interpret faults on the reflection images where the dips of reflectors abruptly change. We are more confident of our fault interpretations where all three of these observations geographically coincide. We interpret fault patterns for both the SBR and SBHR profiles, but because of the differing orientations and the difference in basin width along the two profiles, individual strands of the faults cannot be confidently correlated from profile to profile. In this section, we discuss fault structures along the SBR profile (Fig. 14).

There are abrupt near-vertical offset of basement rocks and an appreciable increase in sediment thickness southwest of the I-215/I-10 Interchange (near meter 3000) that correlates with the projected near-surface trace (Morton and Miller, 2004) of the Rialto-Colton fault zone (RCFZ) (Figs. 13 and 14). Because of the appreciable vertical offset in basement northeast the RCFZ, we suggest that the RCFZ, rather than the SJFZ, bounds the southwestern edge of the San Bernardino Basin. There are likely several strands of the RCFZ, along which the sedimentary basin deepens (Catchings et al., in prep), but the RCFZ may merge with the San Jacinto fault zone (SJFZ) at depth. The SJFZ consists of multiple strands that merge at depth, with the near-surface trace of the SJFZ is centered slightly northeast of the I-215/I-10 Interchange (Fig. 14). In the upper few kilometers, individual strands of the SJFZ encompass about a 3.5-km-wide zone, and most of these strands are within or bound the deepest part of the San Bernardino Basin. Additional faults that may merge with the SJFZ at depth are located between meters 7000 and 11000 of the SBR profile. The most recognizable cultural feature that is closest to these faults is Tippecanoe Avenue. For purposes of discussion, we refer to these faults as the Tippecanoe fault zone (TFZ). Although the TFZ may extend from the Loma Linda fault to the southeast, it appears to be one of the primary faults that accommodates the transfer of slip from the San Jacinto fault to the San Andreas fault, and unlike the mapped part of the Loma Linda fault, the TFZ is not parallel to the San Jacinto fault farther north, beneath the central part of the San Bernardino Basin. To the northeast, a fourth principal fault zone is located near Highway SR-30. We interpret strands of this fault zone to extend from about meter 12,000 to about meter 16,000 of the SBR profile. This fault zone appears to be related to a relative high in basement rocks that likely trends parallel to the San Andreas Fault from the northern Crafton Hills to the Shandin Hills. For purposes of discussion in the report, we refer to this fault zone as the East Highlands fault zone (EHFZ). We do not see a clear expression of a possible San Andreas Fault zone (SAFZ) because the seismic profile does not extend far beyond its surface expression, but there appears to be a possible expression of it at meter 19000, where it appears that the fault dips to the northeast at about 38 degrees.

Seismicity Along the SBR Profile

Earthquakes recorded in southern California during the years 1984 to 2002 have been relocated (Hauksson et al., 2003) using double difference techniques, which are

currently considered the most accurate location techniques (Waldhauser, 2001). We used the double-difference earthquake locations of Hauksson et al., (2003) to construct cross sections of seismic events within 3 km (Fig. 15) and 1km (Fig. 16) of the SBR seismic profile. The events are projected normal to our seismic profile. The seismicity cross sections show that earthquakes occur along most of the SBR seismic profile, suggesting a wide area of faulting along the profile. Many of the events outline well-defined, near-vertical fault zones that extend to more than 20 km depth. In the upper 10 km, hypocenters are most concentrated beneath the TFZ, with fewer events beneath the SJFZ and EHFZ (Figs. 15 and 16). At depths below 10 km, the largest concentration of events is located between the near-surface expressions of the SJFZ and TFZ, suggesting that the faults may merge well above 20 km depth. Although the SJFZ is considered the most seismically active fault in the area, the bulk of the seismicity is located northeast of its mapped surface trace at all depths (Figs. 15 and 16). For earthquake hazard purposes in the upper crust, the SJFZ and the other faults to the northeast within the San Bernardino Basin could be considered separate faults.

Lithology (SBHR Profile)

As discussed for the SBR profile, we generally categorize the rock types along the SBHR profile as (1) unconsolidated and unsaturated alluvial deposits, (2) unconsolidated and saturated alluvial deposits, (3) partially consolidated to consolidated alluvial deposits, (4) Pliocene and Pleistocene (old) alluvial deposits, and (5) basement. Along the SBHR profile, we have seismic tomographic velocities for only the first three categories of rock types.

Empirical studies have shown that saturated sediments (water table) have P-wave velocities of about 1500 m/s in unconsolidated sediments (Schon, 1996) and can be mapped in the subsurface by seismically mapping the 1500 m/s velocity contour (Catchings et al., 1999; Gandhok et al. 1999). Along the SBHR profile, deposits with P-wave velocities less than about 1500 m/s are probably unsaturated and unconsolidated (Fig. 17). Shallow-depth and thin (a few meters thick) aquifers in the upper few meters along parts of the seismic profiles would be considered part of the largely unsaturated sediments because such thin aquifers may not be imaged with relatively low-frequency seismic data. The unconsolidated and largely unsaturated sediments range in thickness from about 25 m near Inland Drive to more than 75 m near 28th Street. Lithologically, these low-velocity sediments correspond to the same deposits observed at the surface and near surface (Dutcher and Garrett, 1963; Izbicki et al., 1998; Morton and Miller, 2003). Saturated (unconsolidated) deposits have velocities between about 1500 and 2200 m/s, and they are highly variable in thickness along the seismic profile. These deposits comprise the bulk of the shallow water table.

We have velocity measurements (2200 m/s to 3000 m/s) for only the very tops of the partially consolidated to consolidated deposits, but these deposits extend for hundreds of meters in depth, varying between unconsolidated and partially consolidated (Izbicki et al., 1998). These deposits are highly variable in velocity along the profile and are segmented into multiple relatively low- and high-velocity zones and apparently tilted blocks (Fig. 17).

Because velocity data are largely limited to the upper 150 m along the SBHR profile, our interpretation of deeper basin structure and lithology along the SBHR profile is largely based on reflection patterns (Figs. 17 and 18). The sediments are not highly reflective at frequencies above 10 Hz, suggesting that high-frequencies are highly attenuated within the near-surface deposits, the sediments are not well layered, and/or

they are highly deformed. However, relatively low frequencies, combined with the densely spaced shots and geophones largely delineate the prominent features of the subsurface along the SBHR profile.

Basin Structure (SBHR Profile)

The sediment/basement interface is not apparent as a high-amplitude reflector along the SBHR profile, suggesting that the transition from sedimentary rocks to metamorphic/crystalline rocks may be gradational. If such is the case, the top of the metamorphic/crystalline rocks is probably weathered. On the basis of the SBR seismic images, we interpret basement to be at least 1000 m deep on the south end of the profile, but based on its proximity to the SBR seismic profile, the basin is probably much deeper than 1000 m. Unfortunately, the SBHR data do not have sufficient signal-to-noise ratios to image much deeper than about 1000 m. The SBHR images show basin sediments that dip sharply northward near the southern end of the profile and more gently southward from the northern end (Fig. 18). From the southern end of the seismic profile to just north of Orange Show Drive (meter 1800), sediments below 100 m depth are largely sub-horizontal; however, from about meter 1800 to about meter 3000 along the SBHR profile, these sediments dip steeply. From about meter 3000 to about meter 7000, sediments below 100 m depth dip more gently southward, as seen along the SBR profile. The basin shape, as revealed by the seismic reflection images, is consistent with gravity measurements (Fig. 18a), whereby gravity values decrease markedly from the south and moderately from the north, toward the center of the profile. The gravity high near the southern end of the profile is likely due to the regional effect of high-density rocks immediately south of the SBHR profile (see Fig. 14).

Fault Structures (SBHR Profile)

We interpret multiple fault strands along the SBHR profile on the basis of (a) vertically offset layers on the reflection images, (b) inferred lateral variations in the depths of the ground water table, (c) low-velocity zones in the upper few hundred meters and (d) topographic variations (Figs. 19 and 20).

We interpret vertical offsets in reflectors over a range of depths on the seismic reflection images to indicate faults. In many cases, the apparent faults are also accompanied by changes in dip of the reflectors (Fig. 20). On the velocity image, vertical offsets of a few tens of meters in the 1500 m/s velocity contour, which is often indicative of the ground water table, suggest that some of these faults may locally act as ground-water barriers (Fig. 19b). Between the apparent faults, there are segments of the SBHR profile where the topography has consistent dips over hundreds of meters to several kilometers (Fig. 19a), suggesting that the faults may bound blocks that are rotated. Some of the apparent faults coincide with low-velocity zones seen on the velocity image (Fig. 19b), and empirical studies elsewhere have shown that faults form low-velocity zones (Catchings et al., 2002).

On the basis of the cumulative data, we suggest that the SBHR seismic profile obliquely crosses three to four faults, each with near-surface splays, along the 8.2-km-long SBHR seismic profile. Similar numbers of splays within relatively short distances are exposed at the surface in multiple locations in the nearby San Bernardino Mountains, and along the northwest projection of the SJF, near its intersection with the SAF (Fig. 1). Such fault splays in the near surface are probably not individual faults that extend through the crust; instead, most of these near-surface fault splays probably merge to form several well-defined fault zones at relatively shallow depths.

The RCFZ is located south of the I-215/I-10 Interchange and should not be imaged on the SBHR profile (Figs. 1 and 20). However, the principal part of the SJFZ is imaged in the vicinity of Inland Drive, with individual strands extending between Orange Show Road (meter 800) and Inland Center (meter 2000). This part of the SJFZ correlates with its northwestward projection from the SBR profile (Fig. 14). There is a large (>50 m) vertical offset in shallow reflectors (Fig. 20) and refractors (Fig. 19b) associated with the SJFZ, with the largest vertical offsets occurring between Orange Show Drive and Inland Drive. Along the SBHR profile, the northwestward continuation of the TFZ is probably centered near downtown San Bernardino, near 3rd Street. As discussed above, this fault may be a continuation of the Loma Linda faults zone, but the TFZ likely acts as a fault that transfers slip from the SJF to the SAF. The series of faults north of 16th Street are probably additional transfer faults.

Seismicity Along the SHBR Profile

Double-difference-located earthquakes (Hauksson et al., 2003) within 1 km and 3 km of the SBHR seismic profile are shown in figure 21. Within 3 km of the SBHR profile, near-vertical alignments of hypocenters infer several fault zones that extend from the near surface to at least 20 km depth, suggesting that separate faults extend through the seismogenic crust. Because the hypocenters are distributed over the length of the SBHR profile, the seismicity data suggest that there are multiple faults at all levels of the crust, much like those seen in our seismic images. Although distribution of seismic events suggest that there has likely been movement on many of the imaged fault zones at depth during the past 20 years, the TFZ appears to have been most active fault zone in the San Bernardino Basin.

Comparison with the Stephenson et al. (2002) Seismic Profile

Stephenson et al. (2002) acquired a seismic reflection profile from Colton to the Perris Hills (Fig. 1). Because their profile was located approximately half way between our SBHR and SBR profiles (north of I-10), we can use their reflection image and interpretations to help constrain the 3-D variation in the large-scale structures observed on our seismic profiles. We refer to the Stephenson et al. (2002) profile as the SBS reflection profile (Fig. 22a,b). The SBS reflection profile was largely coincident with the SBR profile between La Cadena Avenue and the I-215/I-10 Interchange. Northward of the Interchange, the SBS reflection profile trended more northerly than our SBR profile and more northeasterly than our SBHR profile. The SBS and SBR reflection images (Fig. 22) show the similar general reflectors in the upper 1000 m, and both images show a likely basement reflection beneath the I-215/I-10 Interchange.

Because tomographic velocity data were not available for the SBS reflection profile, Stephenson et al. (2002) principally based their structural interpretation on reflection and gravity data, which provide limited constraints. Although the SBS reflection model and our combined seismic images show similar overall structural features of the San Bernardino Basin, there are some differences in the structural interpretations based on the two data sets. On the basis of comparisons of the SBR and SBS reflection data (Fig. 22) and velocity data (Fig. 23), we suggest several modifications to the Stephenson et al. (2002) model. First, the relatively low velocities beneath the I-215/I-10 Interchange area indicate that the San Bernardino Basin extends farther south than suggested by Stephenson et al. (2002), whereby the Rialto-Colton fault forms the basin boundary (Fig. 23). Second, the San Bernardino Basin appears to be deeper than indicated by the SBS model, whereby low-velocity (< 4000 m/s) strata

extend more than 2 km in depth (Figs. 22 -24). Third, the depth to basement may depend on the definition of basement, but the relatively high velocities (>4000 m/s) below 2 km depth at the I-215/I-10 Interchange suggest the presence of crystalline or metamorphic rocks. (Christensen, 1982; Catchings et al. in press). Fourth, high-velocity rocks south of the I-215/I-10 Interchange are underlain by lower velocity, layered rocks, suggesting that sedimentary or metamorphic rocks may underlie the near-surface crystalline rocks (Fig. 23). Fifth, although Stephenson et al. (2002) acknowledge that additional faults could be interpreted from their reflection image, they showed only 8 faults along the profile (Fig. 24a). We interpret faults similar to those interpreted along the SBS seismic profile, but on the basis of offset strata, tilted sedimentary packages, and offset basement reflectors, we interpret additional faults within the San Bernardino Basin (Fig. 24b, c). Our interpreted fault structures also correlate with variations in basement velocities (Fig. 23), whereby a prominent low-velocity zone is associated with the active TFZ, and lateral low-velocity zones in basement coincide with strands of the SJFZ and EHFZ.

Faults Lengths and Orientations

Although the SBR, SBHR, and SBS reflection profiles are not oriented in the same directions, each profile can be interpreted similarly. In particular, the deep (~2000 m) basin near the I-215/I-10 Interchange, a northeastward rise in basement, and several zones of faulting are consistent features on all three (SBR, SBS, and SBHR) profiles. Because the RCFZ, SJFZ, TFZ, EHFZ, and additional faults (herein collectively called "basin faults") can be inferred from all three seismic profiles, we suggest these fault zones to have lateral continuity of at least 9 km, the maximum distance between the profiles along a northwest regional trend.

To better estimate the 3-D variation in the imaged fault zones, we plotted double-difference earthquake locations for the San Bernardino Basin area in map view (Fig. 25). The epicenters show several linear trends that geographically coincide with the imaged faults. The trends of epicenters imply that a series of “connector” faults extend from the SJFZ to the SAFZ at high angles (~75 to 80 degrees) to both principal faults (Figs. 25-27). Collectively, these faults form classic structures associated pull-apart basins (Aydin and Nur, 1982; Hempton and Neher, 1986) and strike-slip fault duplexes (Woodcock and Fisher, 1986). In cross section and in seismic reflection images, these faults form a negative flower structure that accommodates the stepover between the two fault zones. The basin faults may be up to 30 km long, suggesting that they can generate moderate-magnitude earthquakes. However, because these basin faults connect both the San Jacinto and San Andreas faults, the maximum-magnitude earthquakes on the basin faults could be considered the same as those of the San Andreas and San Jacinto faults.

Some of the imaged faults trend along the deepest parts of the San Bernardino Basin, as inferred by gravity anomalies (Fig. 26). Generally, high gravity gradients can indicate large changes in basement depth. In the San Bernardino area, lateral variations in the high gravity gradients probably indicate near-vertical offsets in basement caused by faulting. The northwesterly trend of the high gravity gradients is consistent with the concept that the basin fault zones trend northwestward across San Bernardino Basin, connecting to the San Andreas Fault. A similar, but smaller, linear trend in the gravity field can be inferred near the center of the San Bernardino Basin (Fig. 26). Assuming that vertical slip is less than the lateral slip, the geographic correlation between the deepest basin depths and the highest seismicity rates suggest that the basin faults may have been active for a long period of time.

Discussion

The seismic images and existing geologic surface mapping suggest that the San Bernardino Basin is associated with parts of at least five fault zones. These fault zones include the Rialto-Colton (RCFZ), San Jacinto (SJFZ), San Andreas (SAFZ), and two lesser known or unknown fault zones, which we refer to here as the Tippecanoe (TFZ) and East Highlands (EHFZ) fault zones. Each of these fault zones appear to be several kilometers wide and contain multiple fault strands that likely merge at depth. Most of the fault zones appear to form flower structures that are commonly associated with strike-slip fault zones (Harding, 1985).

The RCFZ bounds the southwestern end of the San Bernardino Basin, where basement rocks have apparent vertical offsets of about 1000 m. The RCFZ probably has several near-surface strands in the upper crust where it crosses the SBR profile. The SJFZ, also located near the southwestern edge of the San Bernardino Basin, has additional apparent vertical offsets of basement rocks of about 1000 meters. Although the SJFZ is centered near the I-215/I-10 Interchange, individual strands of the fault zone probably extend about 1.5 km to the northeast and about 2 km to the south west along the SBR profile. The RCFZ and SJFZ may merge at depths of 5 to 10 km in the vicinity of the I-215/I-10 Interchange. Thus, the two faults can probably be considered one fault zone that is more than 5 km wide near the southwestern edge of the San Bernardino Basin. The TFZ may also be part of the SJFZ and may merge with the SJFZ at greater depths. Over the past 20 years, appreciable seismicity has been focussed on TFZ (Figs. 15, 16, 21 and 25), and based on seismicity trends, the TFZ be an extension of the Loma Linda fault (Fig. 25). There also are likely additional faults that transfer slip from the San Jacinto Fault to the San Andreas Fault northeast of the TFZ, but these faults probably merge with other faults at depth. Farther northeast, we interpret a fourth fault zone (EHFZ), centered along a basement high, possibly connecting the Shandin and Crafton Hills. In the upper few kilometers, the EHFZ is several kilometers wide, and there has been a moderate amount of seismicity associated with this fault zone east of I-215 over the past 20 years. However, west of I-215, there appears to be considerable seismicity associated with the EHFZ where it merges with transfer faults in the Shandin Hills area (Figs. 25-27). The SAFZ is located on the northeast boundary of the San Bernardino Basin, but fault strands, including the main trace of the SAFZ, are not clearly imaged on our profiles. The lack of a clearly imaged fault zone near the SAFZ may indicate that the SAFZ zone dips northeastward. There is relatively little seismicity associated with the SAFZ over the past 20 years, suggesting that it is either locked or that most of its slip is transferred to the SJFZ south east of San Bernardino.

Strands of each of the SJFZ, TFZ, and other slip-transfer faults extend beneath the I-215 freeway. In the upper 100 m, these fault strands appear to tilt and offset near-surface alluvial layers and vertically offset the ground-water table by about 10 to 25 m in places (Figs. 28 and 29). Most individual fault strands correlate with low-velocity zones in the near-surface sedimentary deposits. In the near surface, the largest vertical offsets of alluvial deposits are associated with the SJFZ, where fault strands located in the vicinities of Orange Show Road to Inland Drive offset near-surface sediments (Fig. 19). Similarly, strands of transfer faults between 18th Street to Highland Avenue also bound southerly dipping sediments at several hundred meters depth. At depth, the seismicity data suggest that most of the basin fault zones have been active over the past 20 years, with earthquakes occurring across most of the San Bernardino Basin. The wide lateral and vertical distribution of earthquakes demonstrates the distributed nature of faulting in the San Bernardino area, as faulting is not confined to one or two discrete fault planes

(Figs. 25, 26, 28, and 29). We interpret multiple fault splays to underlie much of the I-215 freeway between the I-215/I-10 Interchange and Highway SR-30, but many of these fault splays may be part of a few discrete fault zones at depth. The I-215 freeway trends sub parallel to these faults that transfer slip from the SJFZ to the SAFZ (see Figs. 25-27).

To better understand the faulting in the vicinity of the I-215 freeway and in the San Bernardino Basin, we recommend conducting more targeted high-resolution imaging at lower angles to the slip-transfer faults and perpendicular to I-215. However, we suggest that data be acquired at night, during periods of low traffic volume, and/or along side streets away from the freeway noises. Remote methods, such as INSAR, may be useful in locating potential sites to seismically image. We also recommend trenching studies to understand which faults have been most active at the surface in the recent past.

Acknowledgements

We thank the City of San Bernardino, the San Bernardino Valley Water District, and Caltrans for granting permission to place seismographs and shot points along the seismic profiles. We also thank Caltrans for providing boreholes that were used as shot points. We thank John Bowman and Martha Merriam (both with Caltrans) for invaluable help in setting up the seismic profiles. We thank L. Behera, Coyn Criley, Sam Gudino, Sr., Sam Gudino, Jr., Linda Nyguen, G. Rao, Jose Rodriguez, Mike (of Caltrans), and Beldon Schroeder for assistance in data acquisition. We thank the PASSCAL (Marcos Alveraz, Mike Fort, Tim Parker; Galen Kaip-UTEP), Rob Williams, and John Childs for providing seismic equipment and assistance. We thank scientists form the National Geophysical Research Institute - India for technical assistance. Caltrans and the USGS Earthquake Hazards Program provided funding for the work. Reviews by Gary Fuis and Janice Murphy are greatly appreciated.

References

Aki, K., and W.H.K. Lee, 1976, Determination of three-dimensional velocity anomalies under a seismic array using P-arrival times from location earthquakes. I. A homogenous initial model, J. Geophys. Res., 81, 4381-4399

Anderson, M.L., R. Jachens, and L. Woolfenden, 1999, Structural model of the San Bernadino strike-slip basin, southern California, from regional gravity data: Eos, Transactions AGU, v.80, p. F 1002.

Aragaon, G., 2004, On the road in southern California: A review of major projects and priorities in http://california.construction.com/features/archive/0304.

Aydin, A. & A. Nur, 1982, Evolution of pull-apart basins and their scale independence. Tectonics 1, 91-105.

Brocher, T.M., A. L. Ruebel, and E. E. Brabb, 1997, Compilation of 59 sonic and density logs form 51 oil test wells in the San Francisco Bay area, California, U.S. Geol. Surv. Open-File Report 87-987, 75 pp.

Brouwer, J. and K. Helbig, 1998, Shallow High-Resolution Reflection Seismics, Handbook of Geophysical Exploration, Volume 19, Section I. Seismic Exploration (K. Helbig and S. Treitel, eds.), Elsevier, New York, 391 pp.

Carmichael, R. S., 1989, Practical Handbook of Physical Properties of Rocks and Minerals, CRC Press, Boca Raton, Florida, 583 pp.

Christensen, N. I., 1982, Seismic velocities in R. S. Carmichael ed., Handbook of Physical Properties of Rocks, V. II, CRC Press, Boca Raton, Florida, 583 pp.

Catchings, R. D., G. Gandhok, M. R. Goldman, E. Horta, M. J. Rymer, P. Martin, and A. Christensen, 1999, Subsurface, high-resolution seismic images from Cherry Valley, San Bernardino County, California: Implications for water resources and earthquake hazards, U.S. Geol. Surv. Open-File Report 99-26, 57 pp.

Catchings, R. D., M. R. Goldman, G. Gandhok, M. J. Rymer, and D. H. Underwood, 2000, Seismic imaging evidence for faulting across the northwestern projection of the Silver Creek fault, San Jose, California, U.S. Geol. Surv. Open-File Report 00-125, 29 pp.

Catchings, R. D., M. J. Rymer, M. R. Goldman, J. A. Hole, R. Huggins, and C. Lippus, 2002, High-resolution seismic velocities and shallow structure of the San Andreas fault zone at Middle Mountain, Parkfield, California, Bull. Seism. Soc. Am., 92, 2493-2503

Catchings, R. D. M. J. Rymer, M. R. Goldman, G. Gandhok, and C. E. Steedman, (in press), Structure of the San Bernardino Basin from the Rialto-Colton/San Jacinto fault zone to the San Andreas fault zone, U.S. Geol. Surv. Open-File Report.

Catchings, R. D., G. Gandhok, M. R. Goldman, and R. Hansen (in press), Basin structure and velocities from the 2000 Santa Clara Seismic Investigation (SCSI) as related to earthquake hazards and water resources, western Santa Clara Valley, California, U.S. Geol. Surv. Open-File Report.

Dobrin, M. B., and C. H. Savit, 1988, Introduction to geophysical prospecting, McGraw-Hill Book Co., San Francisco, California, 867 pp.

Dutcher, L. C. and Garrett, A. A., 1963, Geologic and hydrologic features of the San Bernardino area, California-with special reference to underflow across the San Jacinto fault: U.S. Geol. Surv. Water-Supply Paper 1419, 114p.

Fuis, G. S., Ryberg, T., Godfrey, N. J., Okaya, D. A., and J. M. Murphy, 2001, Crustal structure and tectonics from the Los Angeles basin to the Mojave Desert, southern California, Geol. Soc. Am. Bull, 29, 15-18.

Fumal, T. E., R. J. Weldon, II, G. P. Biasi, T. E. Dawson, G. G. Seitz, W. T. Frost, and D. P. Schwartz, 2002, evidence for large earthquakes on the San Andreas fault at the Wrightwood, California, Paleoseismic site: A.D. 500 to Present, Bull. Seism. Soc. Am., 92, 2726-2760.

Gandhok, G., R. D. Catchings, M. R. Goldman, E. Horta, M. J. Rymer, A. Christensen, and P. Martin, 1999, High-resolution seismic reflection/refraction imaging from I-10 to Cherry Valley Blvd., Cherry Valley, Riverside County, California: Implications for water resources and earthquake hazards, U.S. Geol. Surv. Open-File Report 99-320, 56 pp.

Harding, T. P., and J. D. Lowell, 1979, Structural styles, their plate tectonic habitats, and hydrocarbon traps in petroleum provinces, Am. Assoc. Pet. Geol. Bull., 63, 1016-1058.

Hill, D. P., J. P. Eaton, and L. M. Jones, 1990, Seismicity, 1980-86, in The San Andreas Fault System, California, R. E. Wallace, editor, pp. 115-151, U.S. Geol. Surv. Profess. Paper 1515, Washington, D.C., 283 pp.

Hauksson, E., 2000, Crustal structure and seismicity distributions adjacent to the Pacific and North American plate boundary in southern California, J. Geophys. Res., 105, 13875-13903.

Hauksson E., W-C. Chi, P. Shearer, and A. Michael, Comprehensive waveform cross-correlation of southern California seismograms: Part 1. Refined hypocenters obtained using the double-difference method and tectonic implications (abstract), Fall. Ann. Meeting, American Geophys. Un., Dec. 8-12, 2003, San Francisco CA.

Hempton, M. R., and K. Neher, 1986, Experimental fracture, strain and subsidence patterns over en echelon strike-slip faults: implications for the structural evolution of pull-apart basins, J. Structural Geol., 8, 597-605

Hole, J. A., 1992, Nonlinear high-resolution three-dimensional seismic traveltime tomography, Journal of Geophysical Research, v. 97, p. 6553-6562.

Hole, J. A., R. D. Catchings, K. C. St. Clair, M. J. Rymer, D. A. Okaya, and B. J. Carney, 2001, Steep-dip seismic imaging of the shallow San Andreas fault near Parkfield, Science, 294, 1513-1515

Izbicki, J. A., W.R. Danskin, and G.O. Mendez, 1998, Chemistry and isotopic composition of ground water along a section near the Newmark area, San Bernardino County, California, U.S. Geological Survey Water Resources Investigation Report 97-4179

Matti, J. C. and D. M. Morton, 1993, Paleographic evolution of the San Andreas fault in southern California: A reconstruction based on a new cross-fault correlation, in R. E. Powell, R. J. Weldon, and J. C. Matti, editors, The San Andreas Fault System: displacement, Palinspastic Reconstruction, and Geologic Evolution, Geol. Soc. Am. Mem. 178, 107-159.

Matti, J. C., D. M. Morton, B. F. Cox, and K. J. Kendrick, Geologic map and digital database of the Redlands 7.5' Quadrangle, San Bernardino and Riverside Counties, Califonia, U.S. Geol. Surv. Open-File Report 03-30

Mooney, W. D., and J. H. Luetgert, 1982, A seismic refraction study of the Santa Clara Valley and southern Santa Cruz Mountains, west-central California, Bull. Seism. Soc. Am., 72, 901-909.

Morton, D.M., and J.C. Matti, 1993, Extension and contraction within an evolving divergent strike-slip fault complex: The San Andreas and San Jacinto fault zones at their convergence in southern California, in R.E. Powell, R.J. Weldon II, and J.C. Matti, editors., The San Andreas Fault System: Displacement, Palinspastic Reconstruction, and Geologic Evolution, Geol. Soc. Am. Mem. 178, 107-159

Morton, D.M., and F.K. Miller, 2003, Preliminary Geologic Map of the San Bernardino 30'x 60' Quadrangle, California., U. S. Geol. Surv. Open-File Report 03-293, 189 pp.

Schon, J. H., 1996, Physical Properties of Rocks: Fundamentals and Principals of Petrophysics, Handbook of Geophysical Exploration, Seismic Exploration , Volume 18, Elsevier Science, Inc., Tarrytown, New York

Sharp, R.V., 1972, Map showing recently active breaks along the San Jacinto fault zone between the San Bernardino area and Borrego Valley, California: U.S. Geol. Surv. Misc. Geol. Invest., Map I-675, scale 1:24,000, 3 sheets

Stephenson, W. J., J. K. Odum, R. A. Williams, and M. L. Anderson , 2002, Delineation of Faulting and Basin Geometry along a Seismic Reflection Transect in Urbanized San Bernardino Valley, California, Bull. Seismol. Soc. Am., 92, 2504-2520

Vernon, F.L., 1989, Analysis of Data Recorded on the ANZA Seismic Network, Doctor of Philosophy in Earth Sciences Thesis, University of California San Diego

Waldhauser, F., 2001, HypoDD – A program to compute double-difference hypocenter locations (hypoDD version 1.0 – 3/2001). U.S. Geol. Surv. Open-File Report 01-113

Wallace, R. E., 1990, General Features, *in* The San Andreas Fault System, California, R. E. Wallace, *editor*, pp. 3-14, U.S. Geol. Surv. Prof. Paper 1515, U. S. Government Printing Office, Washington, D.C., 283 pp.

Woolfenden, L. R., and D. Kadhim, 1997, Geohydrology and water chemistry in the Rialto-Colton basin, San Bernardino County, California: U.S. Geological Survey Water-Resources Investigations Report 97-4012, 101p.

Woodcock, N. H., and M. Fisher, 1986, Strike-slip duplexes, J. Structural Geol., 8, 725-735.

Yule, D. and K. Sieh, 2003, Complexities of the San Andreas fault near San Gorgonio Pass: Implications for large earthquakes, J. Geophys. Res. 108, 2548, doi:10.1029/2001JB000451.

Figures

Figure 1. Map of the San Bernardino area showing the locations of seismic profiles relative to known geologic structures, major roadways, and various cities. The profiles jointly acquired by the USGS and Caltrans are shown in red. The dashed gray line between the USGS/Caltrans profiles shows a seismic profile acquired by Stephenson et al., (2002). Yellow lines are seismic profiles acquired by the USGS (Catchings et al., in prep). The gray shaded areas refer to bedrock outcrops. Major known faults are shown by solid (mapped) and dotted (inferred below alluvium) lines. Geology from Morton and Miller (2003).

Figure 2. Part of the San Bernardino South, San Bernardino North, Harrison Mountain, and Redlands USGS 7.5-minute quadrangle maps, with the locations of the San Bernardino Low Resolution (SBR) and the San Bernardino High Resolution (SBHR) seismic profiles. Individual seismograph locations (dots) and shot point (SP #) locations are shown along the SBR profile. Because of the 5-m spacing of geophones along the SBHR profile, the general location of the SBHR profile is shown with dashed black lines.

Figure 3. Seismograph and shot geometry for the SBR seismic profile. (a) Elevation of seismographs as a function of distance along the profile. (b) Variation of seismographs from a linear array as a function of distance along the seismic profile. (c) Shot point elevation as a function of distance along the profile. (d) Variation of shot points from a linear array along the profile. All of the above measurements are in units of meters. (e) Fold as a function of distance along the profile for stacked images.

Figure 4. (a) Shot gather from shot point 1 (see figure 2 for geographic location) of the SBR profile. The horizontal axis shows the channel numbers. The vertical axis is time in milliseconds. Elevation along the SBR profile is shown above the shot gather. (b) Shot gather from shot point 2, plotted as in figure 4a. (c) Shot gather from shot point 3, plotted as in figure 4a. (d) Shot gather from shot point 4, plotted as in figure 4a. (e) Shot gather from shot point 5, plotted as in figure 4a. (f) Shot gather from shot point 6, plotted as in figure 4a. (g) Shot gather from shot point 7, plotted as in figure 4a. (h) Shot gather from shot point 8, plotted as in figure 4a. (i) Shot gather from shot point 9, plotted as in figure 4a. (j) Shot gather from shot point 10, plotted as in figure 4a. (k) Shot gather from shot point 11, plotted as in figure 4a. (l) Shot gather from shot point 12, plotted as in figure 4a. (m) Shot gather from shot point 13, plotted as in figure 4a. (n) Shot gather from shot point 14, plotted as in figure 4a. (o) Shot gather from shot point 15, plotted as in figure 4a.

Figure 5. (a) Seismic velocity model along the SBR seismic profile. Depth and distance are in meters. Velocities are in meters per second. Shot points and various cultural features are shown above the velocity model. (b) Ray density diagram showing the areas of the SBR velocity model with the number of ray paths in each 50-m by 50-m square. Depth and distance are in meters. The velocity model is constrained best in areas with the greatest number of ray paths.

Figure 6. Migrated seismic reflection image along the SBR seismic profile, plotted with 2:1 vertical exaggeration. Depth and distance are in meters. Fold, elevation, shot points, and various cultural features are shown above the seismic reflection image.

Figure 7. Seismic reflection image from figure 6, with the velocity image from figure 5a superimposed.

Figure 8 (a) Part of the USGS 7.5-minute San Bernardino South quadrangle map. The black line along the I-215 freeway shows the location of the SBHR seismic profile. The distance scale from the SBHR velocity and reflection images is shown, along with various cultural features. (b) Part of the USGS 7.5-minute San Bernardino North topographic map with the northward continuation of the SBHR profile (black line).

Figure 9. Geophone and shot geometry for the SBHR seismic profile. (a) Elevation of geophones as a function of distance along the profile. (b) Variation of geophones from a linear array as a function of distance along the seismic profile. (c) Shot point elevation as a function of distance along the profile. (d) Variation of shot points from a linear array along the profile. All of the above measurements are in units of meters. (e) Fold as a function of distance along the profile for stacked images.

Figure 10. (a) Shot gather from a shot point (1054) along the southern end of the SBHR profile. Shot points range from 1001 through approximately 2640 along the SBHR profile. The horizontal axis shows the channel numbers. The vertical axis is time in milliseconds. The elevation is shown above the shot gather, which has been top muted. (b) Shot gather from a shot point (1364) along the south-central part of the SBHR profile, plotted as in figure 10a. (c) Shot gather from a shot point (1503) along the central part of the SBHR profile, plotted as in figure 10a. (d) Shot gather from a shot point (2278) along the north-central part of the seismic profile, plotted as in figure 10a. (e) Shot gather from a shot point (2466) on the northern part of the seismic profile, plotted as in figure 10a.

Figure 11. (a) Seismic velocity model along the SBHR seismic profile. Depth and distance are in meters. Velocities are in meters per second. Shot points and various cultural features are shown above the velocity model. The velocity model is plotted with 10:1 vertical exaggeration. (b) Ray density diagram showing the areas of the SBHR velocity model with multiple ray paths in each 5-m by 5-m square. Depth and distance are in meters. The velocity model is constrained best in areas with the greatest number of ray paths.

Figure 12. (a) Seismic reflection image along the SBHR seismic profile, plotted with 2:1 vertical exaggeration. This image includes only the explosive sources. CDP spacing is every 2.5 meters along the profile. Every three traces have been laterally combined. The vertical axis is plotted in units of time (milliseconds), and the horizontal axis is plotted in units of meters. Fold (for all sources), elevation, shot points, and various cultural features are shown above the seismic reflection image. (b) Seismic reflection image from figure 12a. Spaces between every other reflector are highlighted in yellow. (c) Pre-stack Kirchoff-depth-migrated reflection image using only the explosive sources. (d) Seismic reflection depth image along the SBHR profile with both explosives and seisgun blasts included. Shot and geophone spacing is 5 m, CDP spacing is 2.5 m. Vertical exaggeration is 2:1. (d) Vertical exaggeration is 4:1. The vertical and horizontal axes are plotted in units of meters. Other features are plotted as in figure 12a.

Figure 13. (a) Bouger gravity profile along the SBR profile (data from Anderson et al., 1999). (b) Seismic reflection image from figure 6 with spaces between reflectors

highlighted in yellow. Seismic velocities (Fig. 5a) indicate that the deeper layered rocks are probably not sedimentary. Vertical exaggeration is 2:1.

Figure 14. Image from figure 13, with interpretative faults along the SBR seismic profile. Parts of at least four near-surface fault zones are interpreted along the SBR seismic profile. RCFZ, SJFZ, TFZ, and EHFZ refer to the Rialto Colton fault zone, the San Jacinto fault zone, the Tippecanoe (Loma Linda?) fault zone, and the East Highlands fault zone, respectively.

Figure 15. Seismic reflection image from figure 13 with double-difference-located earthquakes (red dots) within 3 km of the SBR seismic profile, recorded from 1984-2002 (Hauksson et al., 2003).

Figure 16. Same plot from figure 15, except earthquakes are within 1 km of the SBR seismic profile.

Figure 17 (a) The upper 500 m of the seismic reflection depth image along the SBHR profile from figure 12d, plotted with 2:1 vertical exaggeration. (b) Seismic reflection image from figure 12d, plotted with 4:1 vertical exaggeration. (c) Seismic reflection image from figure 12d with the velocity model from figure 11b superimposed. Projections of various water wells and logs near the seismic profile (from Izbicki et al., 1998) are shown in yellow. The 1500 m/s velocity contour is shown in red. (d) Seismic reflection image from figure 12d, with the velocity model from figure 11a superimposed, plotted with vertical exaggeration of 4:1.

Figure 18. (a) Gravity profile along the SBHR seismic profile (data from Anderson et al., 1999). (b) Seismic reflection image along the SBHR seismic profile, plotted as in figure 13b.

Figure 19. (a) Topographic profile along the SBHR seismic profile. (b) Velocity image along the SBHR profile with faults from figure 18b. (c) Migrated reflection image along the SBHR profile (from figure 12c). The purple box outlines the dimensions of the velocity model in figure 19b.

Figure 20. Seismic image from figure 18 with interpreted faults zones.

Figure 21. (a) Seismic reflection image from figure 20 with double-difference-located earthquakes (red dots) within 3 km of the SBHR seismic profile. (b) Seismic reflection image from figure 20 with double-difference located earthquakes (red squares) within 1 km of the SBHR seismic profile. Note the multiple near-vertical alignments of seismic events beneath the SBHR profile. Earthquake locations from Hauksson et al. (2003).

Figure 22. (a) Uninterpreted seismic reflection image from Stephenson et al. (2002) (see figure 1 for the location of the SBS seismic profile). (b) Low-fold reflection image along the SBR seismic profile. The magenta box outlines the approximate area of the SBS seismic profile shown in figure 22a. Note, however, that the SBS profile trended more northerly than our seismic profile. Comparison of the SBR and the SBS reflection images show similar structures in the shallow subsurface and in the deeper parts of the San Bernardino Basin.

Figure 23. Comparison of the (a) SBS velocity model of Stephenson et al. (2002) and (b) the SBR velocity model from this study. The white box in figure 23b outlines the approximate area of the SBS velocity model. The dashed white lines out the 2000 m/s (upper) and the 2800 m/s (lower) velocity contours show in the SBS velocity model.

Figure 24. Comparison of interpretations of the SBS and SBR reflection images. (a) Interpreted reflection image from a seismic reflection profile from Stephenson et al. (2002) (SBS seismic profile) located between the SBR and SBHR seismic profiles (see figure 1). (b) Un-interpreted reflection image from Stephenson et al. (2002) with interpretative faults from this study superimposed. (c) SBR seismic reflection image from this study with interpretative faults.

Figure 25. (a) Location map from figure 1 with double-difference-located earthquakes (red dots) recorded during the period 1984-2002 (Hauksson et al., 2003). Note the linear alignments of earthquakes, which correlate with interpreted faults along the SBR and SBHR seismic profiles. (b) Map and earthquakes from figure 25a with the interpretative trend of faults (dashed blue lines) based on seismicity trends. The interpretative trend of faults is associated with the deepest part of the San Bernardino pull-apart basin. Imaged faults at the SBR seismic profile crossing are shown in purple.

Figure 26. (a) Gravity map of the San Bernardino area (from Anderson et al., 1999) with double-difference-located earthquakes (red dots) recorded during the period 1984-2002 (Hauksson, et al., 2003). Note that the I-215 freeway trends obliquely to the highest gravity gradient. (b) Gravity map from figure 26a with interpretative trend of faults (cyan dotted lines) superimposed. Our interpretative trend of faults correlate with the high gravity gradients and the depression in basement rocks as inferred by the low gravity gradients.

Figure 27. (a) Map view of the theoretical orientation of faults that form a pull-apart basin (adapted from Woodcock and Fisher, 1986). The dashed red lines show the orientations of the SBR and SBHR seismic profiles relative to our interpretative trend of faults across the San Bernardino pull-apart basin (see fig. 25b). (b) Block diagram showing the theoretical 3-D geometry of faults that form a pull-apart basin (adapted from Woodcock and Fisher, 1986), with the orientation of the SBR and SBHR seismic profiles relative to our interpretative trend of faults that form the San Bernardino pull-apart basin. In cross section, these faults form a negative flower structure. (c) Line drawings (map view) from clay experiments with from 16 cm of displacement on strike-slip faults (from Hempton and Neher, 1986). The faults that formed at acute angles to the main strike-slip faults are similar those seen in Fig. 27a and inferred in fig. 25b, and are commonly know as Riedel shears. Such faults are expected in a pull-apart basin that develops between stepovers of two discontinuous parallel strike-slip faults. The dashed red lines show the orientation of the SBR and SBHR seismic profiles relative to a similar San Bernardino pull-apart basin. (d) Same diagram as in Figure 27c, except there has been 20 cm of displacement on the strike-slip faults. Note that the acute-angle, slip-transfer faults (Riedel shears) become dominant over high-angle shears (Riedel shears) with greater slip on the main strike-slip faults.

Figure 28. (a) Part of the San Bernardino South USGS 7.5-minute quadrangle map with double-difference-located earthquakes (red dots) recorded during the period 1984-2002 (Hauksson, et al, 2003). RCFZ, SJFZ, and TFZ refer to the Rialto-Colton, San Jacinto, and Tippecanoe fault zones. The stars show the approximate location of our interpretative faults where they cross the SBHR seismic profile. (b) Part of the San Bernardino North USGS 7.5-minute quadrangle map with earthquakes and interpretative faults plotted as in figure 28a.

Figure 29. (a) Cross section along the I-215 area (from Izbicki et al., 1998) based on groundwater and borehole data. The approximate location of the SBHR seismic profile is shown by the box. Interpretative faults are shown in red, wells are show in white, and well logs are shown in yellow. (b) Cross section from figure 29a with the SBR seismic image, interpretive faults splays (green), and revised interpretative basin structure from this study superimposed. Most of the splay faults (green) are likely near-surface splays associated with stepover faults between the San Jacinto and the San Andreas faults. The seismic profile crosses the stepover faults at low angles.

Appendix 1

Geometry for the SBR seismic profile. Distances are relative to the southwestern-most (first) shot point along the profile, and elevations are relative to topographically lowest shot point along the profile. Geo No. refers to seismograph number, Geo X refers to the distance of each seismograph from the first shot point, Geo Y refers to the lateral variation from a line connecting the first and last seismograph, Geo Z. refers to the elevation of each shot point relative to the first shot point. Shot No. refers to the shot point number, Shot X. refers to the distance of each shot point from the first shot point, Shot Y refers to the lateral variation of each shot point relative to a line connecting the first and last shot point, Shot Z. refers to the elevation of each shot point relative to the first shot point.

Geo No.	Geo X (m)	Geo Y Variation (m)	Geo Z (m)	Shot No.	Shot X (m)	Shot Y Variation (m)	Shot Z (m)
1	4.00	217.50	2.20	1	0.00	225.38	2.00
2	51.44	215.27	2.50	2	763.43	355.34	5.00
3	98.35	212.99	2.80	3	1777.61	171.81	6.71
4	151.76	215.77	3.00	4	2578.17	-141.94	7.71
5	201.92	216.03	3.14	5	3658.40	57.72	16.29
6	257.17	219.61	2.86	6	4098.74	-214.82	24.00
7	303.59	225.87	3.00	7	5240.80	280.93	29.14
8	345.73	226.96	3.00	8	6057.66	-213.61	32.14
9	398.74	230.65	3.00	9	7693.34	203.58	43.57
10	446.77	233.25	3.00	10	9708.08	-268.94	60.14
11	496.42	232.18	3.14	11	10728.21	-366.79	68.00
12	550.89	247.45	3.43	12	13797.03	-1021.63	99.14
13	591.96	263.37	4.14	13	14961.18	-541.28	106.00
14	636.91	285.36	4.14	14	16458.47	-124.99	129.00
15	682.66	305.53	4.71	15	19429.56	34.98	220.00
16	765.45	286.29	5.71				
17	818.87	224.60	6.00				
18	869.60	144.23	6.00				
19	908.47	105.63	5.71				
20	948.58	74.13	5.14				
21	985.03	41.02	4.86				
22	1032.48	49.91	5.43				
23	1084.50	60.82	5.71				
24	1134.36	64.22	6.57				
25	1184.44	72.09	7.86				
26	1233.61	79.56	8.57				
27	1282.77	87.02	9.29				
28	1332.45	95.80	9.43				
29	1382.53	103.67	8.43				
30	1432.21	112.45	8.14				
31	1479.76	123.58	7.43				
32	1531.38	135.40	6.43				
33	1577.69	139.42	5.14				
34	1628.69	147.70	4.57				
35	1676.64	157.91	4.43				

36	1720.72	162.04	4.43				
37	1777.61	171.81	4.43				
38	1833.21	191.95	5.00				
39	1897.55	179.87	6.57				
40	1960.29	144.14	7.14				
41	2001.31	113.05	7.57				
42	2042.05	85.10	8.00				
43	2124.35	37.23	9.00				
44	2167.34	19.03	9.29				
45	2212.25	-5.99	9.86				
46	2255.63	-30.03	10.36				
47	2299.01	-54.07	10.86				
48	2335.29	-44.64	11.14				
49	2396.28	-88.79	10.86				
50	2442.13	-103.55	10.14				
51	2490.21	-118.42	9.00				
52	2535.59	-151.97	7.71				
53	2601.30	-182.02	6.71				
54	2641.75	-169.65	5.57				
55	2694.32	-174.89	4.29				
56	2740.98	-191.48	3.43				
57	2788.15	-206.76	3.29				
58	2835.39	-229.64	4.00				
59	2851.17	-282.79	4.86				
60	2967.97	-339.50	6.00				
61	3031.68	-290.66	8.43				
62	3077.77	-226.63	10.71				
63	3126.82	-221.40	11.29				
64	3177.57	-227.44	12.00				
65	3224.43	-212.25	12.43				
66	3266.15	-182.93	12.43				
67	3301.78	-149.74	13.00				
68	3345.52	-125.00	13.86				
69	3388.45	-98.43	14.57				
70	3474.09	-49.75	15.29				
71	3516.40	-26.73	16.00				
72	3560.35	2.48	16.14				
73	3606.51	21.73	16.29				
74	3652.35	20.62	16.22				
75	3698.19	19.52	16.14				
76	3756.63	5.94	16.35				
77	3815.07	-7.64	16.57				
78	3858.70	-3.71	16.57				
79	3902.32	0.22	16.57				
80	3940.50	2.84	17.29				
81	3987.45	-16.90	17.71				
82	4058.49	-93.77	19.14				
83	4092.34	-116.01	20.57				
84	4160.11	-168.10	22.29				

85	4214.42	-137.61	21.14				
86	4263.51	-122.53	21.29				
87	4307.54	-100.93	21.71				
88	4351.09	-70.81	23.00				
89	4390.46	-43.61	23.71				
90	4435.11	-18.47	24.71				
91	4478.34	4.96	25.43				
92	4533.97	34.94	26.00				
93	4582.44	46.47	26.29				
94	4631.23	64.70	27.14				
95	4713.29	104.15	27.43				
96	4760.64	115.73	27.15				
97	4807.99	127.31	26.86				
98	4886.07	158.45	27.00				
99	4931.71	176.38	27.00				
100	4979.08	192.89	26.43				
101	5024.10	207.27	26.00				
102	5072.89	225.50	26.43				
103	5117.62	243.03	26.86				
104	5163.37	263.20	28.00				
105	5211.65	280.11	29.14				
106	5255.17	277.25	29.33				
107	5298.68	274.39	29.53				
108	5342.20	271.53	29.72				
109	5407.48	267.24	30.01				
110	5472.75	262.96	30.29				
111	5519.89	237.84	31.43				
112	5557.98	210.92	32.71				
113	5605.42	173.54	33.28				
114	5652.86	136.17	33.86				
115	5700.30	98.79	34.43				
116	5741.29	57.85	35.00				
117	5776.89	44.03	35.00				
118	5825.45	20.63	35.00				
119	5917.93	-20.57	34.43				
120	5964.69	-34.92	34.29				
121	6014.03	-70.00	33.71				
122	6058.03	-159.89	32.71				
123	6084.60	-202.82	32.14				
124	6133.84	-202.97	31.86				
125	6184.30	-205.87	32.14				
126	6236.07	-209.28	32.14				
127	6283.27	-214.70	32.43				
128	6332.70	-220.23	32.57				
129	6383.04	-225.36	32.71				
130	6478.16	-230.43	33.43				
131	6524.66	-231.79	33.71				
132	6574.56	-218.54	34.57				
133	6625.77	-205.80	35.14				

134	6673.51	-200.06	35.57				
135	6721.60	-177.76	36.00				
136	6756.78	-163.35	36.29				
137	6805.71	-133.04	36.71				
138	6853.70	-112.98	36.86				
139	6887.02	-72.06	37.29				
140	6932.08	-47.83	37.86				
141	6986.30	-46.88	38.29				
142	7029.52	-23.46	39.00				
143	7077.00	-4.72	39.86				
144	7126.06	0.51	40.43				
145	7176.65	9.70	41.29				
146	7227.64	17.97	41.57				
147	7276.52	28.58	41.86				
148	7370.55	65.66	42.86				
149	7415.90	86.74	42.86				
150	7463.37	105.48	42.86				
151	7509.64	126.97	42.86				
152	7555.06	140.44	43.14				
153	7599.90	160.20	43.14				
154	7646.38	186.15	43.43				
155	7693.34	203.58	43.57				
156	7740.01	224.15	44.43				
157	7785.47	247.46	44.57				
158	7831.62	266.71	45.14				
159	7876.97	287.80	46.00				
160	7970.71	328.02	48.00				
161	8016.17	351.34	49.00				
162	8064.67	372.71	49.14				
163	8108.19	392.99	49.71				
164	8137.06	406.81	50.00				
165	8182.64	367.89	50.14				
166	8226.20	269.06	48.86				
167	8289.93	124.48	48.43				
168	8332.38	30.64	48.14				
169	8379.55	-86.27	49.29				
170	8432.17	-210.61	49.71				
171	8483.01	-251.58	49.86				
172	8529.62	-250.71	50.00				
173	8576.55	-243.14	50.57				
174	8626.39	-249.59	50.71				
175	8675.04	-243.44	50.71				
176	8768.86	-275.30	50.86				
177	8818.77	-289.37	50.71				
178	8866.16	-300.17	50.29				
179	8914.86	-311.49	50.29				
180	8962.97	-316.51	50.71				
181	9016.68	-316.88	51.43				
182	9062.81	-307.48	51.57				

183	9111.68	-296.86	52.57				
184	9159.23	-285.74	53.71				
185	9210.93	-281.53	55.00				
186	9261.52	-272.34	55.57				
187	9311.31	-261.33	56.00				
188	9361.98	-259.76	56.57				
189	9411.84	-256.35	57.14				
190	9461.33	-242.19	57.29				
191	9512.00	-240.62	57.71				
192	9562.35	-245.75	58.71				
193	9611.24	-262.45	59.00				
194	9662.39	-269.41	59.29				
195	9713.76	-271.90	60.14				
196	9763.70	-276.11	60.86				
197	9813.43	-284.79	61.71				
198	9861.21	-296.51	62.00				
199	9911.85	-304.79	61.57				
200	9962.31	-307.69	62.14				
201	10012.44	-317.28	62.57				
202	10061.76	-325.05	63.00				
203	10113.72	-333.84	63.14				
204	10161.32	-340.18	63.57				
205	10212.47	-347.14	64.29				
206	10263.73	-351.86	65.00				
207	10313.67	-356.08	65.29				
208	10363.73	-358.06	65.86				
209	10414.69	-359.64	66.14				
210	10464.01	-367.40	66.86				
211	10515.49	-367.66	67.00				
212	10566.05	-368.32	67.14				
213	10617.13	-367.67	67.29				
214	10668.20	-367.01	67.71				
215	10719.53	-365.70	67.85				
216	10770.86	-364.38	68.00				
217	10821.53	-362.81	68.00				
218	10873.23	-358.60	68.43				
219	10921.77	-354.69	68.71				
220	10973.36	-352.71	68.86				
221	11021.90	-348.80	68.71				
222	11071.69	-337.78	68.43				
223	11121.63	-342.00	68.43				
224	11169.37	-336.26	68.29				
225	11221.66	-338.34	67.86				
226	11267.67	-331.17	67.57				
227	11316.95	-321.48	67.57				
228	11367.43	-314.52	67.57				
229	11416.71	-304.83	67.86				
230	11465.47	-296.45	68.14				
231	11515.36	-283.20	68.71				

232	11562.91	-272.07	69.43				
233	11614.93	-261.16	70.00				
234	11665.74	-247.51	70.71				
235	11713.81	-235.07	71.57				
236	11762.90	-219.99	72.57				
237	11814.22	-205.01	73.43				
238	11860.56	-191.14	73.86				
239	11908.84	-174.23	74.00				
240	11957.42	-160.47	74.57				
241	12007.82	-145.90	74.86				
242	12055.19	-129.40	75.14				
243	12102.15	-111.97	75.29				
244	12149.11	-94.55	75.43				
245	12195.27	-75.30	76.14				
246	12244.46	-57.99	77.14				
247	12291.53	-38.33	78.00				
248	12338.90	-21.82	79.00				
249	12385.97	-2.17	79.86				
250	12433.45	16.57	80.86				
251	12479.49	33.59	82.43				
252	12526.97	52.33	83.43				
253	12591.68	63.37	85.38				
254	12656.39	74.41	87.34				
255	12721.10	85.45	89.29				
256	12770.89	96.46	90.57				
257	12820.67	107.48	92.00				
258	12870.06	119.41	92.86				
259	12919.33	129.11	93.71				
260	12967.18	137.09	94.14				
261	13019.31	150.23	93.71				
262	13066.35	160.03	93.43				
263	13116.94	169.22	92.43				
264	13166.72	180.24	91.00				
265	13214.57	188.21	90.43				
266	13264.25	197.00	89.71				
267	13315.87	208.82	89.43				
268	13366.57	220.24	88.86				
269	13417.05	227.19	89.71				
270	13466.29	240.70	91.29				
271	13515.52	254.21	92.86				
272	13569.02	249.37	94.43				
273	13619.43	250.29	95.86				
274	13669.85	251.20	97.29				
275	13718.33	267.65	98.21				
276	13766.81	284.10	99.14				
277	13814.47	297.46	99.71				
278	13863.56	312.54	99.86				
279	13907.59	334.13	100.43				
280	13952.83	352.98	100.29				

281	14000.41	373.96	100.43				
282	14048.29	391.78	100.57				
283	14096.28	411.84	101.00				
284	14174.55	474.76	101.43				
285	14215.76	502.75	101.57				
286	14257.58	534.31	101.14				
287	14305.76	548.98	100.86				
288	14356.43	550.55	101.29				
289	14407.61	553.44	102.43				
290	14454.43	558.78	103.00				
291	14509.35	555.67	103.86				
292	14559.81	552.77	104.71				
293	14611.61	559.22	106.57				
294	14662.93	574.19	108.14				
295	14714.63	578.40	109.29				
296	14763.17	582.31	109.00				
297	14814.35	585.20	109.71				
298	14867.45	581.28	110.71				
299	14910.56	602.47	111.71				
300	14946.30	600.74	112.43				
301	14995.59	583.12	113.14				
302	15039.79	562.17	113.43				
303	15081.84	533.71	114.57				
304	15160.24	469.91	115.14				
305	15189.07	436.72	115.43				
306	15238.49	394.03	115.29				
307	15286.60	389.01	115.43				
308	15332.75	371.10	115.71				
309	15382.55	354.80	116.43				
310	15428.99	333.75	116.71				
311	15476.78	322.02	116.00				
312	15564.13	267.64	116.14				
313	15604.76	237.46	115.57				
314	15648.23	210.72	115.57				
315	15687.27	194.06	115.00				
316	15769.01	162.33	116.14				
317	15814.35	146.25	116.43				
318	15863.24	129.55	117.14				
319	15912.75	116.40	118.86				
320	15961.45	105.08	119.57				
321	16008.62	89.81	120.86				
322	16056.62	82.56	122.29				
323	16103.28	65.97	124.71				
324	16153.92	57.69	127.71				
325	16209.44	34.62	129.21				
326	16264.96	11.56	130.71				
327	16297.38	-76.88	133.43				
328	16335.59	-166.04	133.29				
329	16381.49	-262.74	131.86				

330	16427.64	-280.65	131.71				
331	16491.22	-308.36	131.71				
332	16542.69	-308.62	132.14				
333	16590.76	-296.18	132.86				
334	16638.63	-278.35	134.00				
335	16686.11	-259.61	135.71				
336	16734.90	-241.38	137.43				
337	16823.07	-195.96	139.29				
338	16871.86	-177.73	139.86				
339	16917.10	-158.88	139.86				
340	16956.99	-130.37	140.00				
341	17002.26	-101.68	139.14				
342	17049.74	-82.94	138.71				
343	17100.63	-76.90	139.00				
344	17150.49	-73.50	138.86				
345	17195.33	-53.73	139.43				
346	17241.00	-25.95	140.43				
347	17288.58	-4.98	141.29				
348	17332.00	13.07	141.71				
349	17379.69	36.27	142.71				
350	17469.79	84.73	145.71				
351	17516.14	98.60	146.86				
352	17564.34	123.13	148.00				
353	17612.03	146.34	149.14				
354	17657.67	164.27	150.86				
355	17701.30	186.78	151.57				
356	17746.65	207.86	152.43				
357	17793.13	233.81	152.29				
358	17837.05	253.17	153.14				
359	17882.81	273.34	154.00				
360	17926.39	248.84	154.57				
361	18013.78	204.30	155.71				
362	18059.71	181.93	157.86				
363	18103.80	158.74	159.71				
364	18149.84	138.60	161.57				
365	18197.19	117.95	163.57				
366	18241.29	94.76	166.00				
367	18286.49	66.60	168.43				
368	18329.60	87.79	171.86				
369	18375.17	113.34	173.57				
370	18433.54	42.90	179.14				
371	18494.44	-95.27	188.29				
372	18551.57	-172.82	193.57				
373	18600.28	-184.14	198.29				
374	18648.85	-170.37	201.86				
375	18695.41	-152.04	205.14				
376	18740.67	-160.50	208.29				
377	18788.04	-143.99	210.86				
378	18832.98	-122.00	213.14				

379	18880.05	-102.34	215.86				
380	18930.13	-94.47	216.14				
381	18978.06	-94.11	217.00				
382	19026.36	-104.52	217.57				
383	19075.63	-94.82	218.14				
384	19126.01	-90.10	219.00				
385	19177.67	-95.74	219.86				
386	19228.34	-94.17	220.00				
387	19277.51	-86.70	220.14				
388	19373.36	-85.98	226.43				
389	19424.06	-74.56	232.00				
390	19458.90	-104.01	238.43				
391	19478.07	-142.55	245.14				
392	19568.75	-174.71	258.57				
393	19606.01	-209.65	263.86				
394	19631.66	-252.98	265.71				
395	19687.88	-330.93	266.43				
396	19755.96	-413.48	264.00				
397	19815.46	-479.05	263.71				
398	19844.99	-516.31	263.57				
399	19885.47	-494.09	263.67				
400	19935.88	-479.52	264.40				
401	19982.38	-480.89	265.50				

Appendix 2

Geometry for the SBHR seismic profile. Distances are relative to the southern-most (first) geophone along the profile, and elevations are relative to topographically lowest geophone along the profile. Station No. refers to geophone number, Receiver Dist. refers to the distance of each geophone from the first geophone, Receiver Elev. refers to the elevation of each geophone relative to the first geophone. Shot No. refers to the shot point number, Shot X. refers to the distance of each shot point from the first geophone, Shot Z. refers to the elevation of each shot point relative to the geophone.

Station No.	Receiver Dist. (m)	Receiver Elev. (m)	Shot No.	Shot Dist. (m)	Shot Elev. (m)
1	0	1.3			
2	5.02	1.22	1001	5.19	1.01
3	9.7	1.16	1002	10.04	1.07
4	14.77	1.01	1003	14.84	0.75
5	19.63	0.79	1004	19.82	0.66
6	24.65	0.69	1005	24.75	0.58
7	29.59	0.63	1006	29.83	0.42
8	34.69	0.76	1007	34.94	0.38
9	39.36	0.91	1008	39.47	0.65
10	44.47	0.69	1009	44.74	0.37
11	49.34	0.65	1010	49.43	0.41
12	53.87	0.66	1011	54.09	0.58
13	59.14	0.77	1012	59.29	0.73
14	64.26	0.94	1013	64.12	0.7
15	68.82	1.12	1014	68.93	0.91
16	73.94	1.24	1015	74.07	0.98
17	78.98	1.19			
18	83.94	1.15	1016	84.1	0.97
19	88.52	1.11	1017	88.77	0.96
20	93.8	1.09	1018	93.51	0.89
21	98.22	1.2	1019	98.84	1.11
22	103.03	1.19	1020	103.66	1.06
23	108.65	0.92	1021	108.64	0.97
24	113.39	0.92	1022	113.62	0.87
25	118.62	0.98	1023	118.78	0.95
26	123.33	1.03	1024	123.55	1.31
27	128.46	1.17	1025	128.54	0.86
28	133.48	1.07	1026	133.68	0.9
29	138.34	1.1	1027	138.52	1.01
30	143.28	1.1			
31	148.99	1.1	1028	148.54	0.89
32	153.84	1.19	1029	153.87	1.01
33	157.96	1.64	1030	157.7	1.41
34	163.58	1.09	1031	163.77	1.21
35	168.71	0.94	1032	168.63	1.15
36	173.73	0.75	1033	173.7	1.03
37	178.8	0.84	1034	178.65	0.96
38	184.2	0.92	1035	184.03	1.19
39	189.09	0.92	1036	189.25	1.07

40	193.95	1.1	1037	193.78	0.94
41	199.06	0.87	1038	199.06	1.05
42	203.16	0.89	1039	203.34	0.99
43	208.5	0.8	1040	208.49	0.99
44	213.36	0.69	1041	213.35	0.99
45	218.73	0.63	1042	218.57	0.86
46	223.61	0.67	1043	223.51	0.79
47	228.35	0.68	1044	228.29	0.75
48	233.5	0.64	1045	233.48	0.73
49	238.41	0.5	1046	238.47	0.54
50	243.38	0.56	1047	243.5	0.66
51	248.42	0.57	1048	248.46	0.72
52	253.13	0.44	1049	253.16	0.34
53	258.16	0.56	1050	258.4	0.56
54	263.29	0.6	1051	263.28	0.55
55	268.02	0.54	1052	268.45	0.55
56	273.2	0.69	1053	273.19	0.64
57	278.14	0.68	1054	278.23	0.68
58	283.09	0.73	1055	283.24	0.73
59	288.1	0.74	1056	288.29	0.76
60	292.85	0.88	1057	293.14	0.83
61	298.09	0.79	1058	298.24	0.75
62	302.86	0.7	1059	302.97	0.75
63	308	0.77	1060	308.11	0.78
64	313.05	0.93	1061	312.94	0.94
65	317.74	0.8	1062	315.56	0.9
66	322.8	0.86	1063	323.06	0.92
67	327.9	1.03	1064	328.02	1.01
68	332.9	1.06	1065	333.06	1.05
69	337.75	1.01	1066	337.94	1.05
70	342.95	1.09	1067	342.96	1.03
71	346.87	0.88	1068	347.91	0.92
72	352.36	1.05	1069	352.39	1.04
73	357.75	1.01	1070	357.99	1.08
74	364.05	0.97	1071	363.95	0.99
75	367.54	0.99	1072	367.86	1.01
76	373.04	1.02	1073	373.13	0.99
77	378.1	1	1074	378.05	0.98
78	382.32	0.92	1075	382.67	1.08
79	387.59	1.15	1076	387.42	1.3
80	392.63	1.19	1077	392.54	1.08
81	397.9	1.03	1078	397.81	1.07
82	402.41	1.02	1079	402.82	1.05
83	407.59	0.97	1080	407.35	0.94
84	412.11	0.97	1081	412.26	0.97
85	416.74	1.02	1082	416.93	0.98
86	422.2	1.06	1083	422.14	1.01
87	427.36	0.98	1084	427.18	0.99
88	431.49	1.01	1085	431.68	1.06

89	436.9	1.1	1086	436.99	1.14
90	442.02	1.13	1087	442.18	1.13
91	446.78	1.14	1088	447.11	1.1
92	451.54	1.21	1089	451.91	1.18
93	456.59	1.27	1090	456.82	1.21
94	461.66	1.21	1091	461.75	1.14
95	466.54	1.05	1092	466.76	1.01
96	471.46	1.04	1093	471.78	1.06
97	476.55	0.8	1094	476.6	0.99
98	481.65	0.9	1095	481.6	0.92
99	487.61	0.87	1096	487.77	0.89
100	491.32	0.87	1097	491.54	0.9
101	496.31	0.89	1098	496.63	0.95
102	501.23	0.84	1099	501.48	0.79
103	505.83	0.75	1100	506.08	0.65
104	511	0.43	1101	510.94	0.38
105	516	0.35	1102	515.41	0.31
106	521.42	0.28	1103	521.5	0.18
107	526.02	0.25	1104	526.09	0.35
108	531.07	0.35	1105	531.01	0.4
109	535.76	0.37	1106	535.81	0.36
110	540.91	0.55	1107	540.85	0.42
111	546.09	0.51	1108	546.11	0.44
112	550.84	0.29	1109	550.83	0.26
113	556.2	0.09	1110	556.25	0.1
114	560.69	0.16	1111	560.78	0.2
115	565.23	0.19	1112	565.34	0.24
116	570.2	0.18	1113	570.33	0.2
117	575.15	0.08	1114	575.23	0.14
118	580.05	0.05	1115	580.17	0.15
119	584.99	0.09	1116	585.15	0.14
120	590.03	0	1117	590.08	0.04
121	594.88	0.25	1118	595.03	0.16
122	600	0.11	1119	600.02	0.18
123	604.8	0.15	1120	604.84	0.19
124	609.74	0.24	1121	609.89	0.22
125	615.32	0.62	1122	615.47	0.57
126	620.01	1.31	1123	620.28	1.51
127	625.01	2.04	1124	625.49	1.99
128	630.31	2.03	1125	630.44	2.02
129	635.12	2.18	1126	635.29	2.11
130	640.05	2.19	1127	640.31	2.08
131	645.19	2.24	1128	645.24	2.23
132	650.26	2.25	1129	650.25	2.22
133	655.18	2.42	1130	655.28	2.25
134	660.2	2.31	1131	660.35	2.24
135	665.18	2.39	1132	665.27	2.37
136	670.22	2.37	1133	670.32	2.28
137	675.19	2.44	1134	675.3	2.48

138	679.66	2.37	1135	680.09	2.41
139	684.97	2.38	1136	684.87	2.38
140	690.43	2.17	1137	689.76	2.37
141	694.49	2.24	1138	694.73	2.38
142	699.9	2.3	1139	699.85	2.44
143	704.37	2.39	1140	704.79	2.41
144	709.8	2.46	1141	709.74	2.53
145	715.38	2.32	1142	715.25	2.36
146	719.51	2.53	1143	719.8	2.51
147	724.67	2.59	1144	724.58	2.63
148	730.2	2.58	1145	729.87	2.75
149	735.35	2.74	1146	735.48	2.81
150	739.9	2.85	1147	739.63	2.93
151	744.86	2.74	1148	744.68	2.8
152	750.1	2.83	1149	749.72	2.89
153	754.91	2.78	1150	754.87	2.9
154	759.63	2.83	1151	759.64	2.88
155	764.7	2.84	1152	764.7	2.89
156	769.9	2.76	1153	769.64	2.82
157	774.45	2.97	1154	774.57	2.9
158	779.64	3.02	1155	779.71	3.02
159	785.24	3.03	1156	784.66	3
160	790.36	3.05	1157	789.87	2.99
161	794.87	3.01	1158	794.96	3.07
162	799.57	2.96	1159	799.57	2.92
163	804.79	2.92	1160	804.88	2.86
164	809.63	2.84	1161	809.69	2.79
165	814.6	2.75	1162	814.55	2.72
166	819.65	2.67	1163	819.62	2.7
167	825.25	2.68	1164	825.52	2.74
168	829.63	2.58	1165	829.63	2.44
169	832.57	2.21	1166	832.61	2.18
170	839.77	1.47	1167	839.5	1.58
171	844.43	1.35	1168	844.17	1.49
172	849.74	1.23	1169	849.52	1.38
173	853.21	1.98	1170	853.1	2.13
174	857.99	2.2	1171	857.77	2.48
175	863.31	2.53	1172	863.03	2.92
176	868.3	3.06	1173	868.29	3.19
183	902.12	3.51	1174	902.06	3.5
184	907.11	3.7	1175	906.84	3.45
185	911.93	3.35	1176	911.63	3.25
186	916.61	3.4	1177	916.38	3.16
187	921.36	3.14	1178	921.13	3.1
188	925.99	3.15	1179	925.83	3.11
189	931.4	3.17	1180	930.91	3.15
190	935.64	3.15	1181	935.53	3.16
191	940.67	3.1	1182	940.2	3.13
192	945.47	3.16	1183	945.09	3.23

193	949.42	3.07	1184	949.82	3.16
194	954.77	3.23	1185	954.5	3.23
195	959.75	3.15	1186	959.36	3.26
196	964.16	3.18	1187	963.98	3.24
197	968.94	3.19	1188	968.82	3.21
198	973.83	3.36	1189	973.6	3.26
199	978.87	3.29			
200	983.27	3.16	1190	982.94	3.24
201	987.95	3.25	1191	988.06	3.16
202	992.79	3.33	1192	992.45	3.37
203	997.29	3.27	1193	996.92	3.28
204	1001.97	3.37	1194	1001.77	3.33
205	1007.06	3.48	1195	1006.65	3.47
206	1011.61	3.56	1196	1011.34	3.49
207	1016.44	3.55	1197	1016.22	3.6
208	1021.13	3.69	1198	1020.76	3.7
209	1025.89	3.73	1199	1025.64	3.67
210	1030.65	3.86	1200	1030.25	3.82
211	1035.62	4.04	1201	1035.24	3.95
212	1040.25	4.15	1202	1039.78	4.01
213	1044.73	4.23	1203	1044.44	4.02
214	1049.33	4.38	1204	1048.95	4.22
215	1053.78	4.11	1205	1053.59	4
216	1058.31	4.15	1206	1058.15	3.99
217	1063.02	4.27	1207	1062.85	4.1
218	1067.49	4.34	1208	1067.28	4.16
219	1072.13	4.46	1209	1071.85	4.27
220	1077.74	4.75	1210	1076.63	4.54
221	1081.4	4.94	1211	1081.25	4.84
222	1086.11	5	1212	1085.85	4.89
223	1090.86	4.94	1213	1090.39	4.82
224	1095.7	4.93	1214	1095.16	4.85
225	1100.01	4.97	1215	1099.76	4.8
226	1104.51	4.83	1216	1104.48	4.84
227	1109.72	4.84	1217	1109.32	4.89
228	1113.87	4.95	1218	1113.38	4.79
229	1118.34	4.88	1219	1118.01	4.87
230	1122.73	4.7	1220	1122.3	4.71
231	1127.12	4.7	1221	1126.97	4.66
232	1131.85	4.67	1222	1131.59	4.69
233	1136.36	4.64	1223	1136.22	4.63
234	1140.83	4.6	1224	1140.72	4.57
235	1145.9	4.46	1225	1145.49	4.66
236	1150.48	4.5	1226	1150.08	4.47
237	1154.69	4.42	1227	1154.42	4.42
238	1159.22	4.5	1228	1158.72	4.43
239	1163.16	4.4	1229	1163.08	4.35
240	1168.29	4.51	1230	1168.01	4.37
241	1172.47	4.35	1231	1172.17	4.35

242	1177.67	4.74	1232	1177.14	4.44
243	1181.82	4.72			
244	1185.97	4.7			
245	1190.8	4.66			
246	1195.62	4.62			
247	1200.45	4.58			
248	1205.27	4.54			
249	1210.1	4.5			
250	1214.92	4.47			
251	1219.75	4.43			
252	1224.57	4.39			
253	1229.4	4.35			
254	1234.22	4.31			
255	1239.05	4.27			
256	1243.48	4.03	1233	1243.37	4.25
257	1248.21	3.69	1234	1247.97	3.92
258	1253.43	3.16	1235	1252.43	3.74
259	1257.83	2.38	1236	1257.55	2.74
260	1262.8	2.34	1237	1262.65	2.6
261	1267.94	2.25	1238	1267.74	2.34
262	1273.75	2.2	1239	1273.41	2.24
263	1277.58	2.25	1240	1277.34	2.24
264	1282.26	2.24	1241	1282.68	2.32
265	1287.41	2.35	1242	1287.05	2.38
266	1292.02	2.58	1243	1291.73	2.34
267	1296.06	2.39	1244	1295.73	2.53
268	1300.86	2.46	1245	1300.46	2.44
269	1305.01	2.42	1246	1304.52	2.44
270	1309.42	2.52	1247	1308.41	2.51
271	1313.88	2.5	1248	1313.34	2.5
272	1318.31	2.52	1249	1317.93	2.49
273	1322.71	2.57	1250	1322.28	2.55
274	1327.02	2.57	1251	1326.72	2.57
275	1331.64	2.6	1252	1331.13	2.56
276	1335.74	2.52			
277	1340.02	2.5	1253	1339.81	2.47
278	1344.55	2.43	1254	1344.3	2.4
279	1349.09	2.39	1255	1348.69	2.36
280	1353.22	2.41			
281	1357.34	2.86	1256	1357.3	2.86
282	1362.14	3.63	1257	1362	3.61
283	1366.74	3.52			
284	1371.35	3.42			
285	1375.95	3.31			
286	1380.56	3.2			
287	1385.16	3.09			
288	1389.76	2.99			
289	1394.37	2.88			
290	1398.97	2.77			

291	1403.58	2.67			
292	1408.18	2.56	1258	1407.94	2.51
293	1412.28	2.39	1259	1412.2	2.26
294	1417.2	2.34	1260	1416.9	2.35
295	1421.15	2.43	1261	1421	2.4
296	1426.14	2.54	1262	1425.73	2.49
297	1430.92	2.58	1263	1430.67	2.57
298	1434.47	2.58	1264	1434.21	2.65
299	1439.4	2.72	1265	1439.02	2.66
300	1443.64	2.6	1266	1443.56	2.63
301	1448.4	2.72	1267	1448.18	2.67
302	1453.03	2.81	1268	1452.57	2.72
303	1457.23	2.78	1269	1457.3	2.75
304	1461.8	2.95	1270	1461.63	2.89
305	1466.42	3.01	1271	1466.28	2.84
306	1470.78	2.83			
307	1475.74	3.01	1272	1475.48	2.96
308	1480.13	3.06	1273	1479.76	2.98
309	1484.44	2.93	1274	1484.24	2.9
310	1490.21	2.96	1275	1489.64	2.78
311	1495.39	2.96	1276	1494.77	2.9
312	1499.68	2.93	1277	1499.25	2.89
313	1507.26	2.78	1278	1506.9	2.74
314	1512.49	2.77	1279	1511.94	2.64
315	1517.52	2.77			
316	1523.14	3.02	1280	1522.71	2.94
317	1528.15	2.93	1281	1527.64	2.85
318	1533.55	2.91	1282	1532.99	2.86
319	1538.75	2.93	1283	1538.13	2.89
320	1542.78	3.12	1284	1542.5	3.12
321	1547.28	3.14	1285	1547.18	3.02
322	1551.48	3.16	1286	1551.56	3.15
323	1556.77	3.12	1287	1556.12	3.07
324	1562.6	3.21	1288	1562.13	3.11
325	1567.52	3.21	1289	1567.14	3.17
326	1572.47	3.19			
327	1579.44	3.17	1290	1579.16	3.12
328	1583.76	3.12	1291	1583.54	3.13
329	1588.11	3.12	1292	1587.78	3.12
330	1592.8	3.35	1293	1592.46	3.25
331	1597.48	3.59	1294	1596.73	3.34
332	1601.91	3.43	1295	1601.54	3.33
333	1607.67	3.46	1296	1607.49	3.47
334	1615.4	3.59	1297	1614.99	3.55
335	1619.84	3.34	1298	1619.39	3.51
336	1625.21	3.39	1299	1624.96	3.54
337	1629.55	3.45			
338	1633.29	3.45	1300	1632.86	3.63
339	1637.55	3.59	1301	1637.46	3.8

340	1642.23	3.65	1302	1642.01	3.81
341	1647.17	3.78			
342	1651.67	3.64	1303	1651.34	3.94
343	1656.2	3.55	1304	1655.86	3.99
344	1660.88	3.81	1305	1660.55	4.11
345	1664.71	3.8	1306	1664.45	4.16
346	1669.97	3.84	1307	1669.61	4.28
347	1673.63	4.27	1308	1673.7	4.44
348	1678.9	4.31	1309	1678.72	4.47
349	1684.09	4.44	1310	1683.63	4.51
350	1687.6	4.29			
351	1692.85	4.35	1311	1692.36	4.72
352	1698.52	4.54	1312	1698.1	4.7
353	1702.48	4.53	1313	1702.5	4.66
354	1704.83	5.38	1314	1704.51	5.45
355	1708.93	5.54	1315	1708.69	5.54
356	1713.58	5.7	1316	1713.34	5.69
357	1718.21	5.82	1317	1717.81	5.79
358	1722.39	5.94	1318	1722.15	5.94
359	1727.27	6.07	1319	1726.81	6.08
360	1731.78	6.46	1320	1731.31	6.44
361	1736.35	6.41	1321	1735.73	6.48
362	1740.66	6.44	1322	1740.02	6.49
363	1745.37	6.55	1323	1744.71	6.52
364	1749.87	6.63	1324	1749.26	6.61
365	1754.26	6.67	1325	1753.55	6.64
366	1758.58	6.73	1326	1758.16	6.8
367	1763.14	6.87	1327	1762.67	6.85
368	1767.72	6.95	1328	1767.23	6.91
369	1772.41	7.05	1329	1771.68	7
370	1776.4	7.06	1330	1776.27	7.08
371	1781.25	7.3	1331	1780.74	7.23
372	1785.38	7.31	1332	1785.24	7.31
373	1790.11	7.43	1333	1789.73	7.41
374	1795.78	7.18			
375	1801.46	6.93			
376	1804.72	7.01	1334	1803.82	6.88
377	1808.35	7.06	1335	1807.66	6.9
378	1813.18	7.12	1336	1812.13	6.91
379	1816.8	7.21	1337	1816.23	7.02
380	1821.62	7.24	1338	1821.28	7.25
381	1826.23	7.37	1339	1825.75	7.28
382	1830.45	7.47	1340	1829.9	7.46
383	1835.16	7.62	1341	1834.58	7.48
384	1840.3	7.82	1342	1839.61	7.46
385	1844.82	7.95	1343	1844.26	7.62
386	1848.92	8.2	1344	1848.34	7.75
387	1853.63	8.44	1345	1853.05	8.05
388	1858.09	8.46	1346	1857.6	8.12

389	1862.61	8.58	1347	1861.82	8.13
390	1865.87	8.24			
391	1871.32	7.79			
392	1875.99	7.84			
393	1880.89	7.88			
394	1884.87	7.97			
395	1889.45	8.05			
396	1894.14	8.14			
397	1898.58	9.87			
398	1903.01	11.6			
399	1907.45	13.33			
400	1911.88	15.06	1348	1911.5	15.04
401	1916.59	15.09	1349	1916.41	15.11
402	1921.63	15.2	1350	1921.3	15.2
403	1926.21	15.23	1351	1925.98	15.21
404	1931.14	15.18	1352	1930.85	15.18
405	1935.96	15.18	1353	1935.75	15.19
406	1940.69	15.2	1354	1940.46	15.21
407	1945.4	15.23	1355	1945.28	15.22
408	1950.22	15.24	1356	1950.06	15.25
409	1955.15	15.26	1357	1954.97	15.24
410	1960.02	15.24	1358	1959.92	15.22
411	1965.82	15.16	1359	1965.74	15.18
412	1969.46	15.18	1360	1969.32	15.2
413	1974.22	15.25	1361	1974.06	15.24
414	1978.8	15.17	1362	1978.77	15.2
415	1983.72	15.2	1363	1983.68	15.13
416	1987.98	15.14	1364	1987.74	15.19
417	1993.5	15.06	1365	1993.19	15.01
418	1998.26	15.06	1366	1998.02	15.01
419	2002.72	15	1367	2002.58	15
420	2007.69	15.01	1368	2007.47	15.03
421	2012.89	14.96	1369	2012.96	14.95
422	2017.5	14.94	1370	2017.36	14.96
423	2022.36	14.93	1371	2022.21	14.9
424	2026.41	14.88	1372	2026.59	14.98
425	2032.24	15.02	1373	2032.15	15.01
426	2036.86	15.03	1374	2036.79	14.98
427	2041.84	14.88	1375	2041.8	14.92
428	2046.72	14.93	1376	2046.81	14.94
429	2051.78	14.85	1377	2051.26	14.8
430	2057.02	14.83			
431	2062.08	14.95	1378	2060.98	14.96
432	2065.27	14.93	1379	2064.83	14.92
433	2069.91	15.04	1380	2069.69	15.01
434	2073.78	15	1381	2073.57	14.94
435	2081.2	14.98	1382	2081.16	14.98
436	2086.34	14.94	1383	2086.25	14.93
437	2090.92	14.88	1384	2090.96	14.9

438	2096.9	14.87	1385	2096.65	14.93
439	2101.11	14.94	1386	2101.08	14.92
440	2106.25	14.88	1387	2106.26	14.88
441	2111.2	14.94	1388	2111.09	14.95
442	2115.8	14.92	1389	2115.93	14.91
443	2120.88	14.91	1390	2120.84	14.87
444	2126.12	14.89	1391	2125.82	14.86
445	2131.56	14.82	1392	2131.42	14.82
446	2135.92	14.78	1393	2136.05	14.81
447	2140.62	14.68	1394	2140.76	14.73
448	2145.59	14.79	1395	2143.24	14.62
449	2150.79	14.83	1396	2150.67	14.8
450	2155.5	14.83	1397	2155.55	14.77
451	2160.4	14.77			
452	2165.16	14.57	1398	2165.68	14.58
453	2170.78	14.51	1399	2170.52	14.58
454	2175.57	14.66	1400	2175.52	14.69
455	2180.87	14.77	1401	2180.88	14.79
456	2185.48	14.81	1402	2185.7	14.88
457	2190.95	14.87	1403	2190.81	14.85
458	2195.85	14.88	1404	2195.8	14.89
459	2200.59	14.88	1405	2200.61	14.83
460	2205.75	14.82	1406	2205.72	14.76
461	2210.21	14.76	1407	2210.61	14.73
462	2215.49	14.6			
463	2220.74	14.57	1408	2220.68	14.55
464	2225.54	14.56	1409	2225.51	14.53
465	2230.73	14.51	1410	2230.7	14.46
466	2235.55	14.44	1411	2235.62	14.41
467	2240.54	14.25	1412	2240.6	14.26
468	2245.55	14.16	1413	2245.44	14.16
469	2250.54	13.94	1414	2250.64	13.99
470	2255.39	13.75			
471	2260.06	13.67	1415	2260.26	13.67
472	2265.67	13.62	1416	2265.93	13.69
473	2270.59	13.71	1417	2270.37	13.81
474	2275.36	13.59	1418	2275.42	13.76
475	2280.05	13.74	1419	2280.32	13.81
476	2285.14	14.03	1420	2285.27	14
477	2290.74	14.02	1421	2291.42	14.16
478	2297.91	14.21			
479	2300.23	14.2	1422	2300.2	14.25
480	2305.2	14.24	1423	2305.2	14.26
481	2310.29	14.38	1424	2310.37	14.44
482	2315.67	14.41	1425	2315.59	14.53
483	2319.88	14.49	1426	2319.84	14.51
484	2325.33	14.57			
485	2330.25	14.86	1427	2330.2	14.75
486	2335.37	14.78	1428	2335.42	14.74

487	2340.16	14.78	1429	2340.12	14.76
488	2344.85	14.7	1430	2345.18	14.77
489	2349.79	14.8	1431	2349.73	14.8
490	2354.77	14.94	1432	2354.78	14.94
491	2359.56	15.03	1433	2359.65	15.07
492	2364.77	15.15	1434	2364.72	15.15
493	2369.66	15.28	1435	2369.67	15.28
494	2374.39	15.36	1436	2374.59	15.33
495	2379.48	15.28	1437	2379.54	15.31
496	2382.95	15.08			
497	2389.16	14.84	1438	2389.29	14.93
498	2394.22	14.84	1439	2394.1	14.98
499	2399.17	14.97			
500	2404.16	15.34	1440	2404.17	15.37
501	2409.04	15.26	1441	2409.01	15.29
502	2414.02	15.15	1442	2413.99	15.2
503	2419	15.15	1443	2418.94	15.15
504	2423.66	15.13	1444	2423.75	15.12
505	2428.8	15.1	1445	2428.88	15.1
506	2433.65	15.07	1446	2433.76	15.12
507	2438.72	15.12	1447	2438.74	15.09
508	2443.62	15.24	1448	2443.7	15.25
509	2448.69	15.11	1449	2448.6	15.08
510	2453.9	15.3	1450	2453.79	15.3
511	2458.53	15.27	1451	2458.44	15.21
512	2463.29	15.31	1452	2463.23	15.28
513	2468.35	15.28	1453	2468.37	15.29
514	2473.17	15.25	1454	2473.25	15.28
515	2478.02	15.2	1455	2478.17	15.23
516	2482.84	15.26	1456	2483.29	15.19
517	2488.09	15.04			
518	2495.03	15.34			
519	2501.98	15.64	1457	2501.91	15.61
520	2506.84	15.51	1458	2506.88	15.52
521	2511.43	15.44	1459	2511.16	15.47
522	2516.56	15.48	1460	2516.55	15.53
523	2521.46	15.68	1461	2521.4	15.67
524	2526.36	15.81	1462	2526.54	15.84
525	2531.56	15.82	1463	2531.5	15.85
526	2536.45	15.8	1464	2536.47	15.81
527	2540.82	15.82	1465	2540.9	15.89
528	2546.4	15.83	1466	2546.42	15.86
529	2551.31	15.85	1467	2551.31	15.87
530	2556.21	15.84	1468	2556.27	15.88
531	2561.32	15.88	1469	2561.42	15.91
532	2566.41	15.88	1470	2566.39	15.95
533	2571.19	15.96	1471	2571.19	15.99
534	2576.12	15.94	1472	2576.09	15.96
535	2580.27	15.96	1473	2580.37	15.99

536	2586.03	15.88			
537	2591.27	15.79	1474	2590.97	15.79
538	2595.92	15.7	1475	2595.95	15.71
539	2600.72	15.66	1476	2600.74	15.67
540	2605.55	15.66	1477	2605.74	15.67
541	2610.74	15.62	1478	2610.94	15.66
542	2615.76	15.58	1479	2615.81	15.61
543	2620.23	15.54			
544	2626.2	15.51			
545	2632.18	15.49			
546	2638.15	15.46			
547	2644.13	15.44			
548	2650.1	15.41	1480	2649.68	15.49
549	2654.49	15.62	1481	2654.51	15.78
550	2658.68	15.8			
551	2664.21	15.61			
552	2669.03	15.72	1482	2668.73	15.78
553	2674.72	15.91	1483	2674.34	15.95
554	2678.72	15.86	1484	2678.68	15.92
555	2683.99	15.88	1485	2683.69	15.93
556	2688.43	15.88	1486	2688.44	15.9
557	2693.87	15.69			
558	2699.56	15.9	1487	2699.55	15.9
559	2703.28	15.66	1488	2703.57	15.69
560	2708.16	15.77	1489	2708.57	15.88
561	2713.17	15.75	1490	2713.27	15.74
562	2718.43	15.75	1491	2718.54	15.73
563	2723.89	15.74	1492	2723.72	15.82
564	2728.75	15.88	1493	2728.72	15.92
565	2733.32	15.76	1494	2733.55	15.73
566	2737.35	15.66	1495	2737.96	15.72
567	2742.9	15.57	1496	2743.64	15.58
568	2747.49	15.21	1497	2748.23	15.22
569	2752.77	15.5	1498	2753.15	15.54
570	2757.57	15.65	1499	2757.95	15.77
571	2762.72	16.07	1500	2762.56	15.94
572	2768.05	16.4	1501	2768.03	16.41
573	2772.58	16.75	1502	2772.84	16.72
574	2777.91	17.33	1503	2778.09	17.29
575	2782.77	17.88	1504	2782.64	17.58
576	2787.55	18.31	1505	2787.78	18.32
577	2792.73	18.09			
578	2797.91	17.87			
579	2803.09	17.65			
580	2808.13	16.46	1506	2808.06	17.14
581	2812.37	16.19	1507	2812.13	16.24
582	2817.53	15.64	1508	2817.77	15.67
583	2822.66	15.58	1509	2822.61	15.7
584	2827.53	15.6	1510	2827.55	15.66

585	2832.43	15.53	1511	2832.42	15.52
586	2837.53	15.53	1512	2837.72	15.59
587	2842.68	15.66	1513	2842.41	15.62
588	2847.89	15.65	1514	2847.84	15.72
589	2852.63	15.75	1515	2852.56	15.81
590	2856.18	15.86	1516	2855.88	15.87
591	2862.1	15.84	1517	2862.24	15.82
592	2867.46	15.84	1518	2867.36	15.86
593	2872.46	15.93	1519	2872.26	15.96
594	2877.36	15.98	1520	2877.47	16.14
595	2882.85	16.07	1521	2882.21	16.06
596	2887.17	16.12	1522	2886.81	16.14
597	2892.4	16.18	1523	2892.21	16.2
598	2896.18	16.16	1524	2896.66	16.14
599	2901.88	16.12	1525	2902.15	16.06
600	2907.15	16.28	1526	2907.14	16.33
601	2912.14	16.41	1527	2912.15	16.43
602	2916.92	16.48			
603	2921.92	16.57	1528	2922.07	16.59
604	2926.87	16.77	1529	2926.93	16.78
605	2931.71	16.97	1530	2932.06	16.97
606	2938.59	17.24	1531	2938.84	17.28
607	2942.35	17.44	1532	2941.98	17.56
608	2947.55	17.64	1533	2947.14	17.75
609	2952.21	17.41	1534	2951.93	17.52
610	2956.68	16.32	1535	2956.76	16.55
611	2961.42	16.09	1536	2961.8	16.27
612	2966.4	15.99	1537	2967.15	16.33
613	2972.12	16.02	1538	2972.12	16.34
614	2978.05	15.96	1539	2977.61	16.03
615	2982.15	16.25	1540	2982.03	16.41
616	2986.31	16.31	1541	2986.57	16.48
617	2991.32	16.64	1542	2991.79	16.76
618	2996.72	16.97	1543	2996.65	17.16
619	2999.63	17.1	1544	2999.41	17.19
620	3006.09	16.19			
621	3011.81	16.36			
622	3017.53	16.54			
623	3023.25	16.71			
624	3028.97	16.88			
625	3034.69	17.05			
626	3040.41	17.23			
627	3046.13	17.4	1545	3046.19	17.44
628	3050.96	17.47	1546	3050.91	17.55
629	3055.28	17.59	1547	3055.18	17.62
630	3061.43	17.81	1548	3061.74	17.96
631	3066.96	17.66	1549	3067	17.75
634	3084.86	17.69	1550	3085.07	17.9
635	3090.55	17.75	1551	3090.58	17.9

636	3095.03	17.72			
637	3101.05	17.87	1552	3101.06	17.88
638	3106.49	17.84	1553	3107.13	17.97
639	3112.3	17.78	1554	3112.25	17.97
640	3117.86	17.69	1555	3117.98	18.02
641	3123.28	17.71	1556	3123.56	18.04
642	3128.68	17.75	1557	3128.82	18.03
643	3134.68	17.87	1558	3134.75	18.11
644	3139.69	17.84	1559	3139.93	18.17
645	3146.1	17.61	1560	3146.44	18.16
646	3151.34	17.67	1561	3151.44	18.18
647	3157.08	17.83	1562	3156.94	18.14
648	3160.87	17.74	1563	3161.21	18.14
649	3164.6	17.63	1564	3165.03	18.09
650	3169.05	17.76	1565	3169.08	18.04
651	3174.5	17.73	1566	3174.56	18.04
652	3179.47	17.77	1567	3179.61	18.1
653	3184.33	17.97	1568	3184.52	18.11
654	3189.32	18.05	1569	3189.68	18.15
655	3194.46	18.12	1570	3194.46	18.14
656	3199.49	18.1	1571	3199.53	18.22
657	3204.43	18.08			
658	3209.31	18.25	1572	3209.42	18.46
659	3214.06	18.39	1573	3214.13	18.63
660	3219.1	18.44	1574	3219.39	18.62
661	3224.08	18.7	1575	3224.22	18.81
662	3229.08	18.82	1576	3229.38	18.88
663	3234.01	19.15	1577	3234.11	19.1
664	3239.13	19.44	1578	3238.86	19.43
665	3243.87	19.77	1579	3244.49	19.71
666	3249.05	20.02	1580	3249.09	19.94
667	3254.04	20.2	1581	3254.11	20.24
668	3258.87	20.4	1582	3259	20.35
669	3263.37	20.43	1583	3263.74	20.42
670	3269.02	20.48	1584	3268.46	20.5
671	3273.65	20.48			
672	3278.65	20.54	1585	3278.69	20.48
673	3283.24	20.49	1586	3283.54	20.53
674	3287.99	20.55	1587	3288.56	20.55
675	3292.6	20.55	1588	3293.52	20.65
676	3298.21	20.59	1589	3298.66	20.63
677	3302.96	20.68	1590	3303.62	20.69
678	3308.02	20.74	1591	3308.59	20.74
679	3312.79	20.81	1592	3313.43	20.77
680	3319.09	20.83	1593	3318.32	20.82
681	3323.31	20.87	1594	3323.3	20.91
682	3328.42	20.9	1595	3328.39	20.98
683	3333.04	20.96	1596	3333.3	21.06
684	3338.44	20.93	1597	3338.43	20.99

685	3343.22	20.94	1598	3343.3	21
686	3348.32	20.97			
687	3353.49	21.02	1599	3353.43	21.06
688	3358.4	21.13	1600	3358.32	21.15
689	3363.19	21.14	1601	3363.18	21.15
690	3368.21	21.17	1602	3368.26	21.09
691	3373.13	21.13	1603	3373.19	21.22
692	3378.28	21.13	1604	3378.1	21.3
693	3383.17	21.13	1605	3383.14	21.32
694	3388.29	21.07	1606	3388.26	21.25
695	3393.06	21.13	1607	3393.09	21.28
696	3398.48	21.2	1608	3398.23	21.36
697	3403.14	21.26	1609	3403.11	21.47
698	3408.25	21.25	1610	3408.17	21.63
699	3413.11	21.36	1611	3413.14	21.62
700	3417.87	21.46	1612	3417.95	21.6
701	3422.91	21.6	1613	3422.96	21.67
702	3427.82	21.69	1614	3427.98	21.68
703	3432.7	21.71	1615	3432.73	21.71
704	3438.02	21.68	1616	3437.92	21.66
705	3442.55	21.65	1617	3442.61	21.66
706	3447.86	21.69	1618	3448.15	21.65
707	3452.51	21.68	1619	3452.65	21.79
708	3457.84	21.94	1620	3457.84	21.84
709	3462.77	22.08	1621	3462.82	22
710	3467.6	21.98	1622	3467.66	22.01
711	3472.49	21.86	1623	3472.55	21.91
712	3475.01	21.9	1624	3475.14	21.93
713	3482.17	21.49			
714	3485.91	20.98			
715	3489.69	21.9			
716	3495.12	21.98	1625	3495.34	21.91
717	3498.19	22.06	1626	3498.34	22.04
718	3501.26	22.15	1627	3501.34	22.16
719	3506.15	22.22	1628	3506.02	22.3
720	3511.9	22.34	1629	3511.36	22.33
721	3516.07	22.39	1630	3516.17	22.4
722	3521.37	22.42	1631	3521.48	22.45
723	3525.49	22.43	1632	3526.09	22.47
724	3531.31	22.4	1633	3531.21	22.44
725	3536.2	22.48	1634	3536.26	22.47
726	3541.3	22.54	1635	3541.18	22.52
727	3545.95	22.61	1636	3545.81	22.58
728	3551.01	22.62	1637	3550.95	22.62
729	3555.93	22.67	1638	3554.74	22.68
730	3560.96	22.76	1639	3560.84	22.71
731	3565.09	22.78	1640	3565.73	22.82
732	3570.51	22.77			
733	3575.51	22.73	1641	3575.85	23.04

734	3580.6	22.85			
735	3585.33	22.78	1642	3585.26	22.77
736	3590.65	22.84			
737	3595.97	22.89			
738	3601.29	22.95			
739	3606.61	23			
740	3611.93	23.06	1643	3611.7	23.06
741	3615.34	23.19	1644	3614.92	23.18
742	3619.69	23.28	1645	3619.9	23.33
743	3625.06	23.29	1646	3624.65	23.4
744	3629.47	23.4	1647	3629.76	23.48
745	3634.84	23.52	1648	3634.63	23.56
746	3639.49	23.65	1649	3639.65	23.65
747	3644.38	23.71	1650	3644.62	23.7
748	3649.09	23.72	1651	3649.1	23.81
749	3654.15	23.78	1652	3654.6	23.78
750	3659.44	23.85	1653	3659.58	23.87
751	3664.23	23.89	1654	3664.41	23.9
752	3669.34	23.96	1655	3669.45	23.98
753	3674.14	24.05	1656	3674.33	24.03
754	3679.23	24.17	1657	3678.82	24.14
755	3683.91	24.27	1658	3684.28	24.2
756	3688.71	24.35	1659	3688.72	24.35
757	3693.92	24.4	1660	3693.91	24.41
758	3698.88	24.37	1661	3699.01	24.4
759	3704.12	24.45	1662	3703.94	24.49
760	3708.99	24.52	1663	3708.95	24.57
761	3713.78	24.54	1664	3714.12	24.53
762	3718.59	24.55			
763	3724.32	24.56	1665	3723.62	24.57
764	3728.77	24.63			
765	3733.69	24.69	1666	3733.66	24.76
766	3738.74	24.69	1667	3738.9	24.86
767	3743.84	24.83	1668	3743.65	24.93
768	3748.71	24.93	1669	3748.66	24.95
769	3753.65	24.9	1670	3753.47	25.12
770	3758.73	25.02	1671	3758.68	25.04
771	3763.67	25.04	1672	3763.6	25.09
772	3768.64	25.09	1673	3768.56	25.2
773	3773.81	25.22	1674	3774.06	25.33
774	3779.3	25.23	1675	3779.53	25.34
775	3784.79	25.25	1676	3784.99	25.35
776	3790.29	25.26			
777	3795.78	25.27			
778	3801.27	25.28			
779	3806.76	25.3			
780	3812.25	25.31			
781	3817.74	25.32			
782	3823.24	25.33			

783	3828.73	25.35			
784	3834.22	25.36			
785	3839.13	25.47	1677	3839.16	25.58
786	3844.68	25.51	1678	3844.46	25.74
787	3849.34	25.58	1679	3849.24	25.76
788	3854.04	25.69			
789	3858.94	25.82	1680	3859.09	25.8
790	3863.65	25.8	1681	3863.33	25.81
791	3869.28	25.94	1682	3869.16	26.02
792	3875.54	26.11	1683	3875.44	26.14
793	3879.33	25.98	1684	3879.09	26.2
794	3883.64	26.02	1685	3883.94	25.95
795	3888.98	26.02	1686	3889.01	26.04
796	3893.56	26.15	1687	3893.29	26.15
797	3899.08	26.06	1688	3898.85	26.16
798	3903.56	26.18	1689	3903.51	26.18
799	3908.71	26.14	1690	3908.51	26.26
800	3913.83	26.22	1691	3913.54	26.26
801	3918.78	26.27	1692	3918.64	26.33
802	3923.39	26.46	1693	3923.35	26.45
803	3928.15	26.47	1694	3928.42	26.56
804	3933.59	26.48	1695	3933.45	26.49
805	3938.34	26.52	1696	3938.24	26.54
806	3942.87	26.62	1697	3943.16	26.63
807	3948.5	26.73	1698	3948.05	26.7
808	3953.42	26.76	1699	3953.19	26.77
809	3957.78	26.83	1700	3957.9	26.84
810	3962.66	27.05	1701	3962.61	27.11
811	3967.81	27.15	1702	3967.78	27.17
812	3973.04	27.29	1703	3972.78	27.31
813	3977.58	27.42	1704	3977.47	27.43
814	3982.61	27.49	1705	3982.52	27.39
815	3987.41	27.48			
816	3992.34	27.45			
817	3996.64	27.39			
818	4001.55	27.44			
819	4006.45	27.5			
820	4011.36	27.55			
821	4016.26	27.6			
822	4021.16	27.66			
823	4026.07	27.71	1706	4026.03	27.72
824	4031.75	27.69	1707	4031.7	27.69
825	4036.16	28.02	1708	4035.99	27.97
826	4041.65	27.95	1709	4041.58	27.97
827	4046.56	28.01	1710	4046.55	28
828	4052.22	28.03	1711	4051.6	28.05
829	4056.55	28.14	1712	4056.42	28.12
830	4061.5	28.16	1713	4061.43	28.13
831	4066.39	28.26	1714	4066.49	28.26

832	4072.14	28.35	1715	4071.97	28.37
833	4076.68	28.38	1716	4076.65	28.33
834	4081.77	28.33	1717	4081.62	28.36
835	4086.74	28.37	1718	4086.47	28.29
836	4091.42	28.36	1719	4091.4	28.29
837	4096.58	28.31	1720	4096.45	28.3
838	4101.25	28.33	1721	4101.17	28.37
839	4106.62	28.32	1722	4106.55	28.39
840	4111.33	28.26	1723	4111.35	28.44
841	4116.63	28.52	1724	4116.51	28.53
842	4122.21	28.44	1725	4122.11	28.47
843	4126.11	28.47	1726	4126.05	28.49
844	4130.89	28.58	1727	4131.02	28.57
845	4135.95	28.57	1728	4135.82	28.58
846	4141.97	28.67	1729	4141.27	28.62
847	4146.55	28.76	1730	4145.96	28.8
848	4151.34	28.72	1731	4151.29	28.75
849	4157.13	28.77	1732	4156.51	28.77
850	4160.33	28.86	1733	4160.19	28.87
851	4163.54	28.88	1734	4164.02	28.91
852	4170.65	28.98	1735	4170.57	29
853	4176.96	29.02	1736	4176.9	29.05
854	4183.83	29.06	1737	4183.16	29.04
855	4189.32	29.18	1738	4188.82	29.17
856	4195.52	29.11	1739	4194.9	29.09
857	4201.4	29.27	1740	4200.66	29.21
858	4205.34	29.07	1741	4205.48	28.97
859	4210.33	29.31			
860	4215.32	29.55	1742	4214.97	29.59
861	4219.73	30.79	1743	4219.81	30.93
862	4224.31	32.41	1744	4224.12	32.46
863	4228.68	33.06	1745	4228.94	33.24
864	4234.29	32.74	1746	4234.3	32.86
865	4239.49	32.39	1747	4239.33	32.49
866	4244.29	32.27	1748	4244.28	32.35
867	4249.35	32.3			
868	4254.41	32.33			
869	4259.46	32.36			
870	4264.52	32.39			
871	4269.5	31.62	1749	4269.28	31.99
872	4274.46	30.87	1750	4274.37	31.76
873	4278.97	30.34	1751	4278.72	30.97
874	4283.66	30.13	1752	4283.73	30.54
875	4289.29	29.98	1753	4289.3	30.32
876	4293.87	30	1754	4293.93	30
877	4298.87	30.12	1755	4298.74	30.12
878	4304.58	30.15	1756	4304.41	30.13
879	4308.87	30.03	1757	4308.77	30.1
880	4314.81	30.21	1758	4314.66	30.29

881	4320.13	30.33	1759	4319.63	30.37
882	4323.79	30.39	1760	4323.44	30.36
883	4328.33	30.32	1761	4328.67	30.3
884	4333.86	30.48	1762	4333.57	30.4
885	4338.09	30.52	1763	4338.83	30.47
886	4342.91	30.56	1764	4343.7	30.57
887	4348.25	30.64	1765	4348.64	30.66
888	4353.79	30.76	1766	4354.06	30.78
889	4358.63	30.71	1767	4358.68	30.76
890	4363.77	30.74	1768	4363.77	30.84
891	4368.31	30.84	1769	4368.35	30.87
892	4373.51	31.04	1770	4373.1	30.98
893	4378.23	31.08	1771	4377.98	31.1
894	4384.09	31.18	1772	4383.02	31.22
895	4388.28	31.21	1773	4388.9	31.24
896	4392.6	31.31			
897	4397.35	31.42			
898	4401.63	31.73	1774	4402.29	31.81
899	4407.07	32.25	1775	4407.47	32.35
900	4412.81	32.97			
901	4416.45	32.85	1776	4416.21	32.54
902	4421.09	32.87			
903	4426.63	32.28			
904	4431.62	32.17			
905	4436.71	32.08			
906	4441.54	32			
907	4445.64	32.77	1777	4445.62	32.09
908	4451.73	31.94	1778	4451.96	31.9
909	4457.09	31.91	1779	4457.09	31.75
910	4462.09	31.84	1780	4462.18	31.69
911	4467.05	31.65	1781	4467.02	31.57
912	4472.04	31.59			
913	4477.05	31.54	1782	4477.2	31.44
914	4481.98	31.49	1783	4482.19	31.37
915	4487.01	31.48	1784	4487.15	31.3
916	4491.99	31.4	1785	4492.07	31.21
917	4496.92	31.38	1786	4497.11	31.16
918	4501.79	31.32	1787	4502	31.05
919	4506.82	31.36	1788	4506.89	31.02
920	4511.17	31.09	1789	4511.5	30.98
921	4516.74	31	1790	4516.92	30.87
922	4521.43	31.14	1791	4521.9	30.76
923	4526.88	31.03	1792	4526.95	30.69
924	4531.88	30.65	1793	4531.87	30.89
925	4536.56	30.55	1794	4536.77	30.69
926	4541.58	30.46	1795	4541.48	30.62
927	4546.84	30.43	1796	4546.78	30.71
928	4551.74	30.31	1797	4551.66	30.7
929	4556.68	30.26	1798	4556.38	30.55

930	4561.92	30.37	1799	4561.91	30.53
931	4566.99	30.07	1800	4566.75	30.84
932	4571.51	29.95	1801	4571.56	30.23
933	4576.16	29.85	1802	4576.27	30.15
934	4580.76	29.74	1803	4580.87	30.12
935	4586.22	30.07			
936	4591.68	30.4	1804	4591.81	30.25
937	4596.89	30.31	1805	4596.91	30.18
938	4601.7	30.25	1806	4601.9	30.09
939	4606.94	30.18	1807	4606.44	30.09
940	4611.53	30.19	1808	4611.49	30.02
941	4616.79	30.17	1809	4616.92	29.84
942	4621.55	30.15	1810	4621.6	29.84
943	4626.58	30.02	1811	4626.7	29.66
944	4631.39	30.04	1812	4631.57	29.86
945	4636.54	30.14	1813	4636.51	29.82
946	4641.6	29.97	1814	4641.56	29.74
947	4645.82	34.09	1815	4645.57	34.39
948	4650.37	34.1	1816	4650.49	34.12
949	4655.57	34.06	1817	4655.38	34.09
950	4660.65	34.05	1818	4660.31	34.06
951	4665.62	34.01	1819	4665.4	34.02
952	4669.95	33.95	1820	4670.33	33.98
953	4675.03	33.95	1821	4675.37	33.96
954	4680.2	33.99	1822	4680.32	33.98
955	4685.06	34.07	1823	4685.1	34.05
956	4690.32	34.16	1824	4690.37	34.16
957	4695.09	34.18	1825	4695.21	34.19
958	4701.33	34.2	1826	4700.89	34.21
959	4705.13	34.26	1827	4704.86	34.26
960	4710.18	34.27	1828	4710.22	34.26
961	4715.26	34.28	1829	4715.25	34.27
962	4720.26	34.32			
963	4725.04	34.3	1830	4725.21	34.33
964	4730	34.3	1831	4730.35	34.31
965	4735.29	34.25	1832	4735.23	34.27
966	4740.26	34.21	1833	4740.02	34.28
967	4745.2	34.33	1834	4745.02	34.31
968	4750.01	34.33	1835	4749.98	34.34
969	4755.14	34.38	1836	4755.03	34.39
970	4760.08	34.45	1837	4759.95	34.42
971	4763.89	34.45			
972	4770.18	34.44	1838	4769.96	34.45
973	4775.05	34.51	1839	4774.93	34.52
974	4780.12	34.51	1840	4779.91	34.48
975	4785.01	34.5	1841	4784.91	34.5
976	4790.1	34.52	1842	4789.96	34.49
977	4794.95	34.57	1843	4794.91	34.55
978	4800.2	34.64	1844	4800.08	34.64

979	4803.93	34.7	1845	4803.66	34.68
980	4809.87	34.7	1846	4809.84	34.71
981	4815.12	34.8	1847	4815.01	34.84
982	4820.18	34.93	1848	4820.04	34.96
983	4825.01	35.07	1849	4824.85	35.06
984	4830.02	35.06	1850	4830.01	35.07
985	4835.19	35.01	1851	4835.03	35.02
986	4840.01	34.99	1852	4839.97	35.01
987	4845	35.01	1853	4844.95	35.02
988	4849.97	35.01	1854	4850.01	34.98
989	4854.84	35.13	1855	4854.74	35.15
990	4859.88	35.11	1856	4859.7	35.18
991	4864.74	35.17	1857	4864.73	35.2
992	4870.16	35.16	1858	4869.99	35.19
993	4874.68	35.25	1859	4874.46	35.27
994	4880.67	35.3	1860	4880.44	35.25
995	4884.82	35.29	1861	4884.69	35.33
996	4889.13	35.34	1862	4889.11	35.32
997	4894.96	35.33	1863	4894.88	35.33
998	4899.73	35.35	1864	4899.7	35.33
999	4904.8	35.41	1865	4904.95	35.43
1000	4909.93	35.42	1866	4909.85	35.42
1001	4914.92	35.43	1867	4914.78	35.44
1002	4919.4	35.53	1868	4919.39	35.47
1003	4924.64	35.74	1869	4924.54	35.7
1004	4929.02	35.78	1870	4929.28	35.78
1005	4933.6	35.83	1871	4933.56	35.82
1006	4939.54	35.7	1872	4939.32	35.69
1007	4944.62	35.92	1873	4944.54	35.97
1008	4949.51	35.98	1874	4949.45	36.03
1009	4954.32	36.06	1875	4954.56	36.01
1010	4959.47	36.05	1876	4959.39	36.08
1011	4964.69	36.16	1877	4964.66	36.2
1012	4969.57	36.16	1878	4969.39	36.2
1013	4974.36	36.21	1879	4974.26	36.24
1014	4979.4	36.28	1880	4979.35	36.34
1015	4984.57	36.28	1881	4984.51	36.33
1016	4989.2	36.35	1882	4989.4	36.39
1017	4994.27	36.48	1883	4994.2	36.5
1018	4999.52	36.58	1884	4999.5	36.6
1019	5004.79	36.61	1885	5004.41	36.59
1020	5009.38	36.68	1886	5009.32	36.69
1021	5015.28	36.75	1887	5015.18	36.67
1022	5019.46	36.69	1888	5019.26	36.68
1023	5024.1	36.8	1889	5023.83	36.76
1024	5029.27	36.82	1890	5029.17	36.83
1025	5034.25	36.94	1891	5034.06	36.93
1026	5038.98	36.92	1892	5038.99	36.93
1027	5044.24	36.91	1893	5044.15	36.88

1028	5049.12	36.91	1894	5049.04	36.88
1029	5054.17	36.92	1895	5054.19	36.91
1030	5059.13	36.97	1896	5059	36.94
1031	5064.34	37	1897	5064.18	36.94
1032	5069.26	37.07	1898	5069.04	37.01
1033	5073.98	37.09	1899	5073.91	37.06
1034	5078.98	37.11	1900	5078.6	37.07
1035	5084.41	37.2	1901	5084.23	37.17
1036	5089.03	37.19	1902	5088.85	37.21
1037	5094.16	37.25	1903	5094.01	37.24
1038	5099.32	37.25	1904	5099.13	37.25
1039	5104.86	37.3	1905	5104.84	37.31
1040	5109.17	37.43	1906	5109.01	37.4
1041	5114.33	37.57	1907	5113.97	37.63
1042	5119.23	37.56	1908	5118.97	37.59
1043	5123.07	37.56	1909	5123.04	37.55
1044	5128.95	37.51	1910	5128.96	37.47
1045	5134.07	37.53	1911	5133.88	37.48
1046	5138.89	37.61	1912	5138.94	37.5
1047	5143.92	37.65	1913	5143.89	37.56
1048	5148.9	37.72	1914	5148.9	37.68
1049	5154.13	37.82	1915	5153.72	37.78
1050	5158.23	37.91	1916	5158.38	37.82
1051	5163.96	38.02	1917	5163.83	37.89
1052	5168.78	38.09	1918	5168.78	38.04
1053	5173.96	38.12	1919	5173.84	38.11
1054	5179.07	38.19	1920	5178.95	38.08
1055	5183.66	38.18	1921	5183.53	38.12
1056	5188.82	38.22	1922	5188.66	38.13
1057	5193.57	38.28	1923	5193.55	38.2
1058	5198.63	38.37	1924	5198.51	38.23
1059	5203.7	38.31	1925	5203.72	38.3
1060	5208.03	38.36	1926	5208.06	38.3
1061	5212.91	38.43	1927	5212.79	38.35
1062	5216.46	38.55			
1063	5222.95	38.59	1928	5222.97	38.58
1064	5228.18	38.76	1929	5227.93	38.72
1065	5232.89	39.01	1930	5232.88	38.97
1066	5237.81	40.33	1931	5237.67	40.28
1067	5241.72	42.12	1932	5241.81	42.1
1068	5246.94	43.87	1933	5246.33	43.75
1069	5251.83	43.82	1934	5251.33	43.72
1070	5256.72	43.77	1935	5256.33	43.69
1071	5261.6	43.71	1936	5261.33	43.67
1072	5266.49	43.66	1937	5266.33	43.64
1073	5271.38	43.61	1938	5271.33	43.61
1074	5275.61	41.64	1939	5275.57	41.63
1075	5281.91	39.19	1940	5281.93	39.23
1076	5284.98	39.25	1941	5285.26	39.21

1077	5289.99	39.19	1942	5289.8	39.16
1078	5295.02	39.25	1943	5294.74	39.23
1079	5300.26	39.22	1944	5299.8	39.26
1080	5304.81	39.27	1945	5304.89	39.27
1081	5309.73	39.33	1946	5310.14	39.32
1082	5315.22	39.37	1947	5315.11	39.42
1083	5319.89	39.42	1948	5319.72	39.35
1084	5324.99	39.44	1949	5324.84	39.35
1085	5329.87	39.46	1950	5329.78	39.38
1086	5334.79	39.5	1951	5334.75	39.48
1087	5339.95	39.58	1952	5339.72	39.53
1088	5345.37	39.55	1953	5344.85	39.57
1089	5350.62	39.68	1954	5350.49	39.64
1090	5354.87	39.62	1955	5354.7	39.6
1091	5359.97	39.75	1956	5359.77	39.68
1092	5364.71	39.8	1957	5364.29	39.75
1093	5369.12	39.81	1958	5369.25	39.79
1094	5374.67	39.93	1959	5374.45	39.88
1095	5379.58	40	1960	5379.45	39.96
1096	5384.38	40.03	1961	5384.31	40.01
1097	5389.59	40.04	1962	5389.29	40.03
1098	5394.38	40.15	1963	5394.26	40.1
1099	5399.24	40.23	1964	5398.73	40.22
1100	5404.01	40.28	1965	5403.91	40.26
1101	5409.07	40.39	1966	5409.01	40.34
1102	5413.97	40.43	1967	5413.98	40.4
1103	5419.26	40.53	1968	5419.04	40.5
1104	5424.38	40.57	1969	5424.18	40.57
1105	5429.02	40.62	1970	5428.75	40.65
1106	5434.11	40.72	1971	5433.94	40.73
1107	5438.7	40.75	1972	5438.5	40.76
1108	5444.25	40.77	1973	5443.94	40.76
1109	5448.82	40.81	1974	5448.68	40.75
1110	5453.8	40.76	1975	5453.61	40.73
1111	5458.71	40.76	1976	5458.6	40.83
1112	5463.71	40.77	1977	5463.69	40.68
1113	5468.61	40.73	1978	5468.42	40.73
1114	5473.77	40.72			
1115	5478.35	40.67			
1116	5482.99	40.62	1979	5482.96	40.63
1117	5488.32	40.55	1980	5488.15	40.57
1118	5493.53	40.33			
1119	5498.75	40.1			
1120	5502.55	39.97	1981	5502.89	40.12
1121	5507.77	40.29	1982	5507.54	40.51
1122	5512.58	40.82	1983	5512.51	40.84
1123	5514.9	40.86			
1124	5522.49	40.92	1984	5522.44	41
1125	5527.56	41.01			

1126	5532.69	41.22	1985	5532.26	41.15
1127	5538.19	41.23	1986	5537.97	41.21
1128	5543.14	41.29	1987	5543	41.34
1129	5547.33	41.44	1988	5547.29	41.42
1130	5552.2	41.4	1989	5552.04	41.42
1131	5556.89	41.54	1990	5556.79	41.53
1132	5562.04	41.6	1991	5561.95	41.66
1133	5567.08	41.71	1992	5566.9	41.74
1134	5571.87	41.85	1993	5571.64	41.85
1135	5576.8	41.93	1994	5576.63	41.9
1136	5581.92	41.93	1995	5581.84	41.94
1137	5586.88	41.99	1996	5586.79	42
1138	5591.9	42.09	1997	5592	42.13
1139	5596.86	42.12	1998	5596.72	42.16
1140	5601.55	42.15	1999	5601.64	42.12
1141	5606.59	42.21	2000	5606.84	42.24
1142	5612.15	42.28	2001	5612.23	42.28
1143	5617.51	42.44	2002	5617.66	42.42
1144	5623.81	42.34	2003	5623.69	42.35
1145	5629.97	42.4	2004	5630.2	42.39
1146	5636.64	42.48	2005	5636.61	42.44
1147	5641.22	42.5	2006	5640.87	42.51
1148	5646.03	42.54	2007	5646.13	42.53
1149	5651.47	42.52	2008	5651.52	42.47
1150	5657.09	42.65	2009	5657.32	42.67
1151	5662.77	42.47	2010	5662.88	42.39
1152	5668.9	42.36	2011	5668.8	42.44
1153	5674.26	42.48	2012	5674.42	42.45
1154	5678.89	42.5	2013	5678.87	42.5
1155	5681.52	42.65	2014	5681.65	42.59
1156	5686.08	42.75	2015	5686.28	42.69
1157	5691.2	42.66	2016	5691.51	42.64
1158	5695.78	42.65	2017	5695.99	42.6
1159	5700.42	42.77	2018	5700.82	42.72
1160	5705.95	42.8	2019	5706.25	42.72
1161	5710.87	42.77	2020	5711.1	42.64
1162	5716.59	42.75	2021	5716.04	42.64
1163	5720.89	42.96	2022	5720.78	42.86
1164	5725.87	43.06	2023	5726.15	42.99
1165	5730.65	43.1	2024	5730.68	43.04
1166	5735.66	43.22	2025	5735.67	43.18
1167	5740.45	43.25	2026	5740.47	43.2
1168	5745.11	43.27	2027	5745.3	43.24
1169	5750.2	43.27	2028	5750.36	43.2
1170	5755	43.43	2029	5755.16	43.38
1171	5759.48	43.44	2030	5759.74	43.37
1172	5764.49	43.55	2031	5765.08	43.56
1173	5769.1	43.58	2032	5769.91	43.53
1174	5775.71	43.64	2033	5775.28	43.57

1175	5780.82	43.67			
1176	5785.4	43.73			
1177	5789.99	43.79	2034	5789.94	43.67
1178	5794.57	43.85	2035	5794.6	43.72
1179	5799.68	43.71	2036	5799.67	43.51
1180	5804.58	43.55	2037	5804.72	43.68
1181	5809.45	43.56	2038	5809.63	43.71
1182	5814.7	43.69	2039	5814.59	43.83
1183	5819.26	43.69	2040	5819.61	43.91
1184	5824.62	43.88	2041	5824.55	43.99
1185	5829.54	43.72	2042	5829.48	43.79
1186	5834.64	44.01	2043	5834.6	44.06
1187	5839.56	44.07	2044	5839.42	44.14
1188	5844.42	44.15	2045	5844.37	44.24
1189	5849.28	44.38	2046	5849.43	44.45
1190	5854.32	44.54	2047	5854.27	44.63
1191	5859.16	44.5	2048	5859.09	44.83
1192	5864.47	44.6	2049	5864.44	44.99
1193	5868.73	44.63	2050	5869.23	44.94
1194	5874.23	44.44			
1195	5879.37	44.8	2051	5879.18	45.17
1196	5884.18	44.99	2052	5884.23	45.11
1197	5889.17	45.05	2053	5888.9	45.11
1198	5893.63	45	2054	5893.73	45.06
1199	5898.89	45.04	2055	5898.8	45.16
1200	5903.62	45	2056	5903.31	45.16
1201	5908.4	45.22	2057	5908.28	45.32
1202	5912.76	45.32	2058	5913.1	45.4
1203	5917.52	45.3	2059	5917.78	45.4
1204	5922.7	45.26	2060	5922.85	45.42
1205	5927.58	45.25	2061	5927.43	45.37
1206	5932.02	45.3	2062	5932.46	45.42
1207	5937.5	45.34	2063	5937.63	45.46
1208	5942.02	45.43	2064	5942.32	45.49
1209	5947.35	45.47	2065	5947.36	45.53
1210	5952.45	45.51	2066	5952.59	45.47
1211	5957.33	45.51	2067	5957.31	45.52
1212	5962.01	45.55	2068	5962.1	45.53
1213	5966.89	45.51	2069	5967.23	45.57
1214	5971.81	45.58	2070	5972.05	45.59
1215	5977.35	45.49	2071	5977.46	45.59
1216	5981.78	45.67	2072	5981.99	45.66
1217	5986.77	45.77	2073	5987.05	45.73
1218	5991.88	45.71	2074	5991.96	45.71
1219	5996.78	45.6	2075	5996.92	45.73
1220	6001.09	45.65	2076	6001.22	45.71
1221	6006.3	45.59	2077	6006.69	45.78
1222	6011.43	45.82	2078	6011.39	45.85
1223	6016.2	45.85	2079	6016.29	45.92

1224	6021.26	45.94	2080	6021.37	45.98
1225	6026.15	45.97	2081	6026.5	45.95
1226	6029.94	46.01	2082	6030.39	45.99
1227	6035.67	45.84	2083	6036.03	46.15
1228	6040.9	45.93	2084	6041.01	46.09
1229	6045.94	45.71	2085	6045.86	46.1
1230	6050.26	45.96	2086	6050.78	46.05
1231	6054.91	46.12	2087	6055.41	46.18
1232	6060.18	46.1	2088	6060.17	46.26
1233	6065.13	46.38	2089	6064.57	46.8
1234	6068.77	43.75	2090	6069.43	43.89
1235	6074.47	44.38			
1236	6080.17	45			
1237	6084.32	46.14	2091	6084.22	46.13
1238	6088.48	47.27	2092	6088.25	47.24
1239	6093.68	47.28			
1240	6098.88	47.28			
1241	6102.39	47.26	2093	6102.87	47.23
1242	6107.64	47.31			
1243	6112.59	47.34	2094	6113.85	47.34
1244	6117.69	47.26	2095	6117.19	47.24
1245	6122.62	47.26	2096	6122.41	46.98
1246	6127.86	47.18	2097	6127.88	47.02
1247	6132.62	47.29	2098	6132.63	47.05
1248	6138.05	47.35	2099	6137.95	47.07
1249	6142.51	47.41	2100	6142.49	47.24
1250	6147.62	47.4	2101	6147.63	47.25
1251	6152.54	47.47	2102	6152.63	47.35
1252	6157.52	47.48	2103	6157.51	47.41
1253	6162.52	47.57	2104	6162.48	47.52
1254	6167.43	47.62	2105	6167.39	47.58
1255	6172.37	47.69	2106	6172.46	47.66
1256	6177.59	47.73	2107	6177.51	47.71
1257	6182.63	47.76	2108	6182.45	47.72
1258	6187.47	47.8	2109	6187.33	47.73
1259	6192.28	47.79	2110	6192.23	47.75
1260	6197.19	47.81	2111	6197.15	47.79
1261	6202.21	47.82	2112	6202.2	47.84
1262	6207.12	47.85	2113	6207.21	47.86
1263	6212.22	47.84	2114	6212.19	47.87
1264	6216.92	47.85	2115	6217.03	47.88
1265	6221.97	47.9			
1266	6227.16	48	2116	6227.06	48.02
1267	6232.21	48.07	2117	6232.01	48.1
1268	6237.53	48.01	2118	6237.17	48.14
1269	6242.18	48.07	2119	6241.98	48.22
1270	6246.98	48.13	2120	6246.94	48.17
1271	6251.89	48.15	2121	6251.88	48.22
1272	6256.97	48.16	2122	6256.91	48.23

1273	6261.74	48.24	2123	6261.78	48.3
1274	6266.88	48.27	2124	6266.84	48.28
1275	6271.63	48.25	2125	6271.6	48.28
1276	6276.66	48.24	2126	6276.45	48.28
1277	6281.62	48.24	2127	6281.59	48.29
1278	6286.76	48.2	2128	6286.7	48.29
1279	6291.65	48.2	2129	6291.47	48.28
1280	6296.55	48.22	2130	6296.57	48.33
1281	6301.6	48.28			
1282	6306.48	48.28	2131	6306.39	48.38
1283	6311.49	48.34	2132	6311.41	48.42
1284	6316.47	48.33	2133	6316.47	48.41
1285	6321.44	48.35	2134	6321.38	48.43
1286	6326.4	48.35	2135	6326.33	48.49
1287	6331.29	48.38	2136	6331.37	48.47
1288	6336.34	48.39	2137	6336.22	48.49
1289	6341.35	48.33	2138	6341.34	48.42
1290	6346.34	48.34	2139	6346.25	48.45
1291	6351.24	48.4	2140	6351.14	48.48
1292	6356.12	48.39	2141	6356.09	48.48
1293	6361.03	48.44	2142	6360.9	48.46
1294	6366.03	48.51	2143	6365.99	48.56
1295	6371.06	48.53	2144	6370.91	48.58
1296	6375.77	48.48	2145	6375.72	48.59
1297	6380.84	48.5	2146	6380.71	48.61
1298	6385.06	48.37	2147	6384.86	48.52
1299	6390.68	48.66	2148	6390.65	48.7
1300	6395.67	48.74	2149	6395.67	48.77
1301	6400.83	48.69	2150	6400.77	48.76
1302	6405.79	48.77	2151	6405.64	48.83
1303	6410.77	48.85	2152	6410.84	48.91
1304	6415.69	48.93	2153	6415.56	48.96
1305	6420.52	48.95	2154	6420.56	49.02
1306	6425.93	49.06	2155	6425.64	49.01
1307	6430.44	49.04	2156	6430.32	49.1
1308	6435.56	49.06	2157	6435.46	49.09
1309	6440.92	49.16	2158	6440.74	49.15
1310	6445.56	49.18	2159	6445.47	49.17
1311	6450.5	49.18	2160	6450.78	49.21
1312	6455.52	49.27	2161	6455.57	49.28
1313	6460.37	49.35	2162	6460.44	49.34
1314	6465.57	49.34	2163	6465.58	49.38
1315	6470.38	49.3	2164	6470.4	49.49
1316	6475.27	49.49	2165	6475.34	49.53
1317	6480.46	49.59	2166	6480.38	49.55
1318	6485.61	49.6	2167	6485.49	49.58
1319	6490.22	49.63	2168	6490.37	49.65
1320	6495.38	49.7	2169	6495.42	49.68
1321	6500.25	49.78	2170	6500.33	49.74

1322	6505.25	49.84	2171	6505.34	49.8
1323	6510.52	49.86	2172	6510.42	49.8
1324	6515.35	49.9	2173	6515.36	49.84
1325	6520.31	49.93	2174	6520.31	49.9
1326	6525.26	49.93	2175	6525.35	49.87
1327	6530.32	49.96	2176	6530.32	49.93
1328	6535.3	50.18	2177	6535.19	49.97
1329	6540.25	49.67	2178	6540.32	50.08
1330	6545.17	50.16	2179	6545.14	50.11
1331	6549.96	50.3	2180	6550.06	50.25
1332	6554.98	50.31	2181	6555.04	50.26
1333	6559.71	50.32	2182	6559.96	50.27
1334	6565.07	50.38	2183	6565.14	50.31
1335	6569.89	50.44	2184	6569.9	50.33
1336	6574.79	50.43	2185	6574.98	50.33
1337	6579.96	50.54	2186	6579.95	50.39
1338	6585.13	50.56	2187	6584.89	50.46
1339	6589.87	50.56	2188	6589.9	50.38
1340	6594.74	50.65	2189	6595.02	50.38
1341	6599.99	50.66	2190	6600.04	50.33
1342	6604.85	50.61	2191	6604.84	50.39
1343	6609.89	50.57	2192	6609.87	50.41
1344	6614.83	50.56	2193	6614.93	50.38
1345	6619.34	50.6	2194	6619.42	50.37
1346	6624.64	50.72	2195	6624.81	50.61
1347	6629.71	51.06	2196	6629.71	50.97
1348	6634.68	51.31	2197	6634.64	51.27
1349	6639.1	51.46	2198	6639.22	51.43
1350	6643.48	51.44	2199	6643.69	51.55
1351	6648.13	51.42	2200	6648.41	51.71
1352	6653.18	50.9	2201	6653.22	51.23
1353	6658.37	51.42	2202	6658.36	51.87
1354	6663.23	51.74	2203	6663.09	51.97
1355	6667.77	51.73	2204	6668.01	51.78
1356	6672.65	51.4	2205	6672.9	51.39
1357	6677.84	51.4	2206	6677.82	51.31
1358	6680.94	51.32	2207	6681.77	51.12
1359	6687.34	51.12			
1360	6692.43	51.25	2208	6692.39	51.06
1361	6697.07	51.25	2209	6697.47	51.11
1362	6702.98	51.03	2210	6702.24	51.07
1363	6707.24	51.19	2211	6707.16	51.16
1364	6712.47	51.36	2212	6712.29	51.14
1365	6717.19	51.45	2213	6717.4	51.39
1366	6722.13	51.31	2214	6722.34	51.31
1367	6727.24	51.5	2215	6727.53	51.41
1368	6732.22	51.48	2216	6732.33	51.36
1369	6737.5	51.61	2217	6737.27	51.51
1370	6742.46	51.49	2218	6742.34	51.4

1371	6745.4	51.52	2219	6745.38	51.49
1372	6751.5	51.49	2220	6751.38	51.4
1373	6757.02	51.69	2221	6757.26	51.66
1374	6762.16	51.81	2222	6762.11	51.72
1375	6766.89	51.81	2223	6767	51.65
1376	6772.51	51.97	2224	6772.21	51.78
1377	6777	52.11	2225	6777.07	51.82
1378	6782.01	51.84	2226	6782.05	51.83
1379	6786.05	52.14	2227	6785.75	51.9
1380	6791.94	52.2	2228	6791.87	51.91
1381	6796.76	51.97	2229	6796.16	51.82
1382	6802.16	52.11	2230	6802.09	52
1383	6806.51	52.29			
1384	6812.22	52.27	2231	6812.09	52.28
1385	6817.13	52.27	2232	6816.88	52.15
1386	6822.21	52.15	2233	6822.23	52.06
1387	6827.26	52.01	2234	6827.01	52
1388	6831.94	52.02	2235	6831.9	52.01
1389	6836.92	52.04	2236	6836.67	52
1390	6841.68	52.06	2237	6841.68	52.04
1391	6846.66	52.09	2238	6846.6	52.07
1392	6851.82	52.1	2239	6851.51	52.11
1393	6856.6	52.16	2240	6856.6	52.12
1394	6861.57	52.21	2241	6861.5	52.2
1395	6867.28	52.36	2242	6867.16	52.31
1396	6871.47	52.29	2243	6871.36	52.31
1397	6876.32	52.34	2244	6876.18	52.36
1398	6881.42	52.4	2245	6881.34	52.39
1399	6886.38	52.38	2246	6886.31	52.44
1400	6891.26	52.39	2247	6891.18	52.37
1401	6896.53	52.42	2248	6896.43	52.43
1402	6901.54	52.62	2249	6901.57	52.64
1403	6906.35	52.8	2250	6906.32	52.55
1404	6911.91	52.55	2251	6911.26	52.55
1405	6916.63	52.64	2252	6916.97	52.64
1406	6921.44	52.63	2253	6921.18	52.68
1407	6926.45	52.72	2254	6926.15	52.73
1408	6931.35	52.75	2255	6931.2	52.77
1409	6936.16	52.88	2256	6936.02	52.86
1410	6941.59	52.9	2257	6941.4	52.93
1411	6946.31	52.99			
1412	6951.39	52.93	2258	6951.55	52.82
1413	6956.21	52.87	2259	6956.01	52.84
1414	6961.08	52.95	2260	6960.97	52.93
1415	6966.07	52.95	2261	6965.91	52.87
1416	6971.14	52.97	2262	6970.96	52.87
1417	6976.09	53.04	2263	6975.89	52.86
1418	6980.97	53.04			
1419	6986.17	53.05	2264	6985.92	52.97

1420	6990.99	53.16	2265	6990.75	53.02
1421	6995.81	53.18	2266	6995.59	53.13
1422	7000.88	53.17	2267	7000.43	53.15
1423	7005.47	53.26	2268	7005.49	53.1
1424	7010.5	53.37	2269	7010.52	53.32
1425	7016.01	53.44	2270	7015.61	53.35
1426	7020.86	53.46			
1427	7025.47	53.46	2271	7025.4	53.47
1428	7030.47	53.51	2272	7030.41	53.48
1429	7035.56	53.64	2273	7035.34	53.52
1430	7040.52	53.65	2274	7040.45	53.57
1431	7045.26	53.74	2275	7045.38	53.68
1432	7050.48	53.76	2276	7050.47	53.73
1433	7055.41	53.88	2277	7055.22	53.73
1434	7060.05	53.98	2278	7059.84	53.93
1435	7062.74	54.02	2279	7062.41	53.91
1436	7065.43	54.07	2280	7064.98	53.88
1437	7070.42	53.93	2281	7070.31	53.91
1438	7075.23	54.19	2282	7074.69	54.07
1439	7080.18	54.15	2283	7079.67	54.11
1440	7085.17	54.29	2284	7084.96	54.18
1441	7090.22	54.25	2285	7090.09	54.23
1442	7094.92	54.33	2286	7095.19	54.25
1443	7102.33	54.53	2287	7102.11	54.39
1444	7104.84	54.48	2288	7104.7	54.39
1445	7109.92	54.56	2289	7109.62	54.46
1446	7115.28	54.56	2290	7114.86	54.49
1447	7120	54.77	2291	7119.69	54.58
1448	7124.66	54.77	2292	7124.47	54.74
1449	7129.87	55.19			
1450	7134.69	55.18	2293	7134.83	54.91
1451	7139.71	55.22	2294	7139.61	55
1452	7144.68	55.24	2295	7144.47	55.03
1453	7149.36	55.47	2296	7149.53	55.19
1454	7154.35	55.63	2297	7154.18	55.3
1455	7158.98	55.74			
1456	7164.06	55.86	2298	7164.2	55.8
1457	7169.21	56.05	2299	7169.23	55.86
1458	7174.02	55.99	2300	7174.07	55.85
1459	7178.46	56.09	2301	7178.45	55.91
1460	7182.52	56.33	2302	7182.35	55.98
1461	7188.19	56.01	2303	7188.19	55.93
1462	7192.43	56.12	2304	7192.39	56
1463	7197.91	56.08	2305	7197.72	56.06
1464	7202.59	56.03	2306	7202.37	55.98
1465	7207.54	56.1	2307	7207.26	56.11
1466	7211.94	56.2	2308	7212.12	56.16
1467	7217.21	56.31	2309	7216.69	56.3
1468	7221.61	56.38	2310	7221.31	56.4

1469	7226.42	56.48	2311	7226.22	56.45
1470	7231.48	56.61	2312	7231.04	56.6
1471	7235.64	56.61	2313	7235.47	56.65
1472	7240.32	56.62	2314	7240.59	56.64
1473	7245.33	56.65			
1474	7250.49	56.72	2315	7250.33	56.73
1475	7255.12	56.85	2316	7255.05	56.86
1476	7260.41	56.97	2317	7260.14	56.96
1477	7265.34	57.08	2318	7265.32	57.06
1478	7270.19	57.07	2319	7270.16	57.1
1479	7275.33	57.09	2320	7275.11	57.09
1480	7280.2	57.23	2321	7280.02	57.22
1481	7285.23	57.23	2322	7285.06	57.22
1482	7290.35	57.25	2323	7290.12	57.24
1483	7293.94	57.29	2324	7293.65	57.32
1484	7297.06	57.33	2325	7296.74	57.31
1485	7300.19	57.36	2326	7299.83	57.31
1486	7304.97	57.45	2327	7304.73	57.41
1487	7309.92	57.52	2328	7309.81	57.44
1488	7315.23	57.74	2329	7314.88	57.6
1489	7320.23	57.82	2330	7319.97	57.72
1490	7325.16	57.98	2331	7324.77	57.78
1491	7330.13	57.96			
1492	7334.23	58.16	2332	7334.21	57.9
1493	7336.92	58.06			
1494	7339.61	57.97	2333	7339.13	58.01
1495	7345.03	58.08	2334	7344.62	57.91
1496	7349.55	58.09	2335	7349.26	57.83
1497	7354.09	58.07	2336	7354.13	57.95
1498	7359.01	58.06	2337	7359.02	57.89
1499	7363.89	58.02	2338	7364.02	57.92
1500	7368.6	58.09	2339	7368.57	58.04
1501	7374.01	58.17	2340	7373.8	57.96
1502	7378.92	58.21	2341	7378.79	58.09
1503	7384.22	58.25	2342	7384.33	58.01
1504	7388.66	58.15	2343	7388.81	58.05
1505	7393.49	58.08	2344	7393.46	58.04
1506	7398.56	58.11	2345	7398.34	58.08
1507	7403.11	58.22	2346	7402.99	58.15
1508	7407.79	58.24	2347	7408.07	58.2
1509	7412.91	58.51	2348	7412.82	58.42
1510	7417.24	58.33	2349	7417.55	58.37
1511	7423.07	58.5	2350	7422.48	58.45
1512	7427.59	58.5	2351	7427.47	58.56
1513	7432.43	58.53	2352	7432.07	58.56
1514	7436.8	58.67	2353	7436.69	58.65
1515	7442.19	58.77	2354	7442.1	58.78
1516	7447	58.89	2355	7446.56	58.88
1517	7451.86	59.06	2356	7452.04	59.06

1518	7456.74	59.12	2357	7456.68	59.12
1519	7460.95	59.15	2358	7461.55	59.18
1520	7466.33	59.19	2359	7466.25	59.16
1521	7470.51	59.24	2360	7470.96	59.23
1527	7500.93	59.44	2361	7500.89	59.39
1528	7505.85	59.49			
1529	7511.23	59.54	2362	7511.25	59.58
1530	7515.62	59.58	2363	7515.44	59.58
1531	7520.08	59.47	2364	7520.15	59.53
1532	7525.29	59.62	2365	7525.44	59.66
1533	7530.21	59.6	2366	7530.36	59.68
1534	7535.13	59.69	2367	7535.04	59.61
1535	7540.16	59.55	2368	7540	59.58
1536	7545.33	59.56	2369	7545.42	59.6
1537	7550.28	59.59	2370	7550.22	59.68
1538	7555.42	59.72	2371	7555.5	59.73
1539	7560.3	59.7	2372	7560.51	59.72
1540	7565.68	59.75	2373	7565.68	59.78
1541	7570.58	59.76	2374	7570.57	59.8
1542	7575.22	59.74	2375	7575.34	59.74
1543	7578.98	59.77	2376	7579.03	59.75
1544	7585.21	59.82	2377	7585.34	59.88
1545	7590.04	59.93	2378	7589.92	59.88
1546	7593.9	59.63	2379	7595.27	59.64
1547	7599.51	59.7	2380	7600.27	59.66
1548	7605.47	59.98	2381	7605.2	59.74
1549	7610.35	59.99	2382	7610.16	59.75
1550	7615.25	60.01	2383	7615.15	59.82
1551	7620.51	60.03	2384	7620.17	59.82
1552	7625.18	60.06	2385	7625.14	59.85
1553	7630.08	60.06	2386	7630.14	59.86
1554	7635.18	60.09	2387	7635.12	59.9
1555	7640.1	60.13	2388	7640.08	59.93
1556	7645.5	60.16	2389	7645.05	59.96
1557	7651.56	60.2	2390	7650.78	59.98
1558	7656.1	60.23	2391	7655.79	60
1559	7661.09	60.26	2392	7660.55	60.03
1560	7665.83	60.28			
1561	7670.78	60.3	2393	7670.8	60.05
1562	7675.68	60.32	2394	7675.73	60.09
1563	7680.55	60.33	2395	7680.7	60.13
1564	7686.11	60.38	2396	7685.74	60.15
1565	7690.91	60.41	2397	7690.56	60.18
1566	7695.68	60.45	2398	7695.58	60.22
1567	7701	60.49	2399	7700.6	60.25
1568	7705.79	60.52	2400	7705.63	60.3
1569	7710.67	60.57	2401	7710.57	60.34
1570	7715.73	60.62	2402	7715.52	60.4
1571	7720.6	60.66	2403	7720.53	60.44

1572	7725.59	60.72	2404	7725.46	60.51
1573	7730.64	60.79	2405	7730.23	60.56
1574	7735.64	60.88	2406	7735.3	60.68
1575	7740.47	60.9	2407	7740.23	60.68
1576	7744.9	60.94	2408	7744.78	60.72
1577	7749.94	61.01	2409	7749.61	60.78
1578	7755.44	61.06	2410	7755.12	60.84
1579	7761.35	61.13	2411	7761.14	60.92
1580	7765.24	61.17			
1581	7770.05	61.23	2412	7769.73	61.01
1582	7775	61.29	2413	7774.78	61.06
1583	7780.05	61.34	2414	7779.75	61.12
1584	7785.32	61.44	2415	7784.78	61.17
1585	7789.98	61.47	2416	7789.74	61.23
1586	7794.69	61.52	2417	7794.75	61.28
1587	7799.96	61.58	2418	7799.68	61.35
1588	7804.94	61.51	2419	7804.64	61.4
1589	7809.8	61.69	2420	7809.38	61.47
1590	7814.14	61.73	2421	7814.47	61.51
1591	7820.14	61.8	2422	7819.4	61.56
1592	7824.34	61.85	2423	7824.44	61.62
1593	7829.34	61.9	2424	7829.43	61.67
1594	7834.44	61.96	2425	7834.43	61.72
1595	7839.46	62.02	2426	7839.4	61.78
1596	7845.91	62.09			
1597	7849.57	62.12	2427	7849.39	61.88
1598	7854.31	62.17	2428	7854.49	61.92
1599	7859.56	62.24			
1600	7864.92	62.28			
1601	7869.75	62.33	2429	7869.48	62.06
1602	7874.86	62.37	2430	7874.52	62.12
1603	7879.82	62.39	2431	7879.52	62.16
1604	7884.85	62.45	2432	7884.49	62.21
1605	7889.49	62.47	2433	7888.78	62.22
1606	7894.52	62.52	2434	7893.67	62.29
1607	7899.87	62.57	2435	7898.59	62.33
1608	7904.41	62.59	2436	7903.49	62.38
1609	7909.12	62.64	2437	7908.46	62.42
1610	7913.28	62.68			
1611	7917.82	62.95	2438	7917.74	62.87
1612	7923.11	63.12	2439	7922.93	62.94
1613	7927.56	63.17	2440	7926.91	62.86
1614	7932.66	63.14	2441	7932.65	62.95
1615	7937.46	63.2	2442	7937.05	62.99
1616	7942.33	63.23	2443	7942.21	63.08
1617	7951.14	63.32	2444	7950.77	63.21
1618	7956.68	63.43	2445	7956.18	63.4
1619	7961.33	63.5	2446	7960.92	63.45
1620	7966.58	63.62	2447	7966.23	63.63

1621	7975.12	63.82	2448	7974.61	63.79
1622	7980.07	63.97			
1623	7983.74	63.95	2449	7983.56	63.94
1624	7989	64.08	2450	7988.37	64.07
1625	7994.03	64.12	2451	7993.83	64.06
1626	7998.83	64.1	2452	7998.46	64.07
1627	8003.83	64.09			
1628	8008.83	64.07			
1629	8013.83	64.06	2453	8013.8	64.04
1630	8020.29	64.15	2454	8020.35	64.16
1631	8026.16	64.19	2455	8026.3	64.14
1632	8032.1	64.18	2456	8031.96	64.17
1633	8038.15	64.33	2457	8038.05	64.3
1634	8042.9	64.35	2458	8042.67	64.37
1635	8047.98	64.42	2459	8048.2	64.35
1636	8053.36	64.5	2460	8053.32	64.39
1637	8058.39	64.56	2461	8058.26	64.46
1638	8063.44	64.7	2462	8063.09	64.43
1639	8068.01	64.52	2463	8067.66	64.43
1640	8072.51	64.65	2464	8072.95	64.51
1641	8077.19	64.42	2465	8076.75	64.28
1642	8082.23	64.78	2466	8082.01	64.67
1643	8087.49	64.69	2467	8086.93	64.63
1644	8091.39	64.78	2468	8091.08	64.71
1645	8096.3	64.8	2469	8095.62	64.67
1646	8100.49	64.83	2470	8100.1	64.72
1647	8104.55	64.71	2471	8103.93	64.6
1648	8109.73	64.71	2472	8109.09	64.69
1649	8114.16	64.75	2473	8113.64	64.72
1650	8118.94	64.95	2474	8118.61	64.8
1651	8122.99	64.85	2475	8122.55	64.77
1652	8127.42	64.99	2476	8127.18	64.87
1653	8131.82	65.04	2477	8131.36	64.84
1654	8136.2	65.1	2478	8136.09	64.87
1655	8140.53	65.15	2479	8140.2	64.95
1656	8145.49	65.29	2480	8144.91	65.13
1657	8148.61	65.21	2481	8148.69	65.15
1658	8152.96	65.31	2482	8152.53	65.24
1659	8157.61	65.49	2483	8156.48	65.28
1660	8162.33	65.57	2484	8161.81	65.44
1661	8166.75	65.73	2485	8166.26	65.58
1662	8171.04	65.87	2486	8170.7	65.71
1663	8175.76	65.99	2487	8175.12	65.85
1664	8179.72	66.09	2488	8178.98	65.87
1665	8184.1	66.16	2489	8183.29	66.01
1666	8187.44	66.23	2490	8187.39	66.29
1667	8191.61	66.35	2491	8191.96	66.31
1668	8195.94	66.22	2492	8195.45	66.14
1669	8199.83	66.39	2493	8199.4	66.3

1670	8204.13	66.35	2494	8203.66	66.2
1671	8207.9	66.35	2495	8207.27	66.17
1672	8212.52	66.44	2496	8211.31	66.23
1673	8216.1	66.44	2497	8215.42	66.27
1674	8221.62	66.7	2498	8221.03	66.42
1675	8224.46	66.74	2499	8223.79	66.48
1676	8228.84	66.8	2500	8228.32	66.61
1677	8232.22	66.73	2501	8231.82	66.6
1678	8235.96	66.82	2502	8235.66	66.61
1679	8239.29	66.76	2503	8239.29	66.73
1680	8243.44	66.64	2504	8243.13	66.61
1681	8246.52	66.59	2505	8246.32	66.54
1682	8252	67			
1683	8257	67			
1684	8262	67			
1685	8267	67			
1686	8272	67			
1687	8277	67			
1688	8282	67			
1689	8287	67			
1690	8292	67			
1691	8297	67			
1692	8302	67			
1693	8307	67			
1694	8312	67			
1695	8317	67			
1696	8322	67			
1697	8327	67			
1698	8332	67			
1699	8337	67			
1700	8342	67			
1701	8347	67			
1702	8352	67			
1703	8357	67			
1704	8362	67			
1705	8367	67			
1706	8372	67			
1707	8377	67			
1708	8382	67			
1709	8387	67			
1710	8392	67			
1711	8397	67			
1712	8402	67			
1713	8407	67			
1714	8412	67			
1715	8417	67			
1716	8422	67			
1717	8427	67			

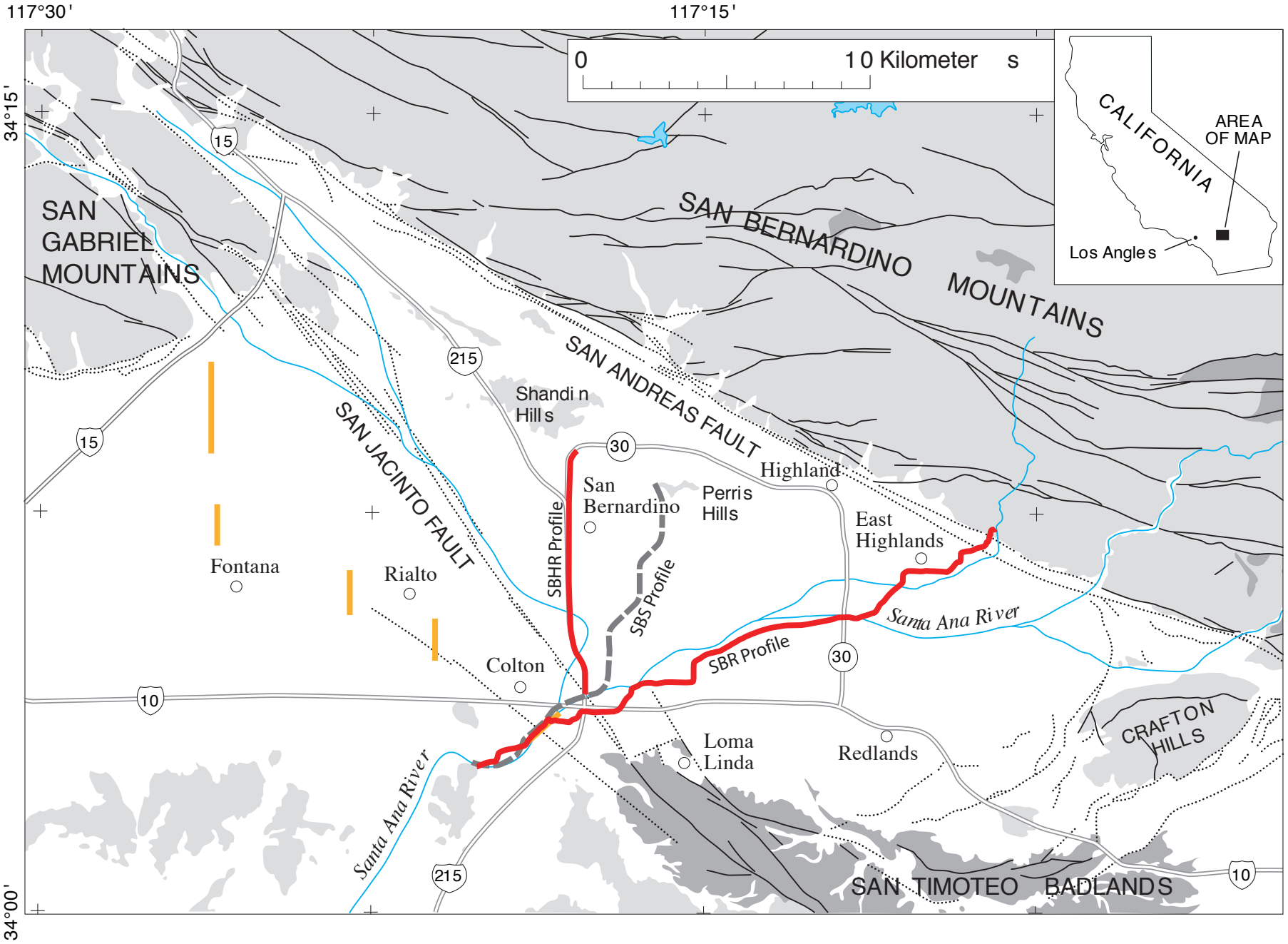
117°30'
117°15'
34°15'
34°00'
0
10 Kilometer s
CALIFORNIA
AREA
OF MAP
Los Angeles
SAN
GABRIEL
MOUNTAINS
SAN BERNARDINO MOUNTAINS
SAN ANDREAS FAULT
SAN JACINTO FAULT
Shandin
Hills
San
Bernardino
Perris
Hills
Highland
East
Highlands
Fontana
Rialto
Colton
SBHR Profile
SBS Profile
SBR Profile
Santa Ana River
Santa Ana River
Loma
Linda
Redlands
CRAFTON
HILLS
SAN TIMOTEO BADLANDS
15
215
30
10

Fig. 1

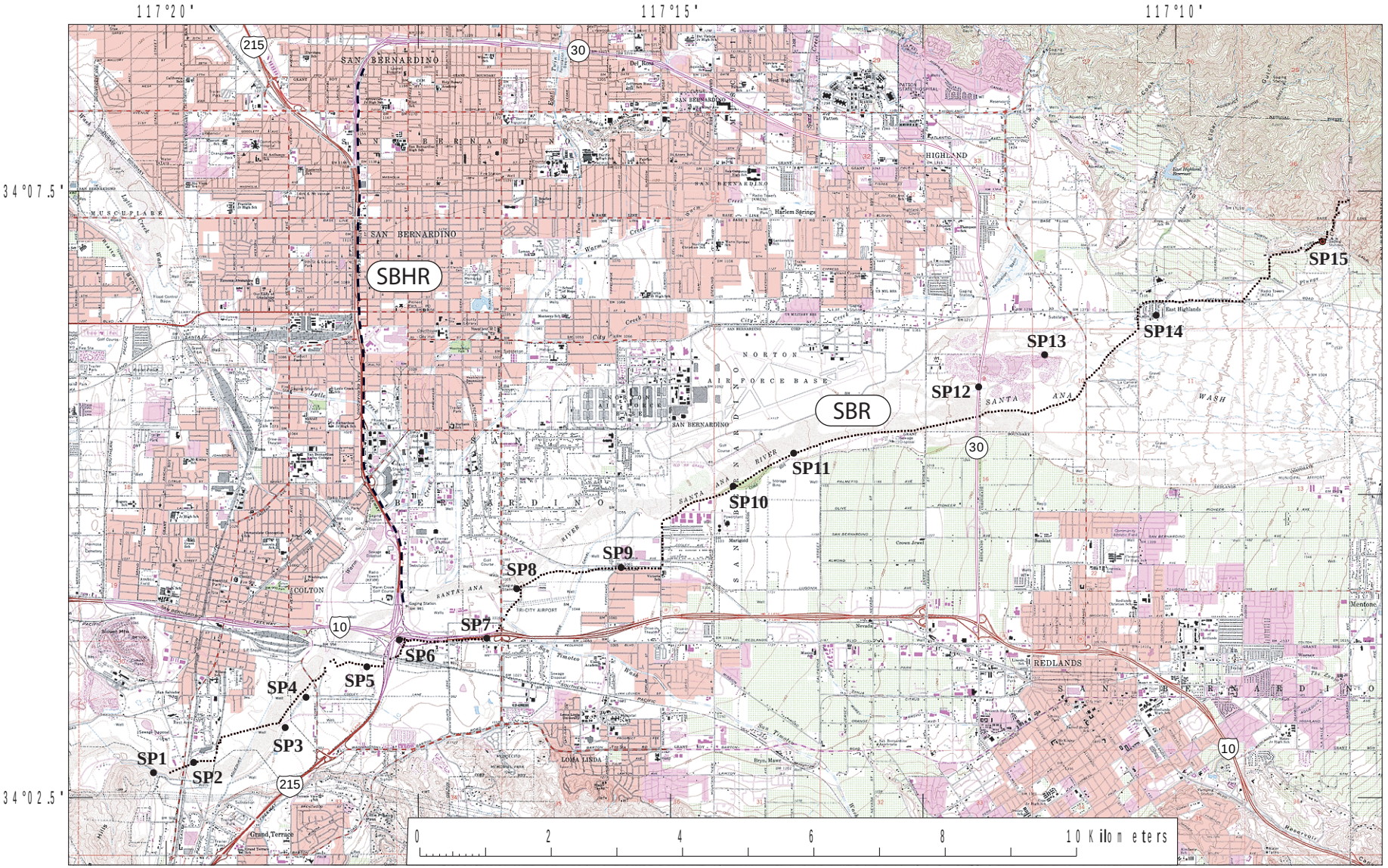
117°20'
117°15'
117°10'
34°07.5'
34°02.5'
SBHR
SBR
SP1
SP2
SP3
SP4
SP5
SP6
SP7
SP8
SP9
SP10
SP11
SP12
SP13
SP14
SP15
SAN BERNARDINO
HIGHLAND
COLTON
REDLANDS
NORTON AIR FORCE BASE
SANTA ANA RIVER
SANTA ANA WASH
0 2 4 6 8 10 Kilometers

Fig. 2

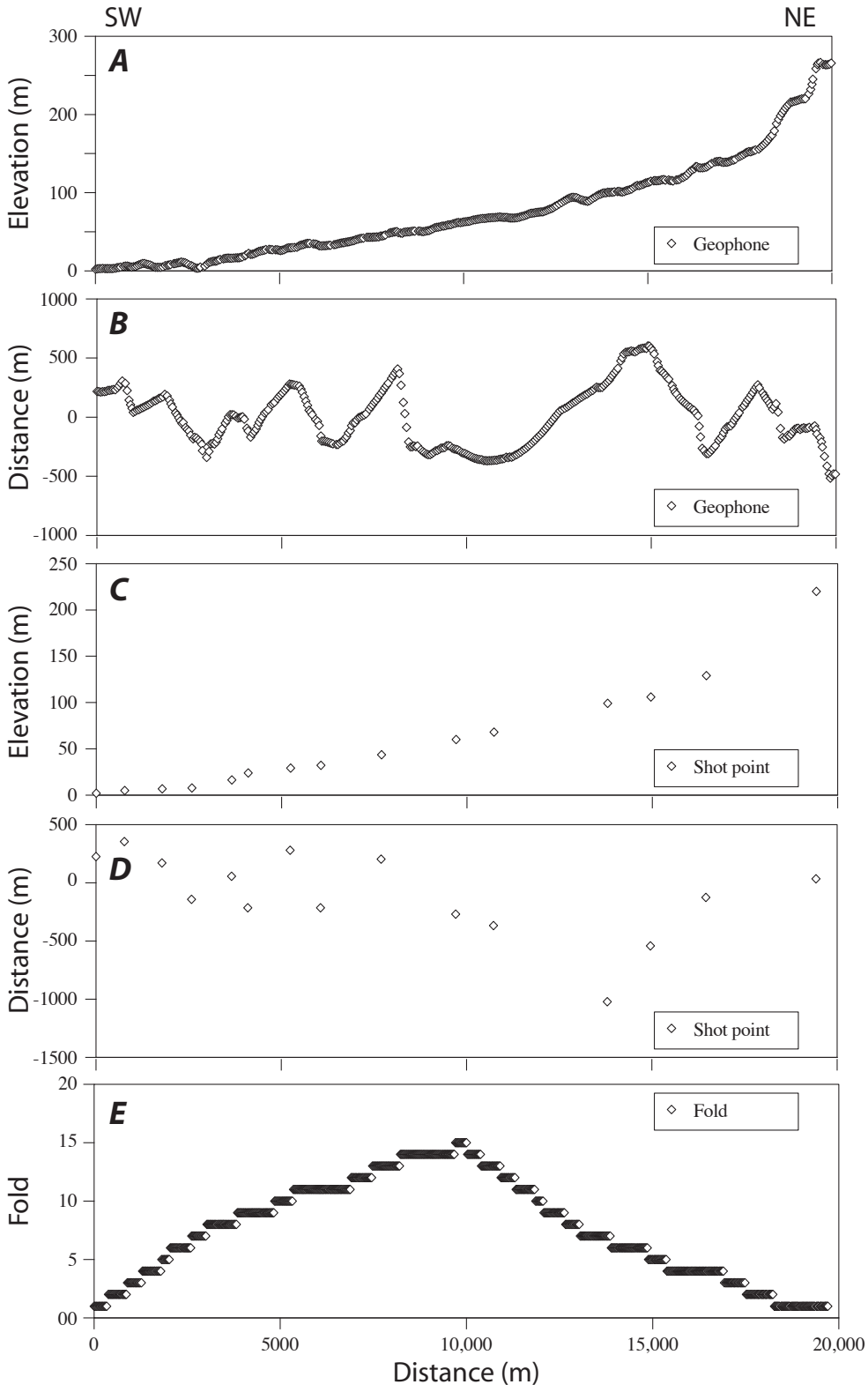
SW
NE
A
Elevation (m)
300
200
100
0
Geophone
B
Distance (m)
1000
500
0
-500
-1000
Geophone
C
Elevation (m)
250
200
150
100
50
0
Shot point
D
Distance (m)
500
0
-500
-1000
-1500
Shot point
E
Fold
20
15
10
5
00
Fold
0
5000
10,000
15,000
20,000
Distance (m)

Fig. 3

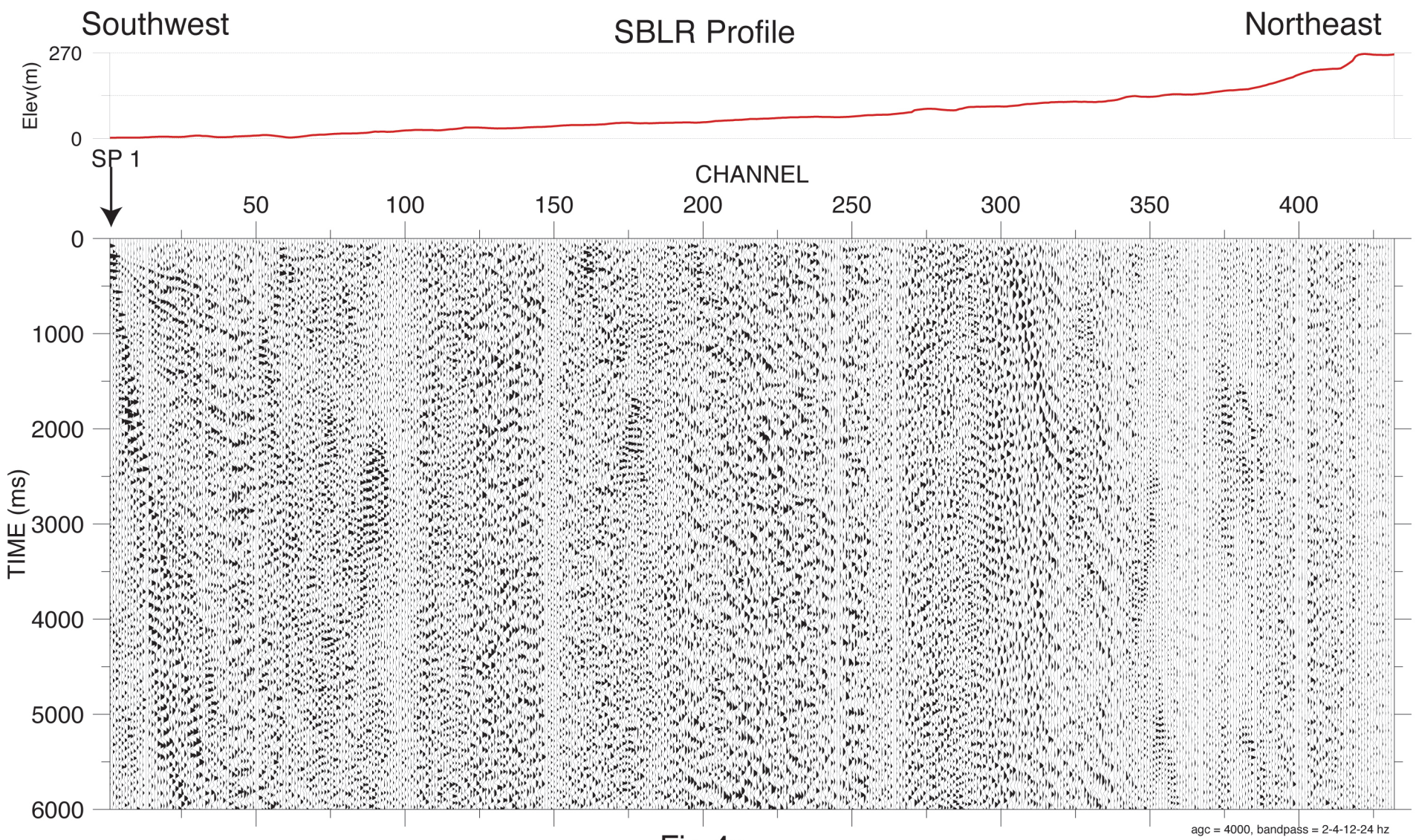
Southwest
SBLR Profile
Northeast
Elev(m)
270
0
SP 1
CHANNEL
50
100
150
200
250
300
350
400
0
1000
2000
3000
4000
5000
6000
TIME (ms)
agc = 4000, bandpass = 2-4-12-24 hz

Fig 4a

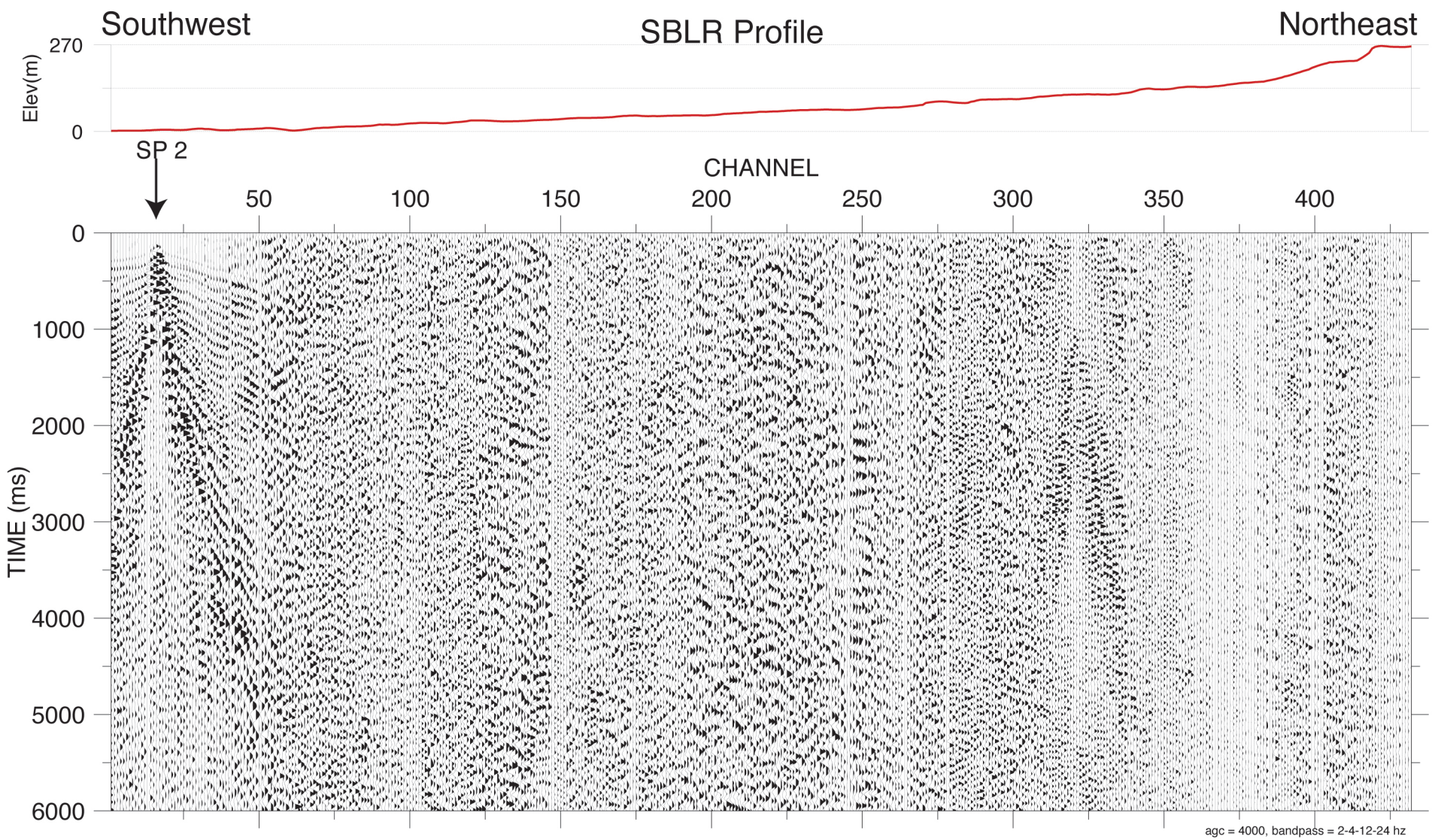
Southwest
SBLR Profile
Northeast
Elev(m)
270
0
SP 2
CHANNEL
50
100
150
200
250
300
350
400
0
1000
2000
3000
4000
5000
6000
TIME (ms)
agc = 4000, bandpass = 2-4-12-24 hz

Fig 4b

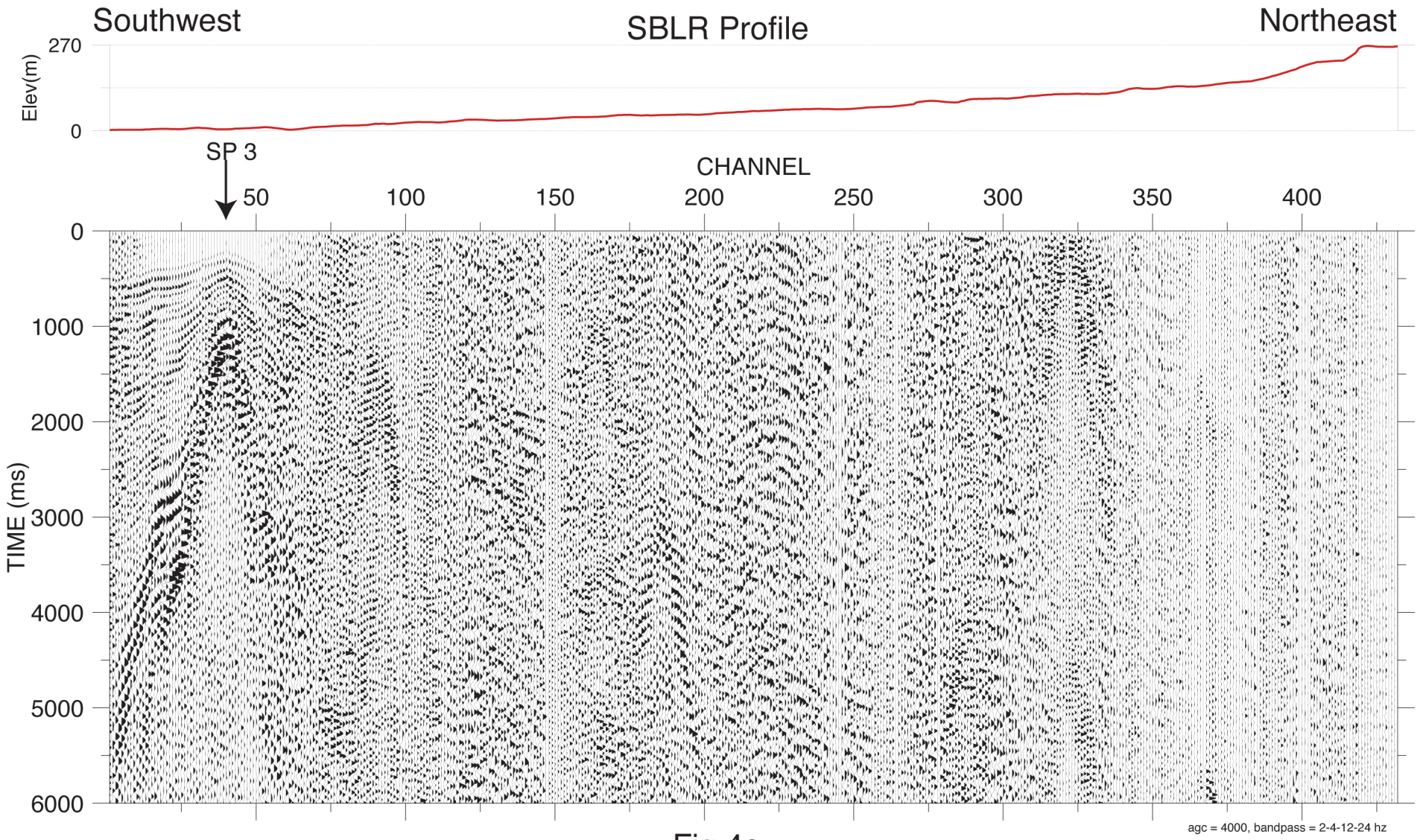
Southwest
SBLR Profile
Northeast
Elev(m)
270
0
SP 3
CHANNEL
50
100
150
200
250
300
350
400
0
1000
2000
3000
4000
5000
6000
TIME (ms)
agc = 4000, bandpass = 2-4-12-24 hz

Fig 4c

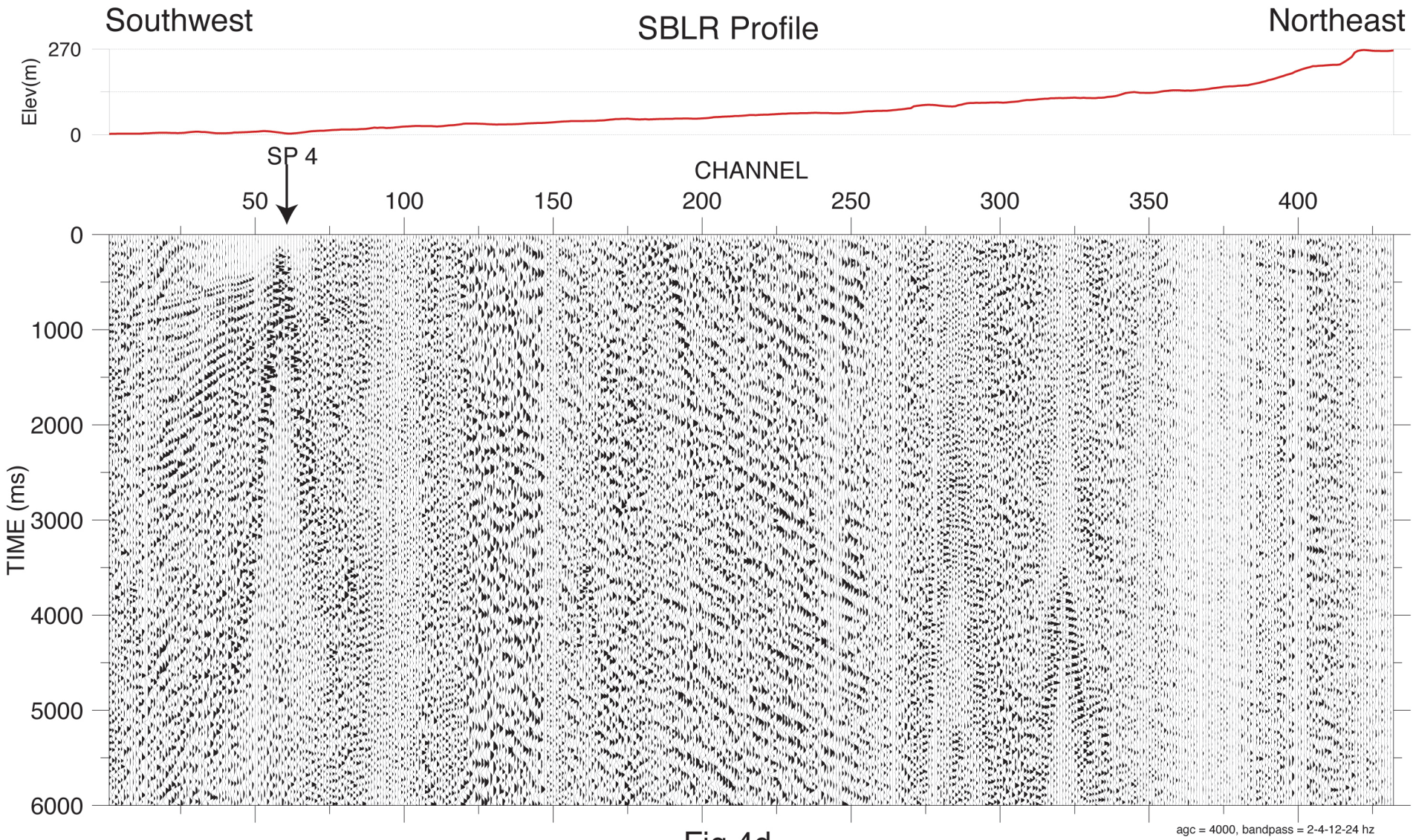
Southwest
SBLR Profile
Northeast
Elev(m)
270
0
SP 4
CHANNEL
50
100
150
200
250
300
350
400
0
1000
2000
3000
4000
5000
6000
TIME (ms)
agc = 4000, bandpass = 2-4-12-24 hz

Fig 4d

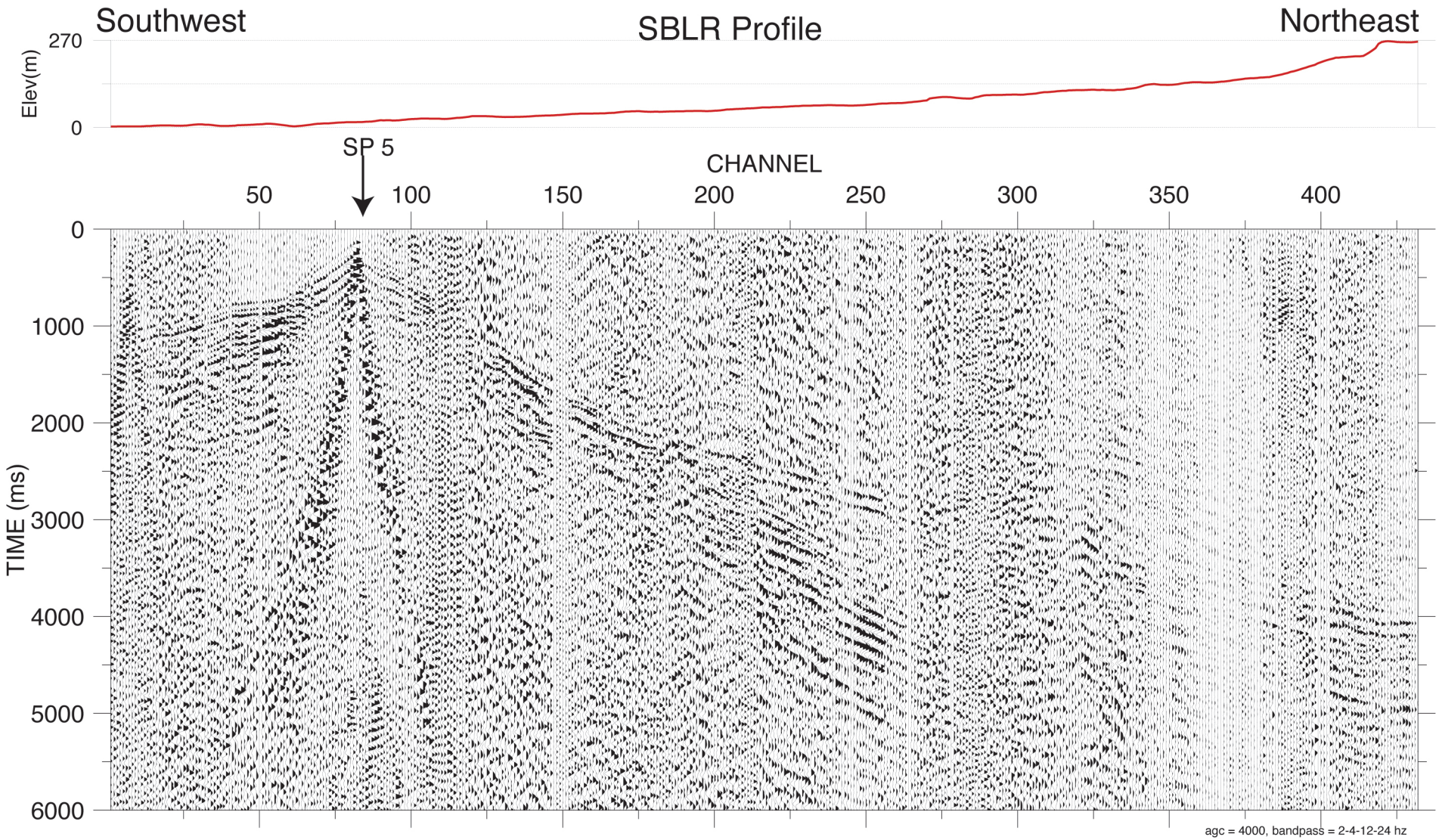
Southwest
SBLR Profile
Northeast
Elev(m)
270
0
SP 5
CHANNEL
50
100
150
200
250
300
350
400
0
1000
2000
3000
4000
5000
6000
TIME (ms)
agc = 4000, bandpass = 2-4-12-24 hz

Fig 4e

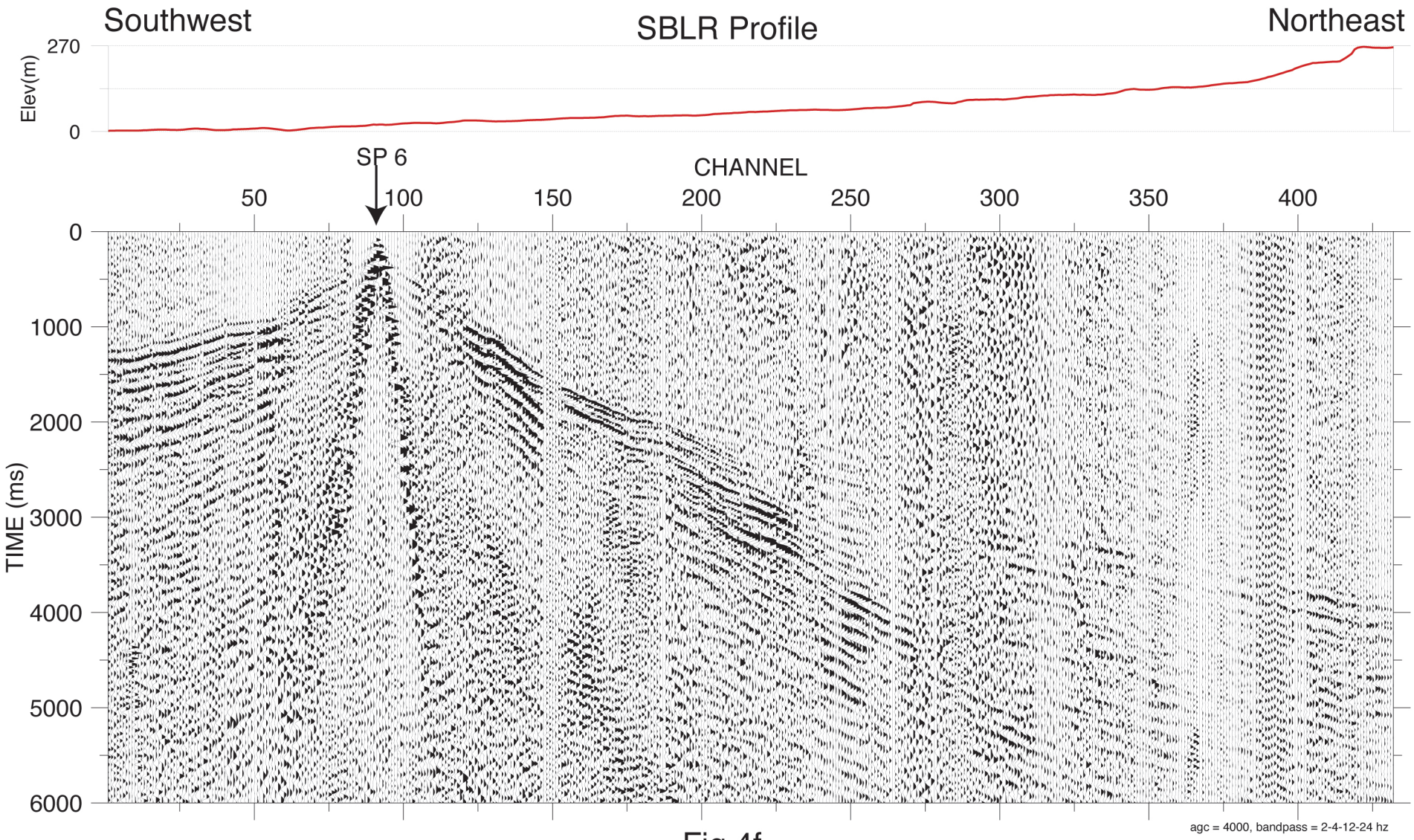
Southwest
SBLR Profile
Northeast
Elev(m)
270
0
SP 6
CHANNEL
50
100
150
200
250
300
350
400
0
1000
2000
3000
4000
5000
6000
TIME (ms)
agc = 4000, bandpass = 2-4-12-24 hz

Fig 4f

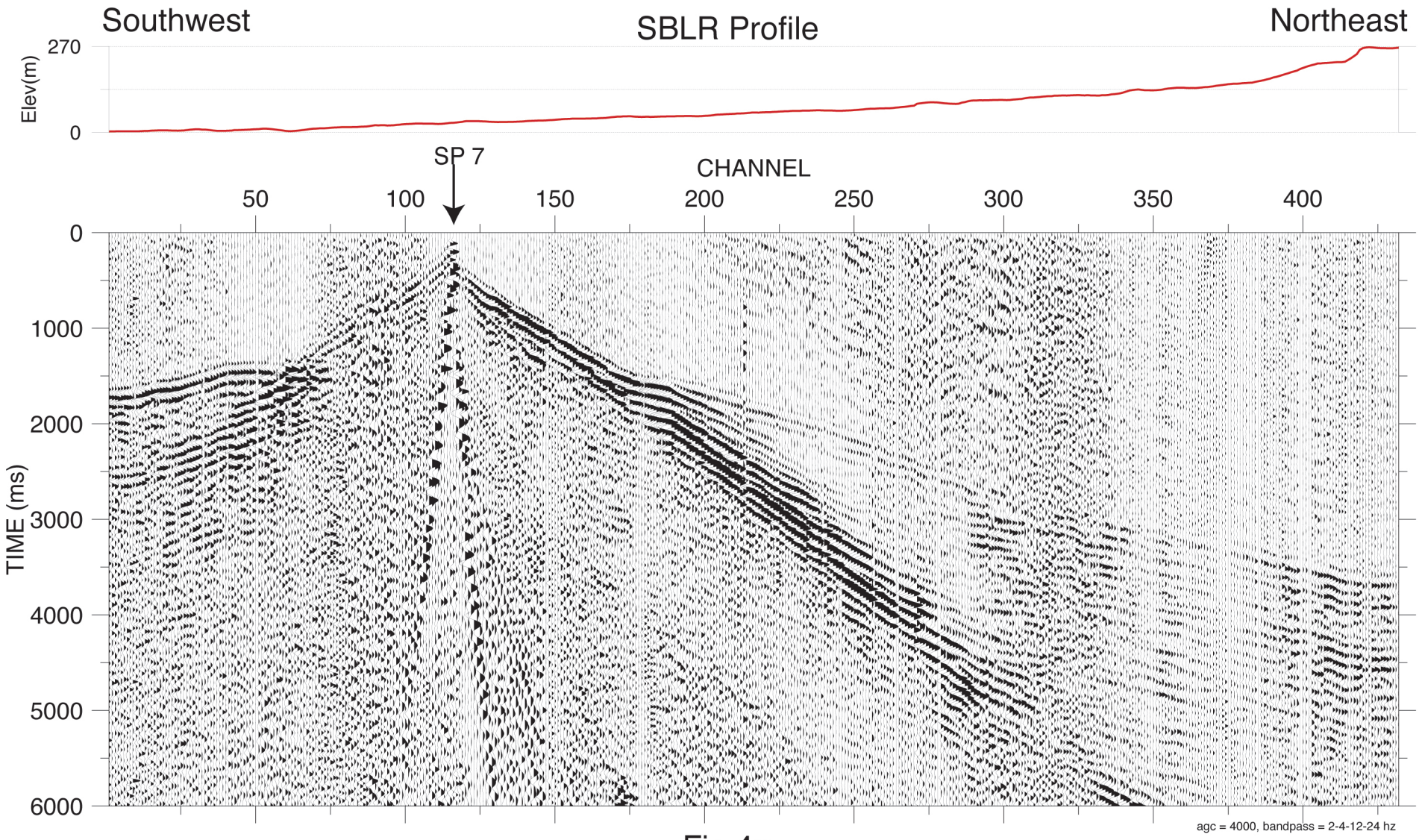
Southwest
SBLR Profile
Northeast
Elev(m)
270
0
SP 7
CHANNEL
50
100
150
200
250
300
350
400
0
1000
2000
3000
4000
5000
6000
TIME (ms)
agc = 4000, bandpass = 2-4-12-24 hz

Fig 4g

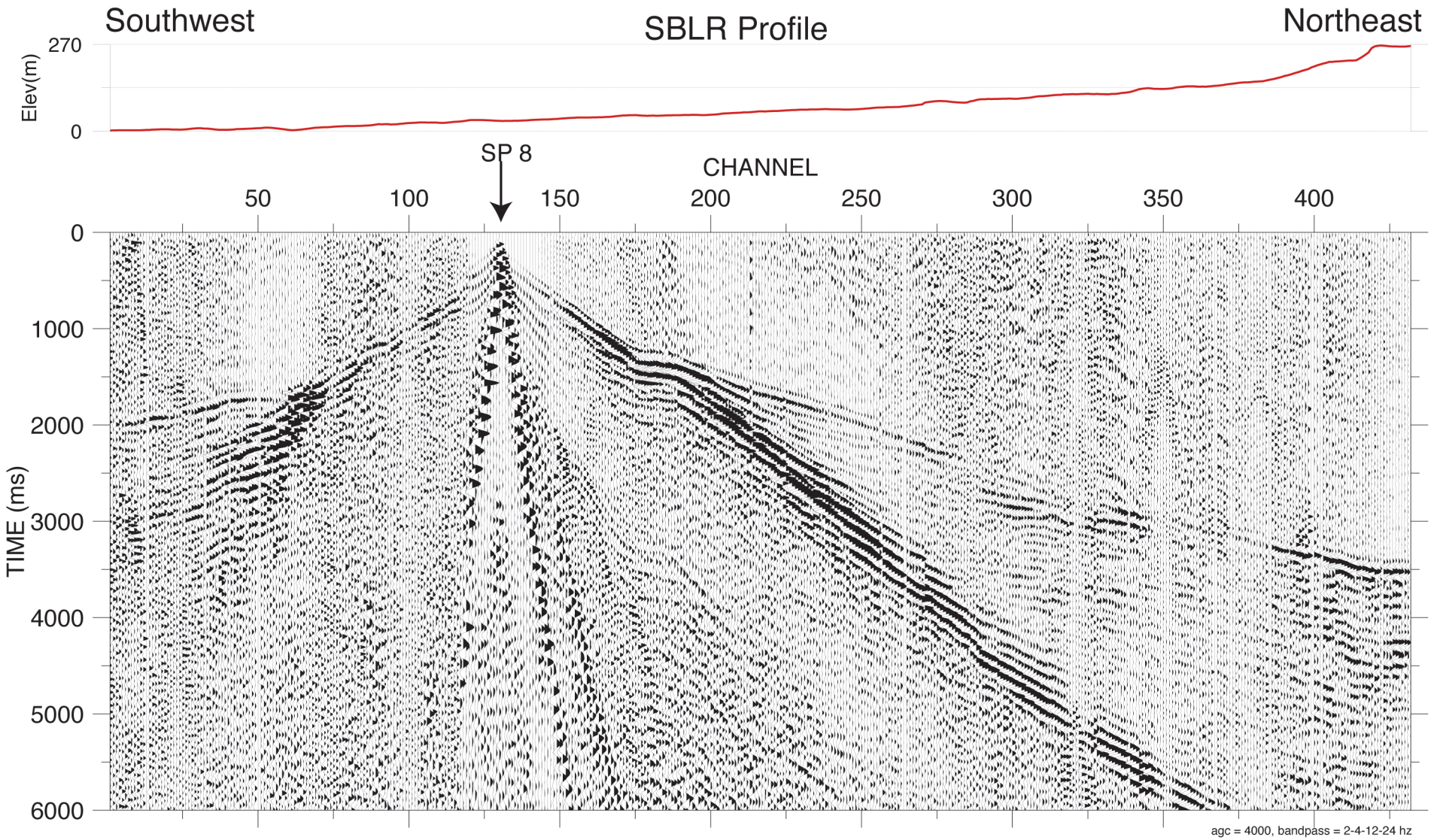
Southwest
SBLR Profile
Northeast
Elev(m)
270
0
SP 8
CHANNEL
50
100
150
200
250
300
350
400
0
1000
2000
3000
4000
5000
6000
TIME (ms)
agc = 4000, bandpass = 2-4-12-24 hz

Fig 4h

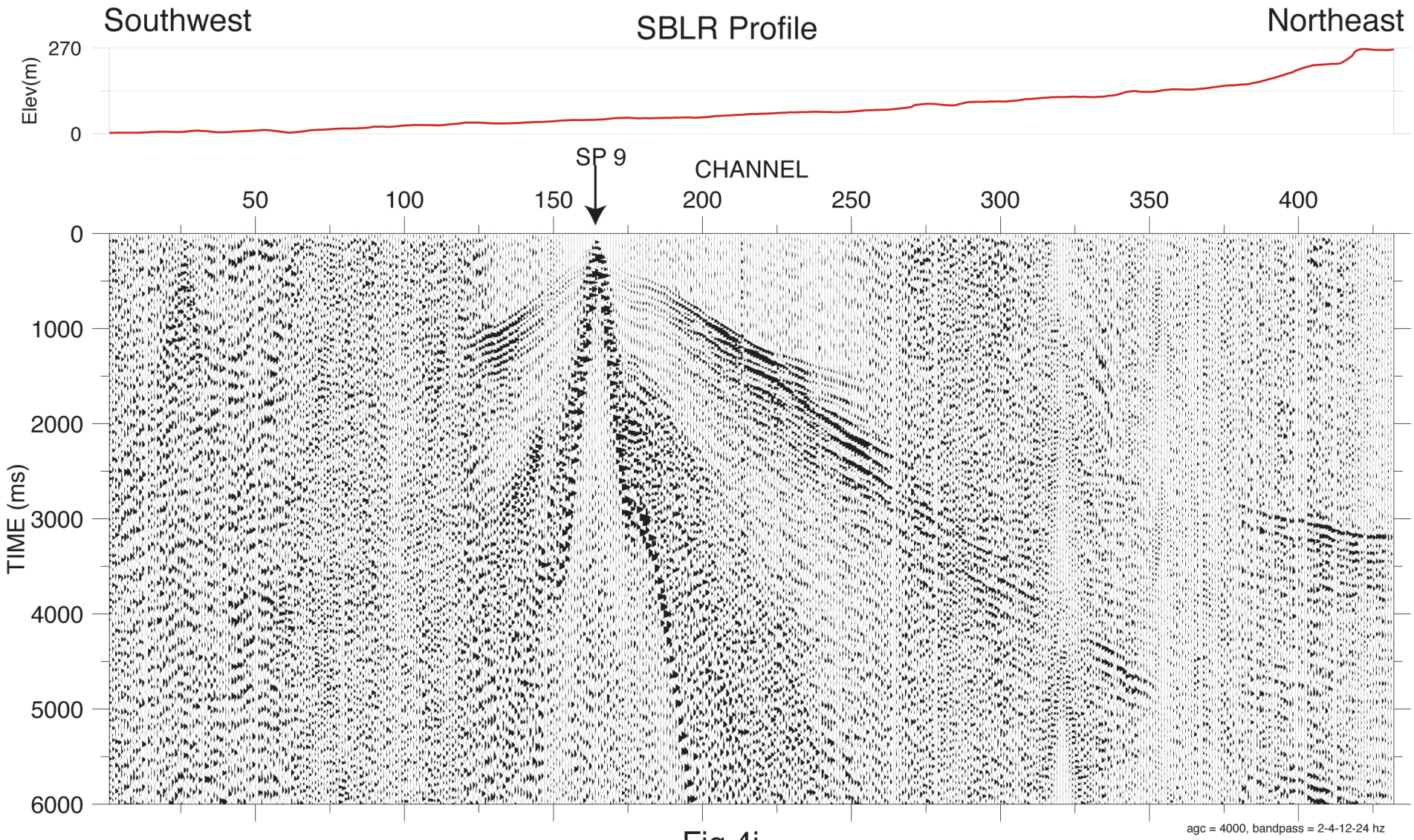
Southwest
SBLR Profile
Northeast
Elev(m)
270
0
SP 9
CHANNEL
50
100
150
200
250
300
350
400
0
1000
2000
3000
4000
5000
6000
TIME (ms)
agc = 4000, bandpass = 2-4-12-24 hz

Fig 4i

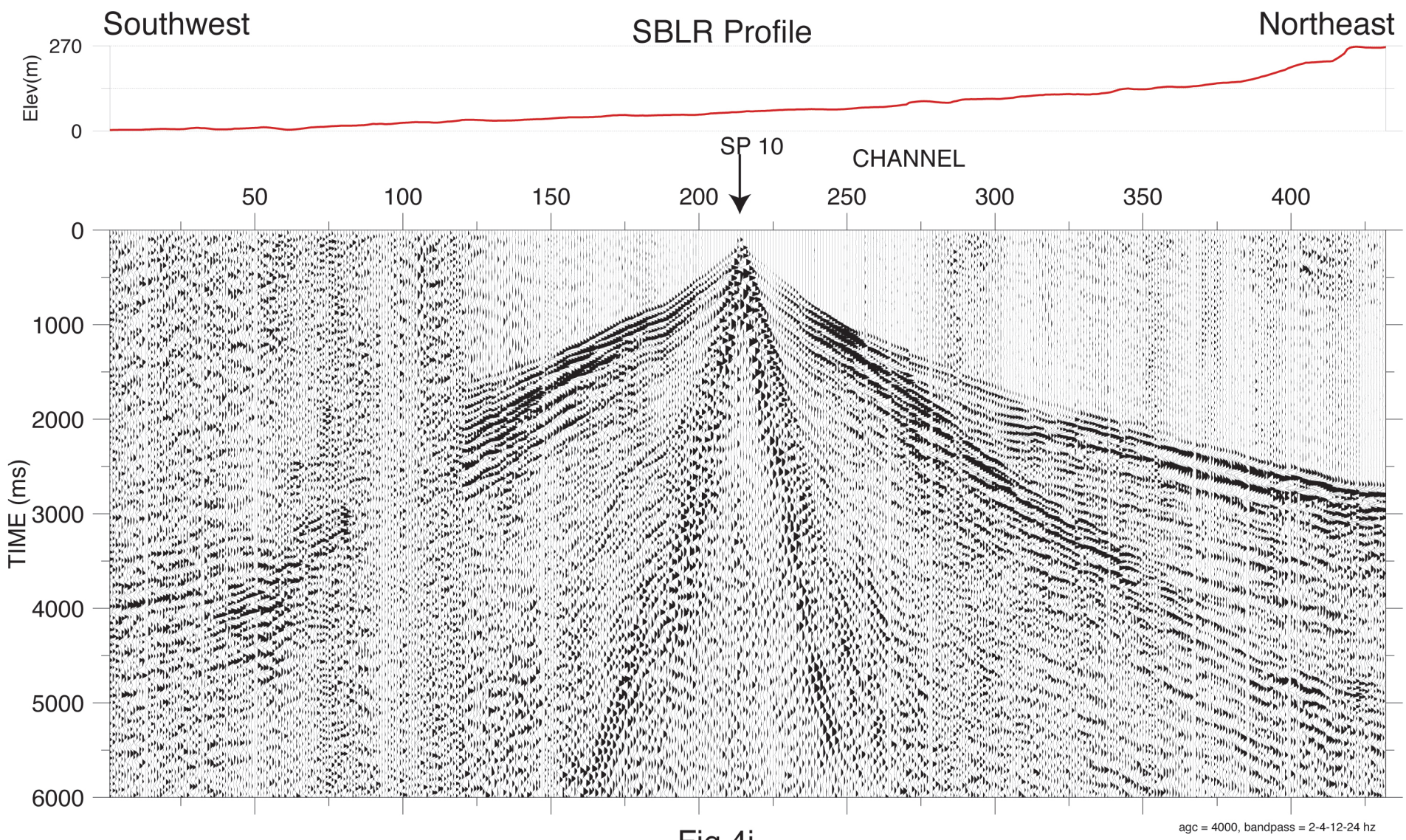
Southwest
SBLR Profile
Northeast
Elev(m)
270
0
SP 10
CHANNEL
50
100
150
200
250
300
350
400
0
1000
2000
3000
4000
5000
6000
TIME (ms)
agc = 4000, bandpass = 2-4-12-24 hz

Fig 4j

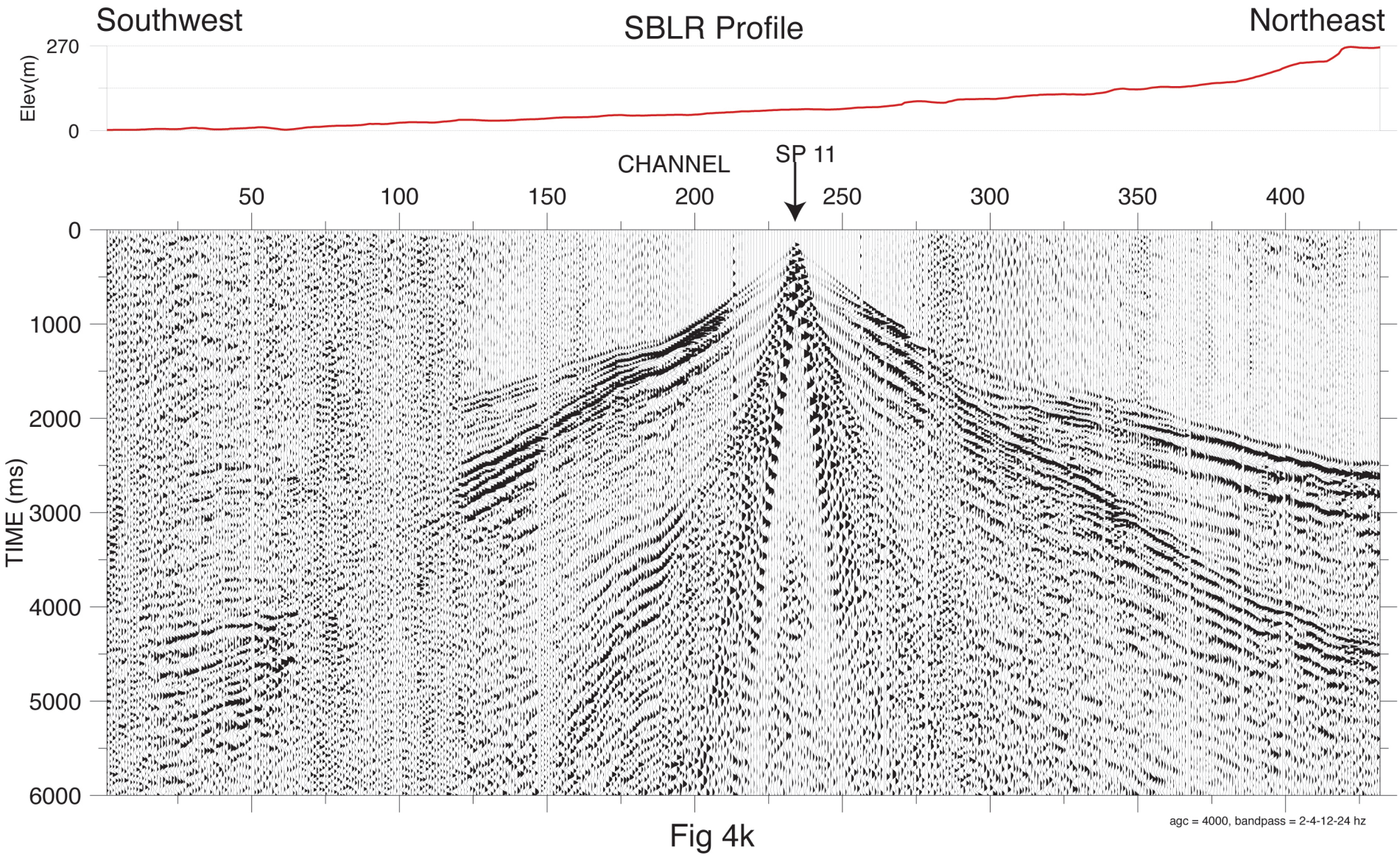
Southwest
SBLR Profile
Northeast
Elev(m)
270
0
CHANNEL
SP 11
50
100
150
200
250
300
350
400
0
1000
2000
3000
4000
5000
6000
TIME (ms)
agc = 4000, bandpass = 2-4-12-24 hz

Fig 4k

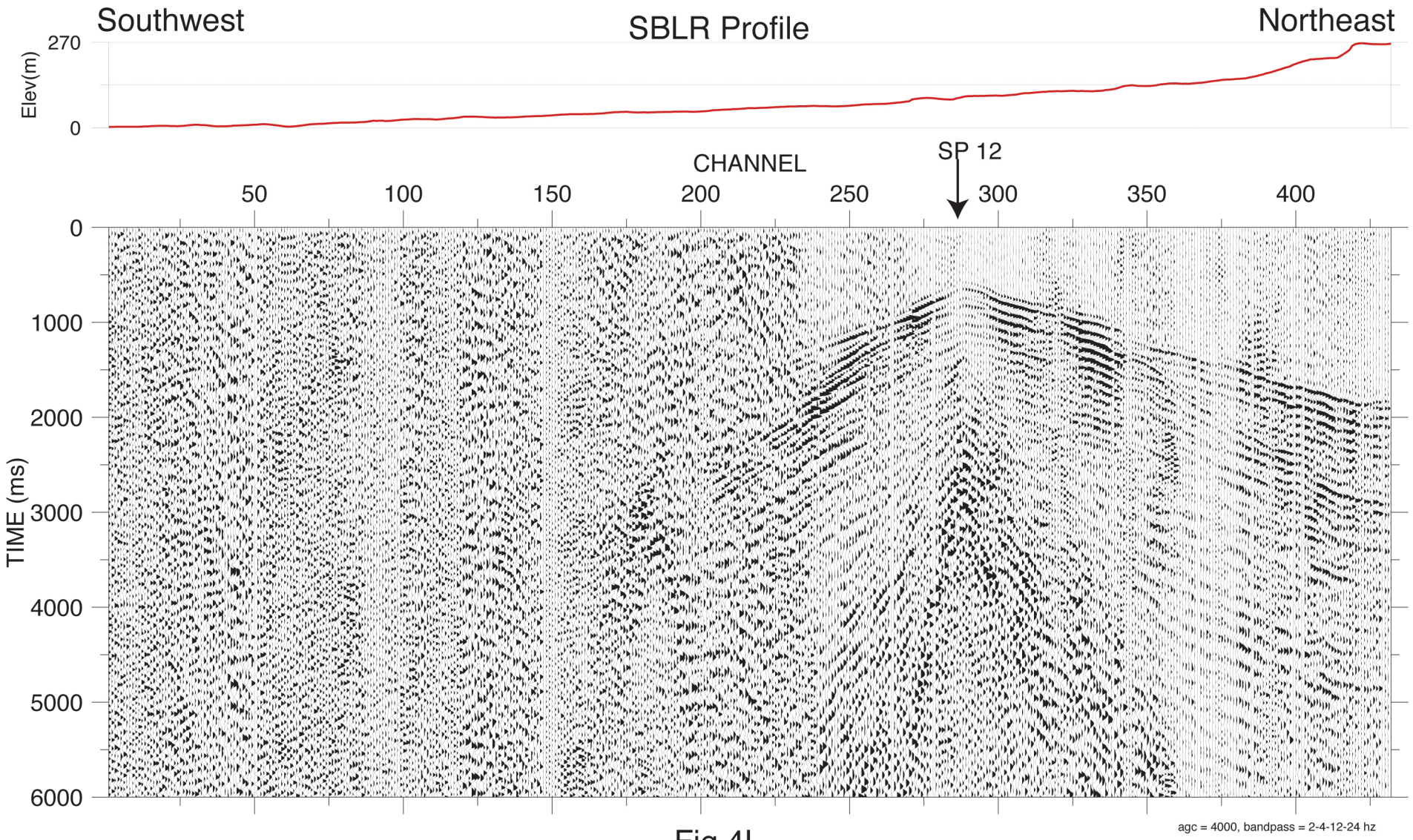
Southwest
SBLR Profile
Northeast
Elev(m)
270
0
CHANNEL
SP 12
50
100
150
200
250
300
350
400
0
1000
2000
3000
4000
5000
6000
TIME (ms)
agc = 4000, bandpass = 2-4-12-24 hz

Fig 4L

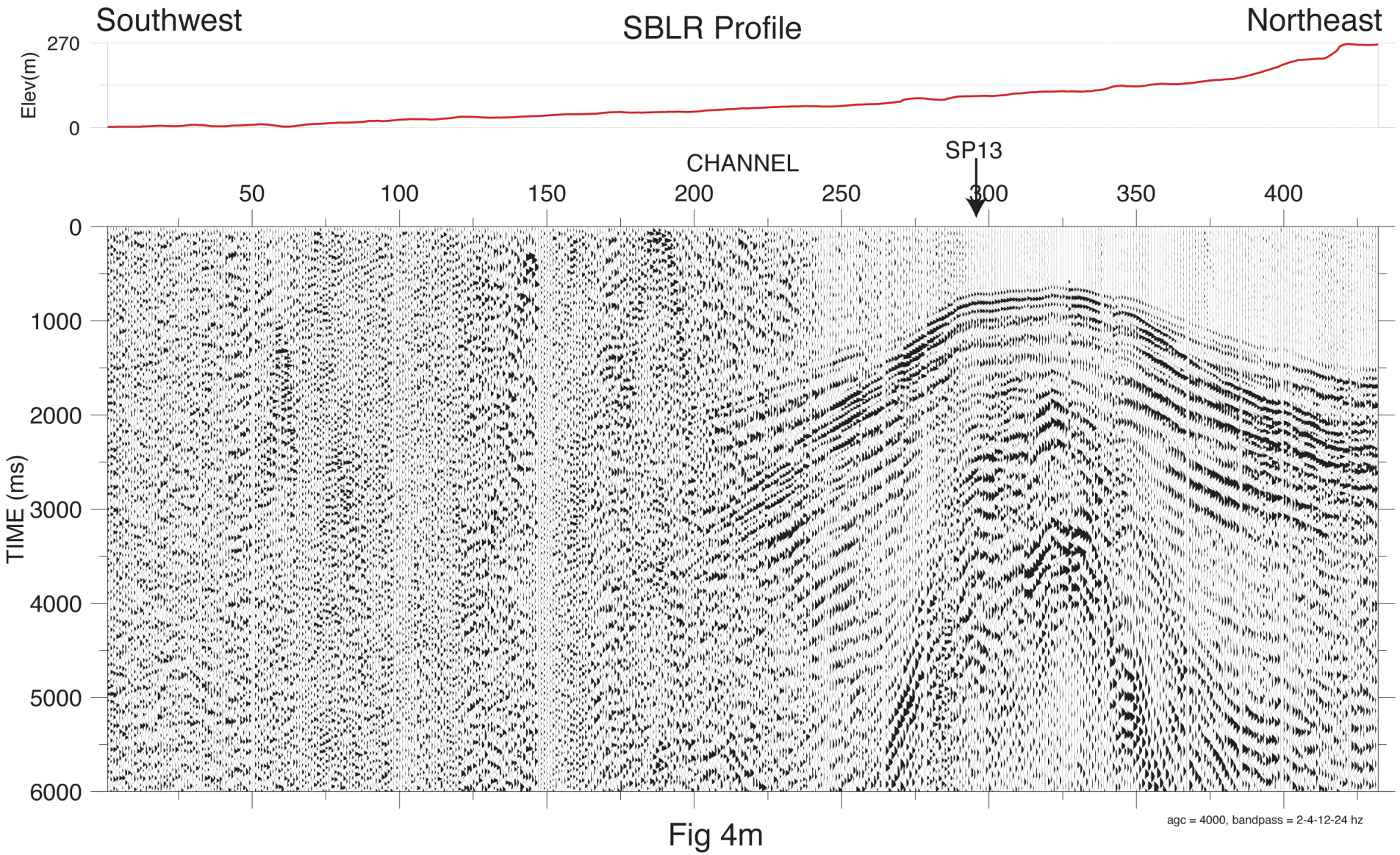
Southwest
SBLR Profile
Northeast
Elev(m)
270
0
CHANNEL
SP13
50
100
150
200
250
300
350
400
0
1000
2000
3000
4000
5000
6000
TIME (ms)
agc = 4000, bandpass = 2-4-12-24 hz

Fig 4m

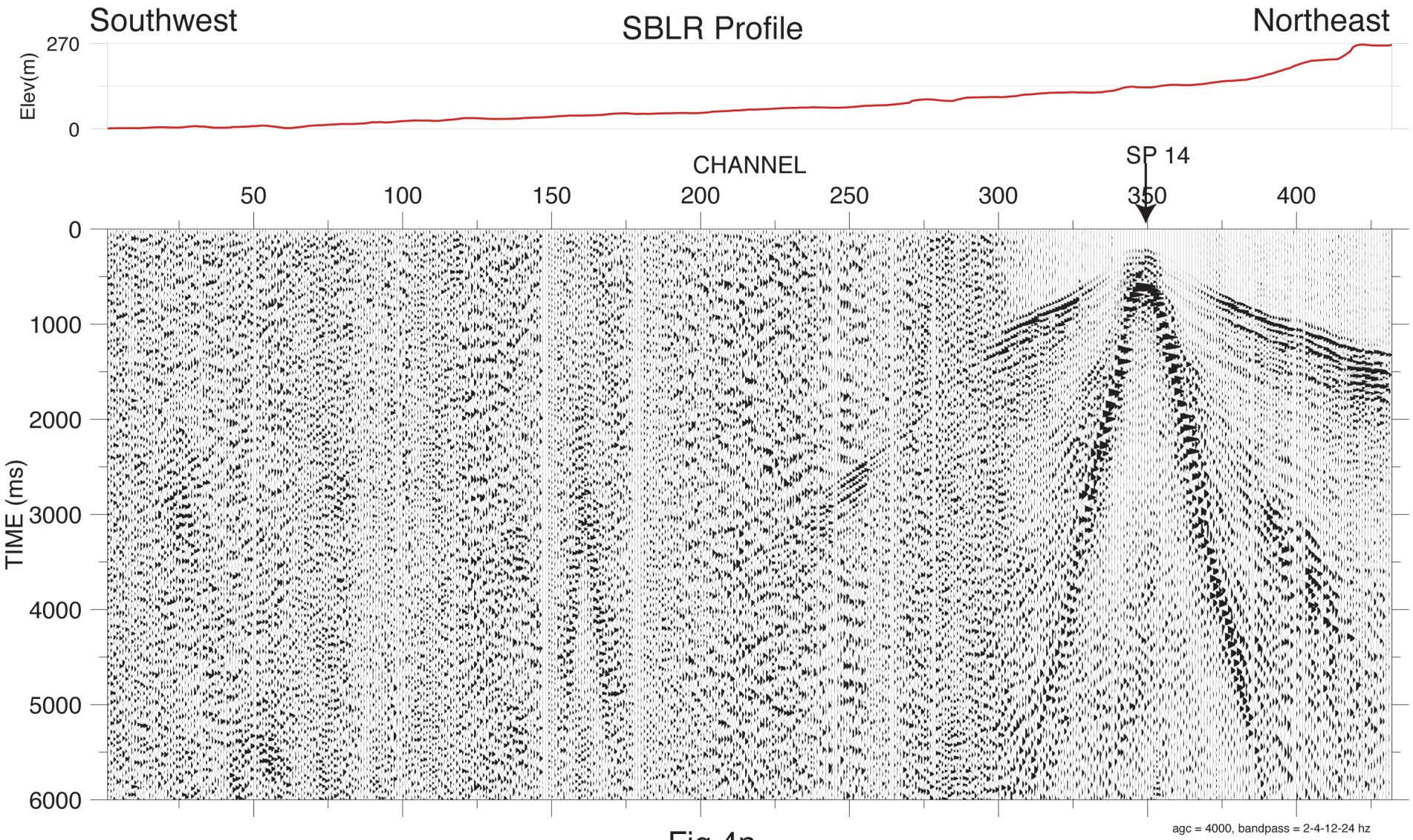
Southwest
SBLR Profile
Northeast
Elev(m)
270
0
CHANNEL
SP 14
50
100
150
200
250
300
350
400
0
1000
2000
3000
4000
5000
6000
TIME (ms)
agc = 4000, bandpass = 2-4-12-24 hz

Fig 4n

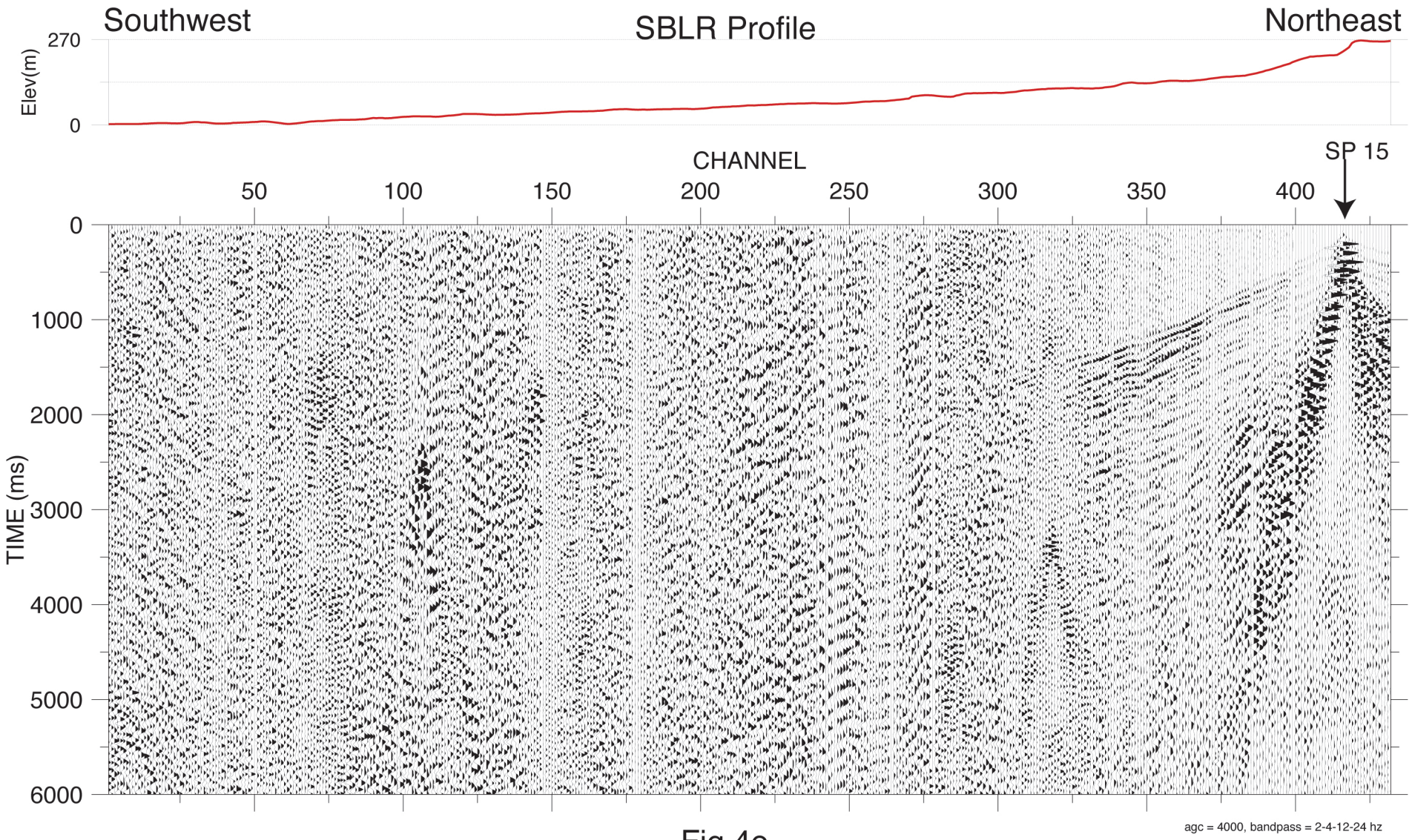
Southwest
SBLR Profile
Northeast
Elev(m)
270
0
CHANNEL
50
100
150
200
250
300
350
400
SP 15
0
1000
2000
3000
4000
5000
6000
TIME (ms)
agc = 4000, bandpass = 2-4-12-24 hz

Fig 4o

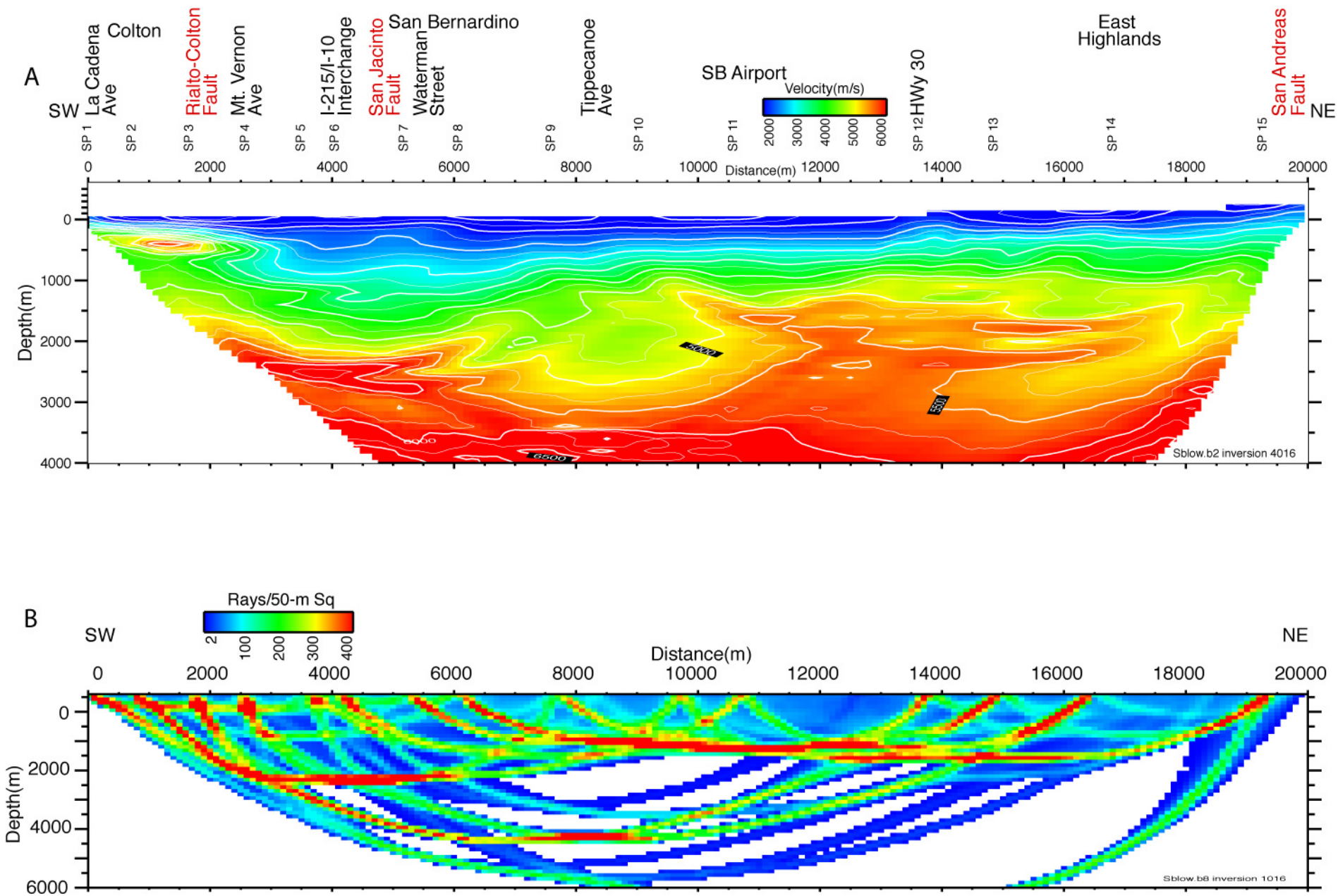
A
SW
NE
La Cadena Ave
Colton
Rialto-Colton Fault
Mt. Vernon Ave
I-215/I-10 Interchange
San Jacinto Fault
San Bernardino
Waterman Street
Tippecanoe Ave
SB Airport
HWy 30
East Highlands
San Andreas Fault
Velocity(m/s)
2000
3000
4000
5000
6000
SP 1
SP 2
SP 3
SP 4
SP 5
SP 6
SP 7
SP 8
SP 9
SP 10
SP 11
SP 12
SP 13
SP 14
SP 15
0
2000
4000
6000
8000
10000
Distance(m)
12000
14000
16000
18000
20000
Depth(m)
0
1000
2000
3000
4000
5000
5500
6000
6500
Sblow.b2 inversion 4016
B
SW
NE
Rays/50-m Sq
2
100
200
300
400
Distance(m)
0
2000
4000
6000
8000
10000
12000
14000
16000
18000
20000
Depth(m)
0
2000
4000
6000
Sblow.b8 inversion 1016

Fig. 5

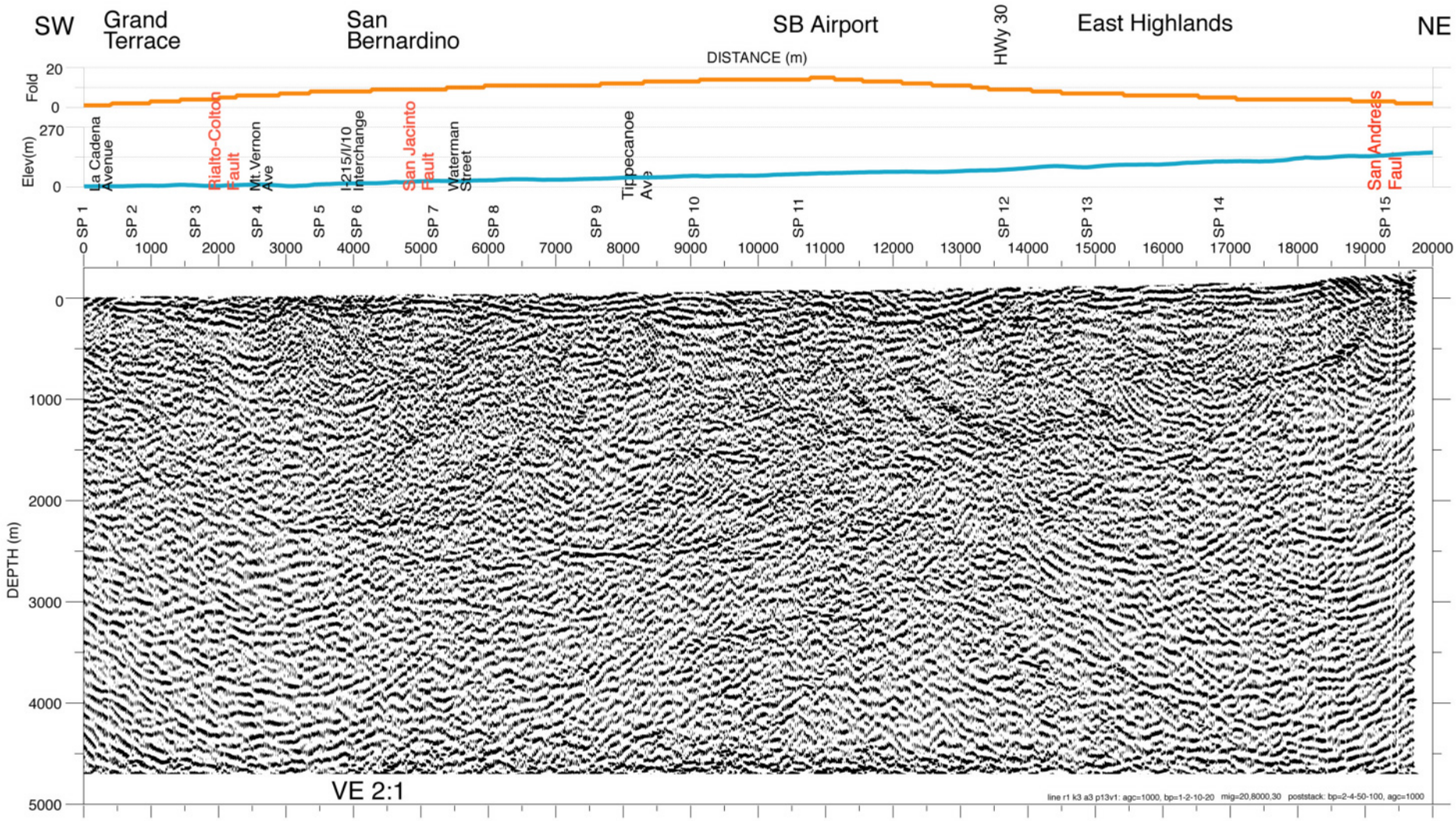
SW
Grand Terrace
San Bernardino
SB Airport
HWy 30
East Highlands
NE
DISTANCE (m)
Fold
20
0
Elev(m)
270
0
La Cadena Avenue
Rialto-Colton Fault
Mt. Vernon Ave
I-215/I-10 Interchange
San Jacinto Fault
Waterman Street
Tippecanoe Ave
San Andreas Fault
SP 1
SP 2
SP 3
SP 4
SP 5
SP 6
SP 7
SP 8
SP 9
SP 10
SP 11
SP 12
SP 13
SP 14
SP 15
0
1000
2000
3000
4000
5000
6000
7000
8000
9000
10000
11000
12000
13000
14000
15000
16000
17000
18000
19000
20000
DEPTH (m)
0
1000
2000
3000
4000
5000
VE 2:1
line r1 k3 a3 p13v1: agc=1000, bp=1-2-10-20 mig=20,8000,30 poststack: bp=2-4-50-100, agc=1000

Fig.6

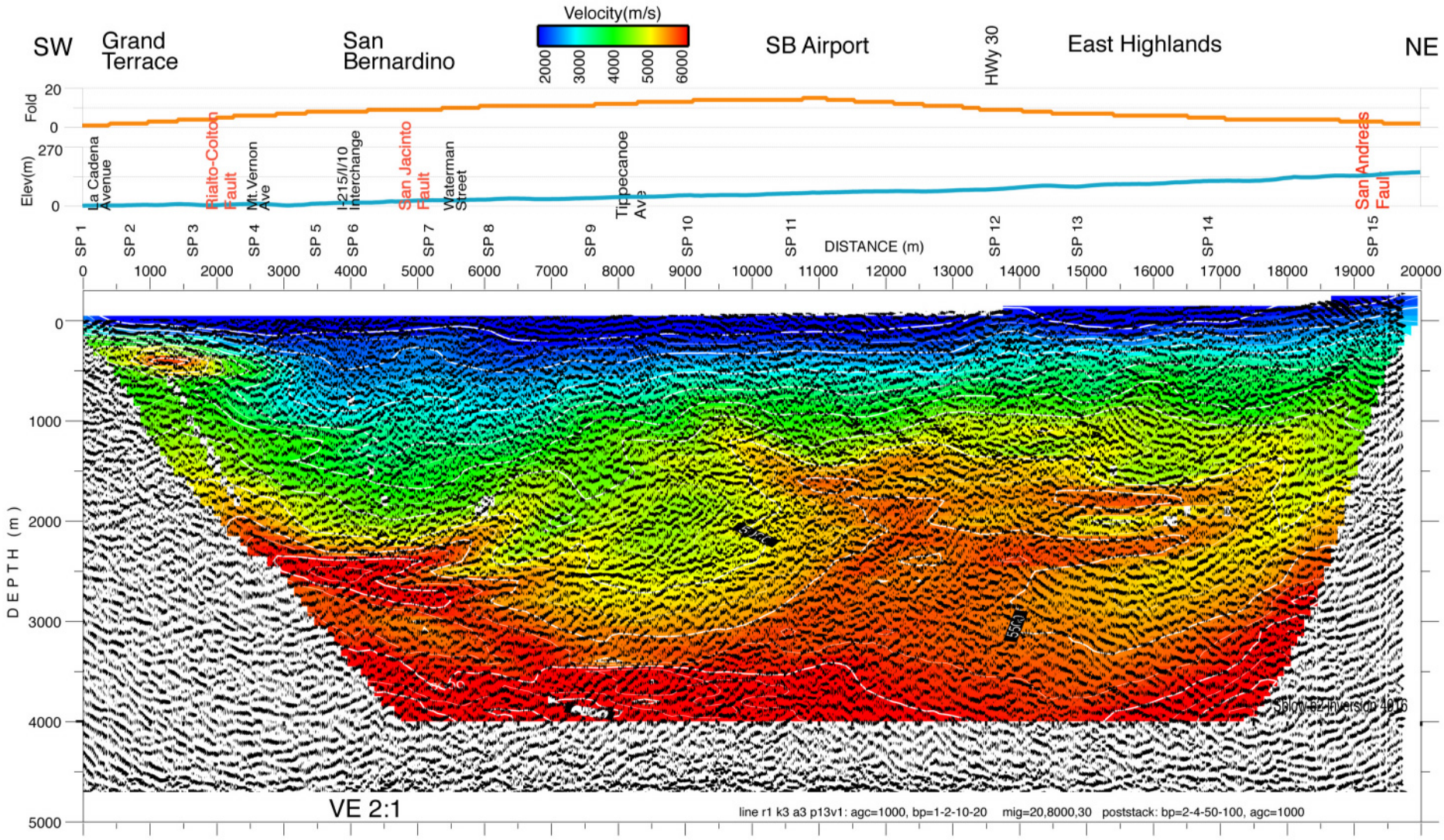
SW
Grand Terrace
San Bernardino
SB Airport
HWy 30
East Highlands
NE
Velocity(m/s)
2000
3000
4000
5000
6000
Fold
Elev(m)
La Cadena Avenue
Rialto-Colton Fault
Mt.Vernon Ave
I-215/I-10 Interchange
San Jacinto Fault
Waterman Street
Tippecanoe Ave
San Andreas Faul
SP 1
SP 2
SP 3
SP 4
SP 5
SP 6
SP 7
SP 8
SP 9
SP 10
SP 11
SP 12
SP 13
SP 14
SP 15
DISTANCE (m)
DEPTH (m)
VE 2:1
line r1 k3 a3 p13v1: agc=1000, bp=1-2-10-20 mig=20,8000,30 poststack: bp=2-4-50-100, agc=1000

Fig. 7

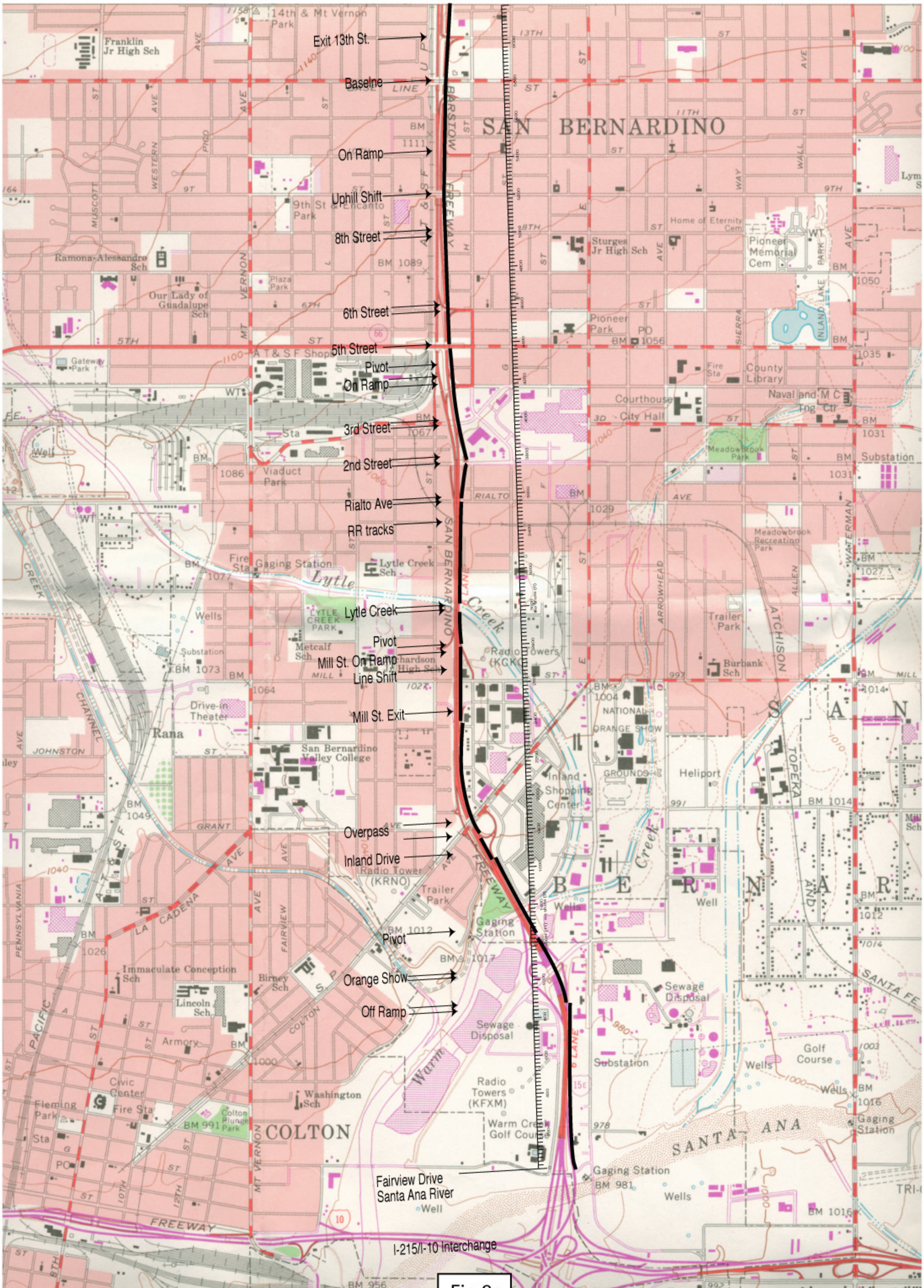
Exit 13th St.
Baselne
On Ramp
Uphill Shift
8th Street
6th Street
5th Street
Pivot
On Ramp
3rd Street
2nd Street
Rialto Ave
RR tracks
Lytle Creek
Pivot
Mill St. On Ramp
Line Shift
Mill St. Exit
Overpass
Inland Drive
Pivot
Orange Show
Off Ramp
Fairview Drive
Santa Ana River
I-215/I-10 Interchange
SAN BERNARDINO
COLTON
SANTA ANA
San Bernardino Valley College
Inland Shopping Center
National Orange Show Grounds
Franklin Jr High Sch
Sturges Jr High Sch
Pioneer Memorial Cem
County Library
Courthouse
City Hall
Meadowbrook Park
Lytle Creek Park
Heliport
Sewage Disposal
Warm Creek Golf Course
Immaculate Conception Sch
Lincoln Sch
Washington Sch
Civic Center
Fleming Park
Colton Plunge Park

Fig 8a

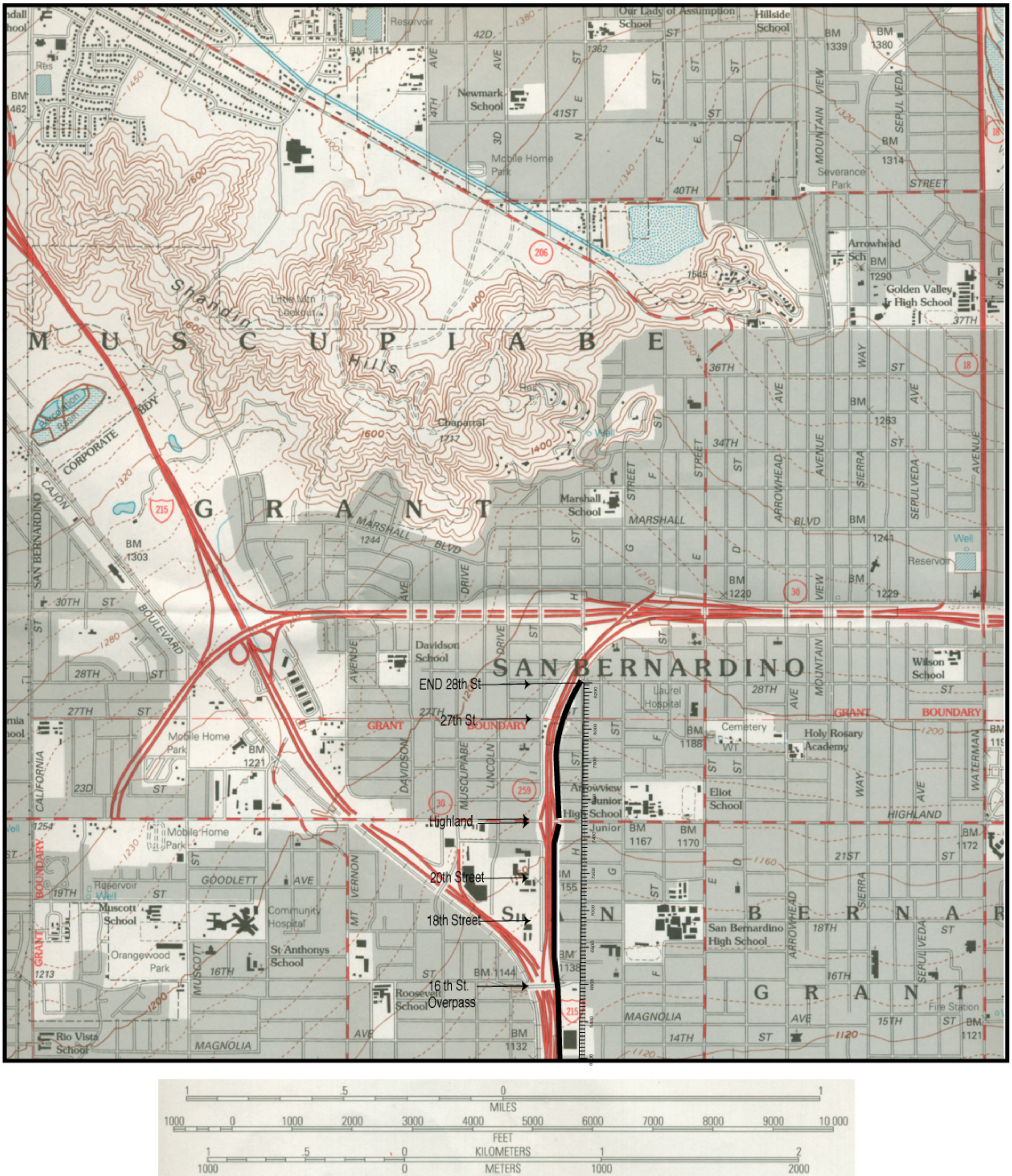
END 28th St
27th St
Highland
20th Street
18th Street
16 th St.
Overpass
SAN BERNARDINO
MUSCUPIABE
GRANT
Shandin Hills
Little Mtn Lookout
Chaparral
1717
Marshall School
Davidson School
Arrowview Junior High School
Eliot School
San Bernardino High School
Muscott School
St Anthonys School
Roosevelt School
Rio Vista School
Newmark School
Our Lady of Assumption School
Hillside School
Arrowhead Sch
Golden Valley High School
Wilson School
Holy Rosary Academy
Laurel Hospital
Community Hospital
Cemetery
Mobile Home Park
Orangewood Park
Severance Park
MARSHALL BLVD
HIGHLAND
MAGNOLIA
GOODLETT
CORPORATE BDY
GRANT BOUNDARY
MILES
FEET
KILOMETERS
METERS
1000 0 1000 2000 3000 4000 5000 6000 7000 8000 9000 10 000

Fig 8b

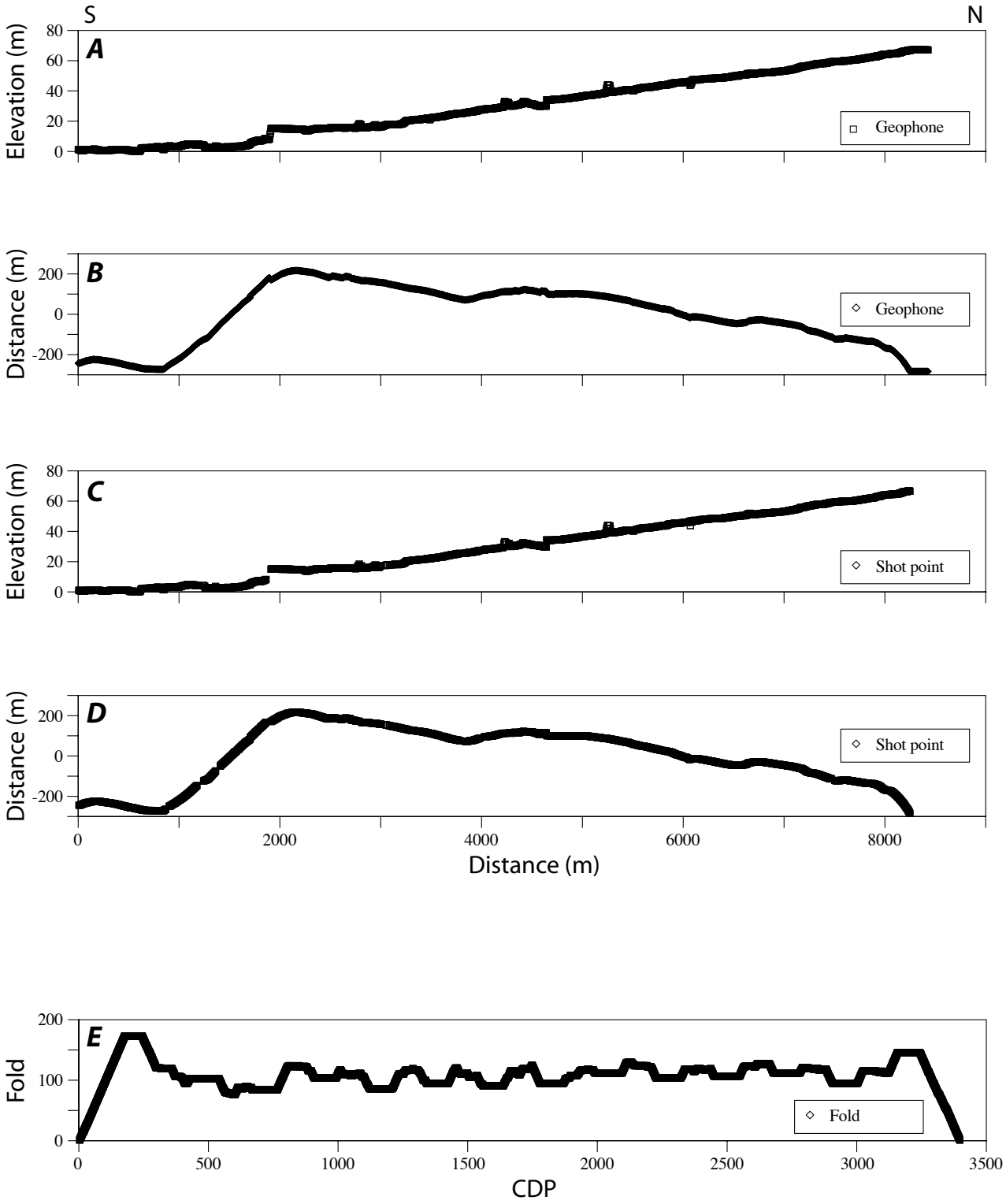
S
N
A
Elevation (m)
80
60
40
20
0
Geophone
B
Distance (m)
200
0
-200
Geophone
C
Elevation (m)
80
60
40
20
0
Shot point
D
Distance (m)
200
0
-200
Shot point
0
2000
4000
6000
8000
Distance (m)
E
Fold
200
100
0
Fold
0
500
1000
1500
2000
2500
3000
3500
CDP

Fig. 9

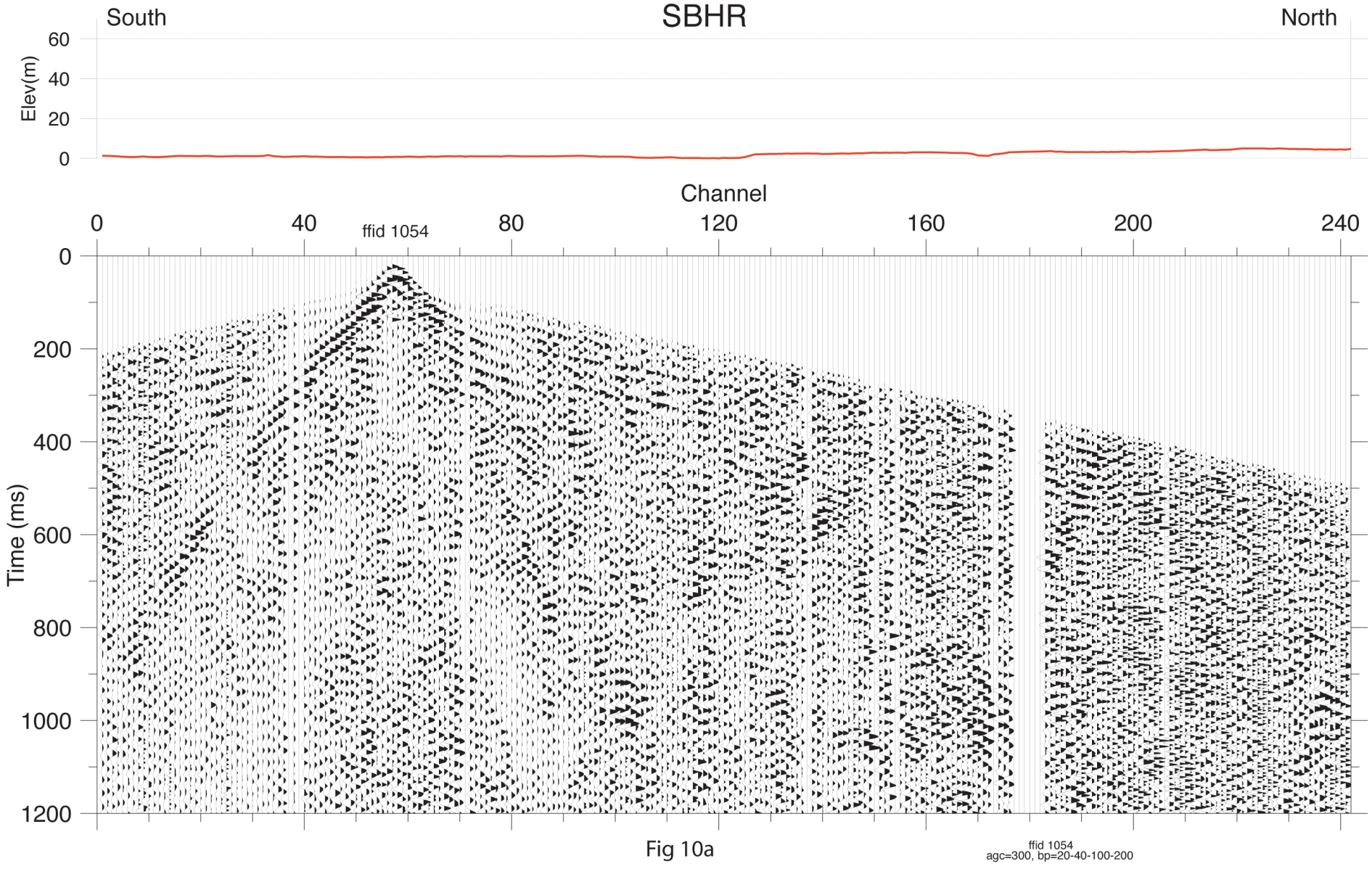
South
SBHR
North
Elev(m)
60
40
20
0
Channel
0
40
80
120
160
200
240
ffid 1054
0
200
400
600
800
1000
1200
Time (ms)
ffid 1054
agc=300, bp=20-40-100-200

Fig 10a

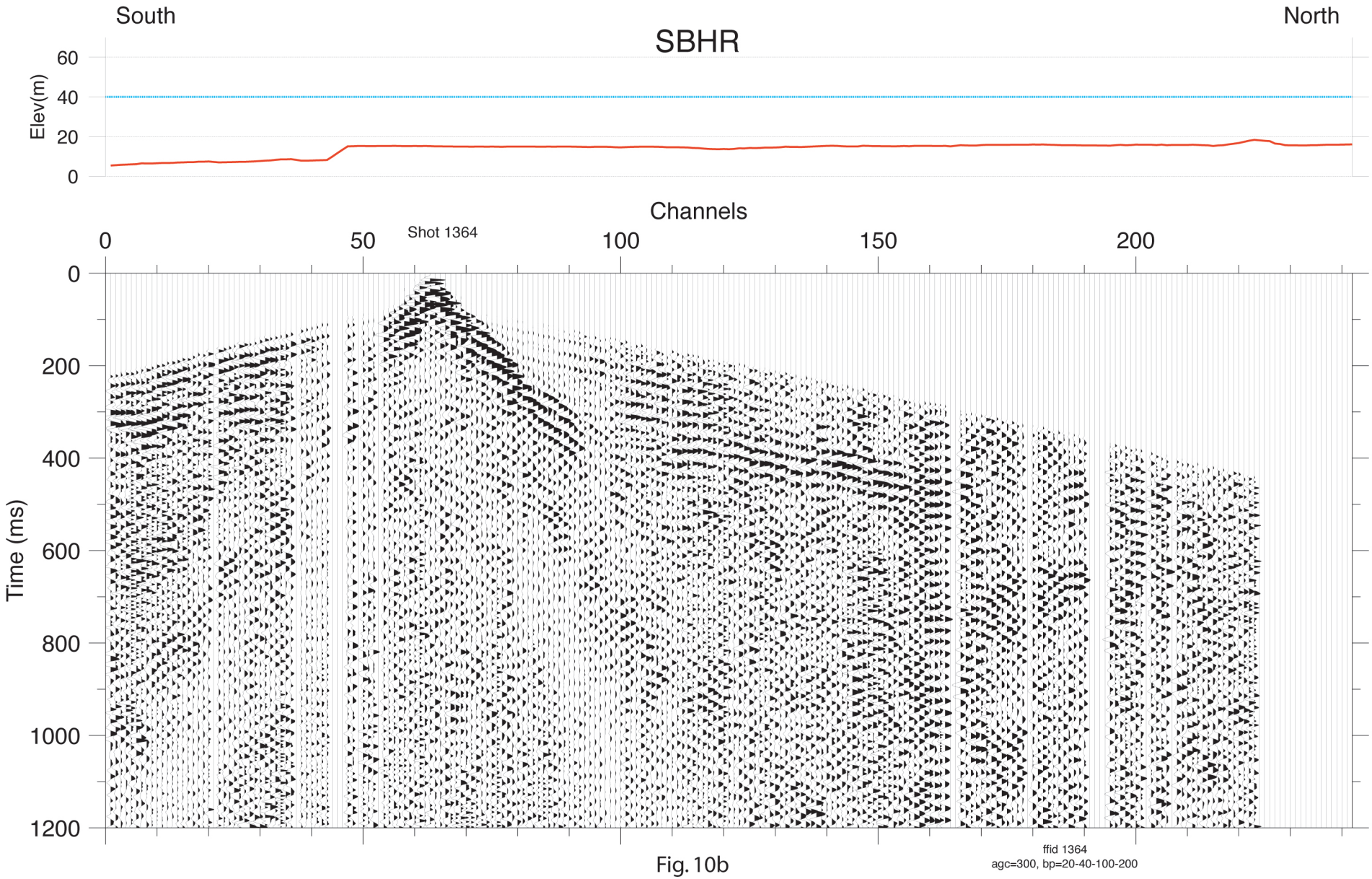
South
North
SBHR
Elev(m)
60
40
20
0
Channels
0
50
Shot 1364
100
150
200
Time (ms)
0
200
400
600
800
1000
1200
ffid 1364
agc=300, bp=20-40-100-200

Fig. 10b

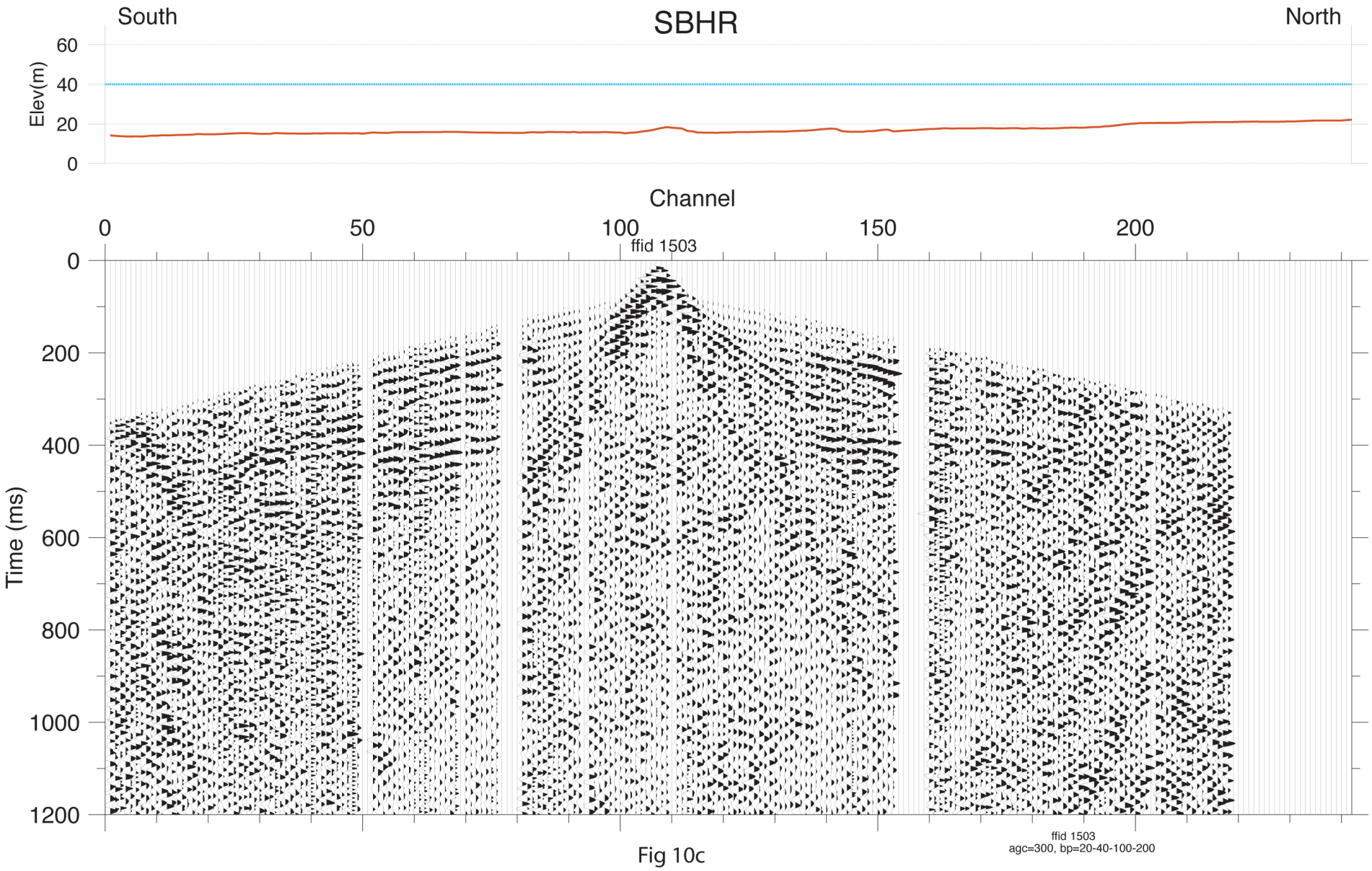
South
SBHR
North
Elev(m)
60
40
20
0
Channel
0
50
100
150
200
ffid 1503
Time (ms)
0
200
400
600
800
1000
1200
ffid 1503
agc=300, bp=20-40-100-200

Fig 10c

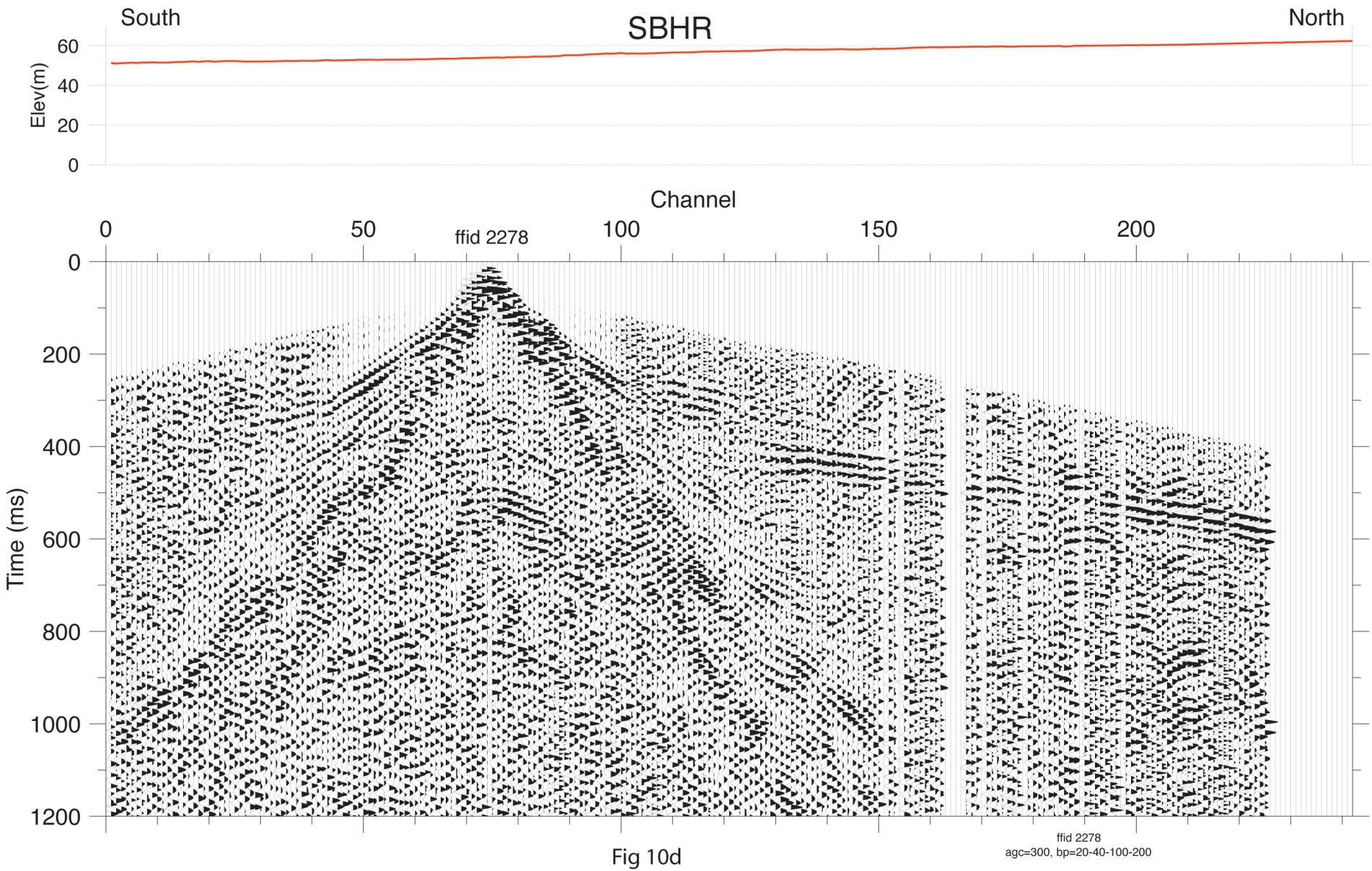
South
SBHR
North
Elev(m)
60
40
20
0
Channel
0
50
ffid 2278
100
150
200
Time (ms)
0
200
400
600
800
1000
1200
ffid 2278
agc=300, bp=20-40-100-200

Fig 10d

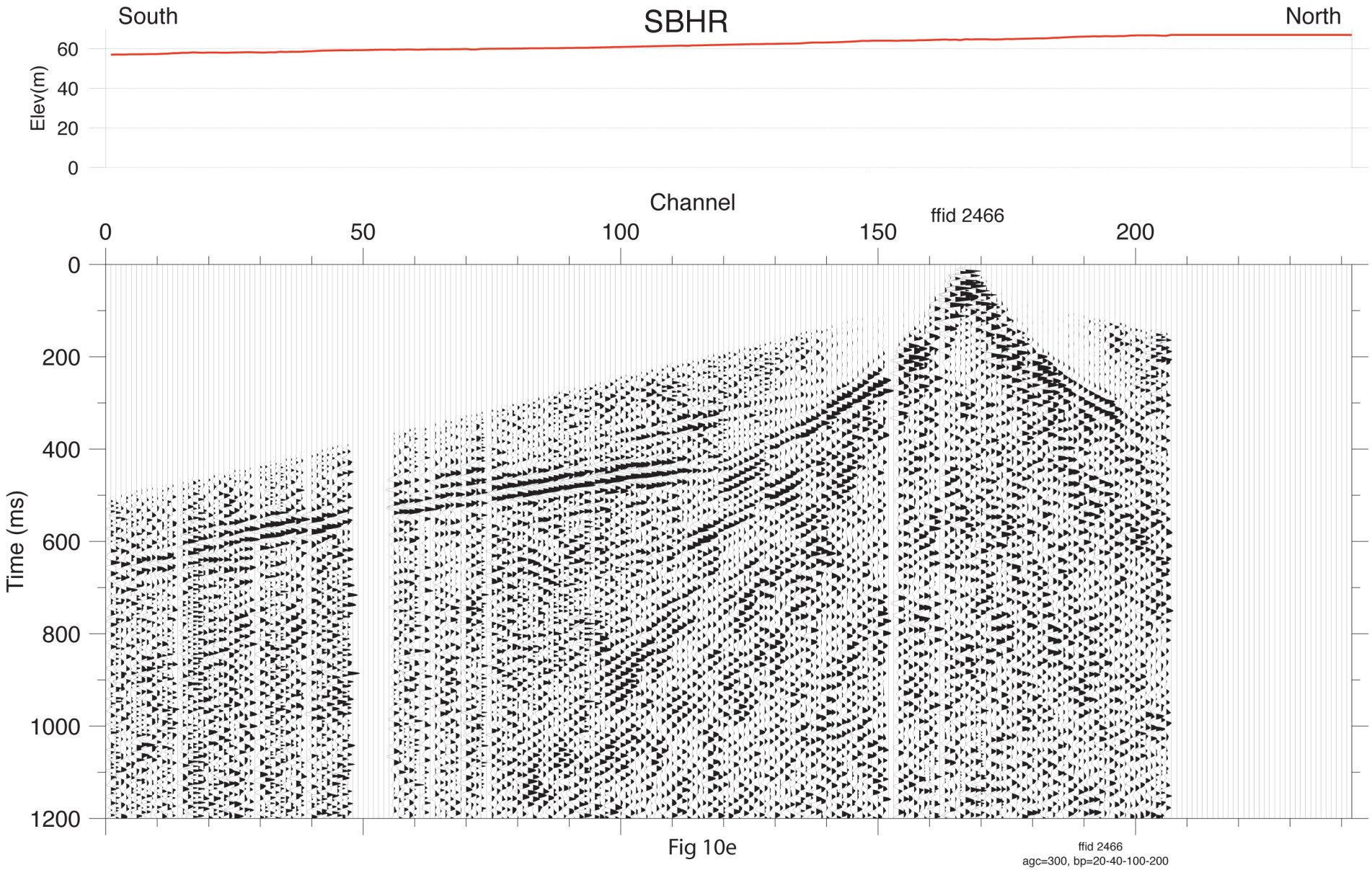
South
SBHR
North
Elev(m)
60
40
20
0
Channel
ffid 2466
0
50
100
150
200
0
200
400
600
800
1000
1200
Time (ms)
Fig 10e
ffid 2466
agc=300, bp=20-40-100-200

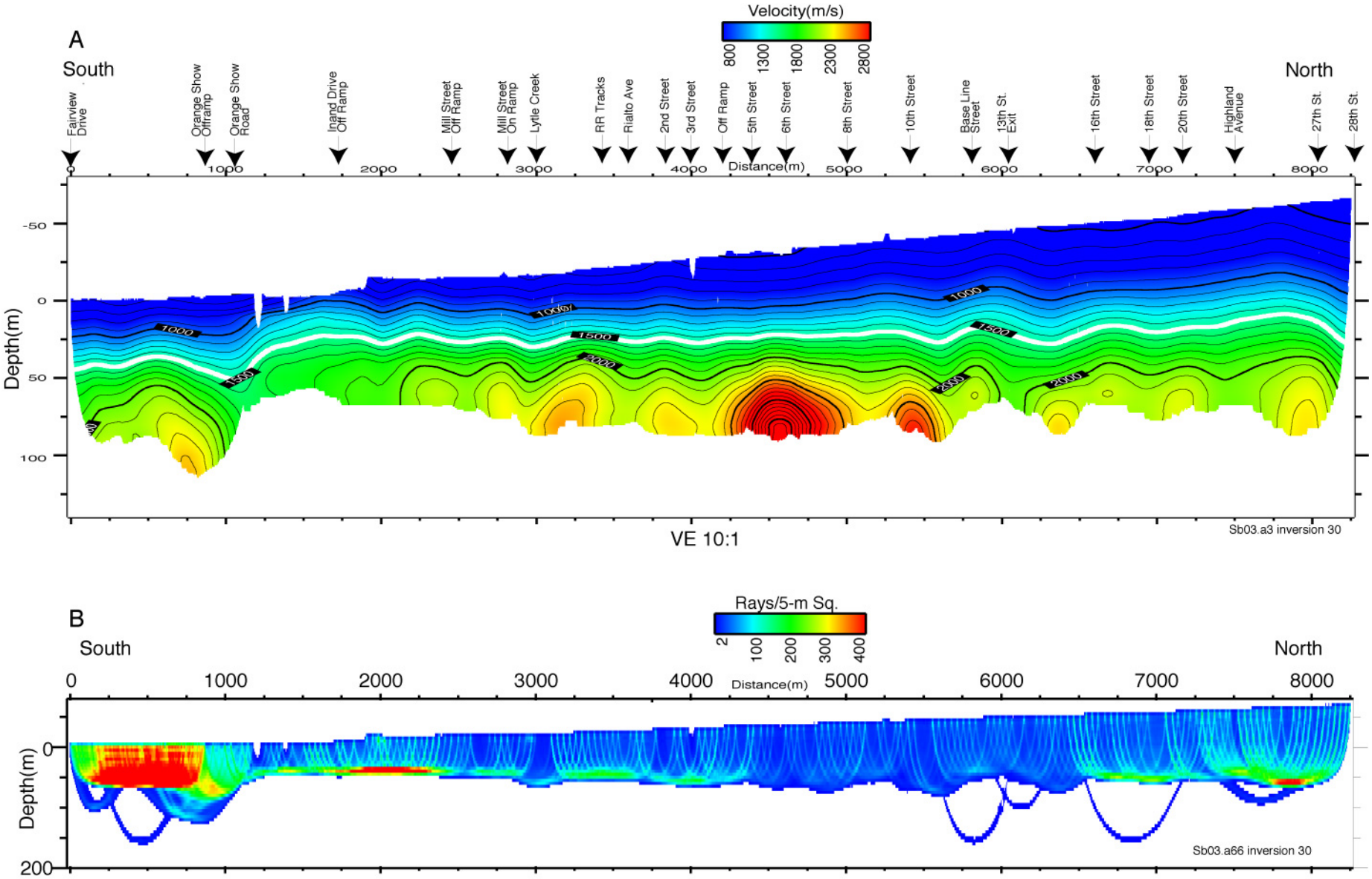
A
South
North
Velocity(m/s)
800
1300
1800
2300
2800
Fairview Drive
Orange Show Offramp
Orange Show Road
Inand Drive Off Ramp
Mill Street Off Ramp
Mill Street On Ramp
Lytle Creek
RR Tracks
Rialto Ave
2nd Street
3rd Street
Off Ramp
5th Street
6th Street
8th Street
10th Street
Base Line Street
13th St. Exit
16th Street
18th Street
20th Street
Highland Avenue
27th St.
28th St.
0
1000
2000
3000
4000
Distance(m)
5000
6000
7000
8000
Depth(m)
-50
0
50
100
1000
1500
2000
VE 10:1
Sb03.a3 inversion 30
B
South
North
Rays/5-m Sq.
2
100
200
300
400
0
1000
2000
3000
4000
Distance(m)
5000
6000
7000
8000
Depth(m)
0
200
Sb03.a66 inversion 30

Fig. 11

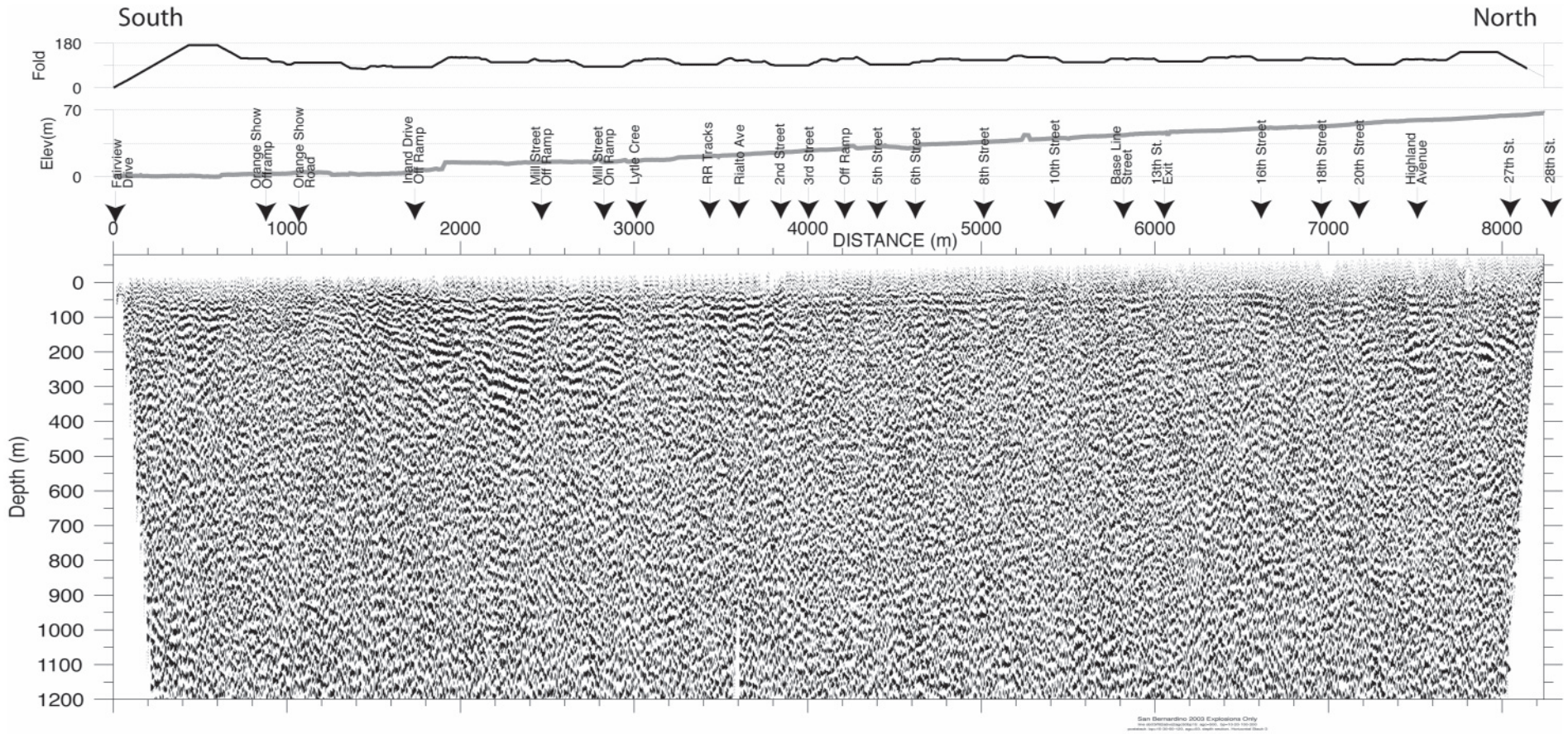
South
North
Fold
180
0
Elev(m)
70
0
Fairview Drive
Orange Show Offramp
Orange Show Road
Inland Drive Off Ramp
Mill Street Off Ramp
Mill Street On Ramp
Lytle Cree
RR Tracks
Rialto Ave
2nd Street
3rd Street
Off Ramp
5th Street
6th Street
8th Street
10th Street
Base Line Street
13th St. Exit
16th Street
18th Street
20th Street
Highland Avenue
27th St.
28th St.
0
1000
2000
3000
4000
5000
6000
7000
8000
DISTANCE (m)
Depth (m)
0
100
200
300
400
500
600
700
800
900
1000
1100
1200
San Bernardino 2003 Explosions Only

Fig. 12a

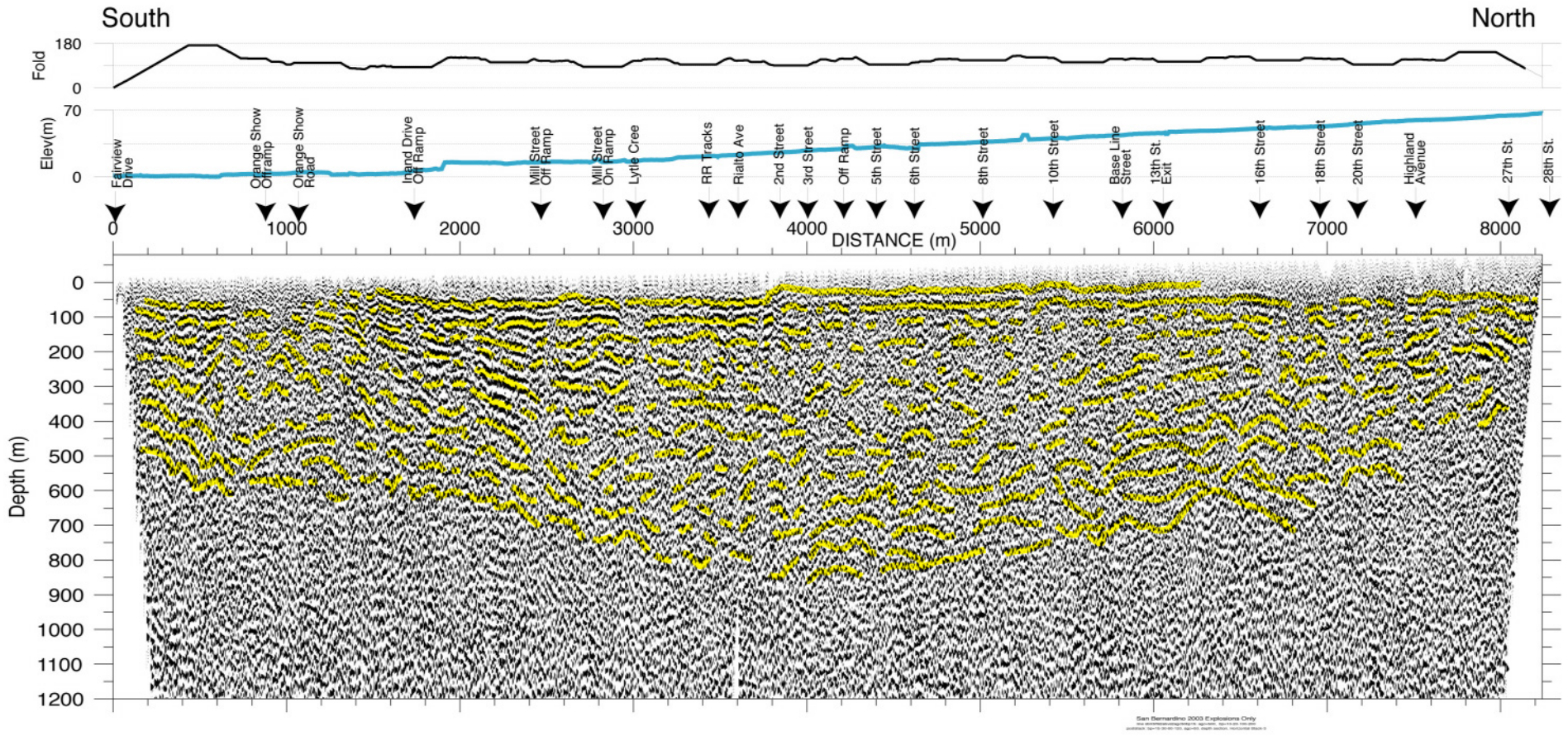
South
North
Fold
180
0
Elev(m)
70
0
Fairview Drive
Orange Show Offramp
Orange Show Road
Inland Drive Off Ramp
Mill Street Off Ramp
Mill Street On Ramp
Lytle Cree
RR Tracks
Rialto Ave
2nd Street
3rd Street
Off Ramp
5th Street
6th Street
8th Street
10th Street
Base Line Street
13th St. Exit
16th Street
18th Street
20th Street
Highland Avenue
27th St.
28th St.
0
1000
2000
3000
4000
DISTANCE (m)
5000
6000
7000
8000
Depth (m)
0
100
200
300
400
500
600
700
800
900
1000
1100
1200
San Bernardino 2003 Explosions Only

Fig. 12b

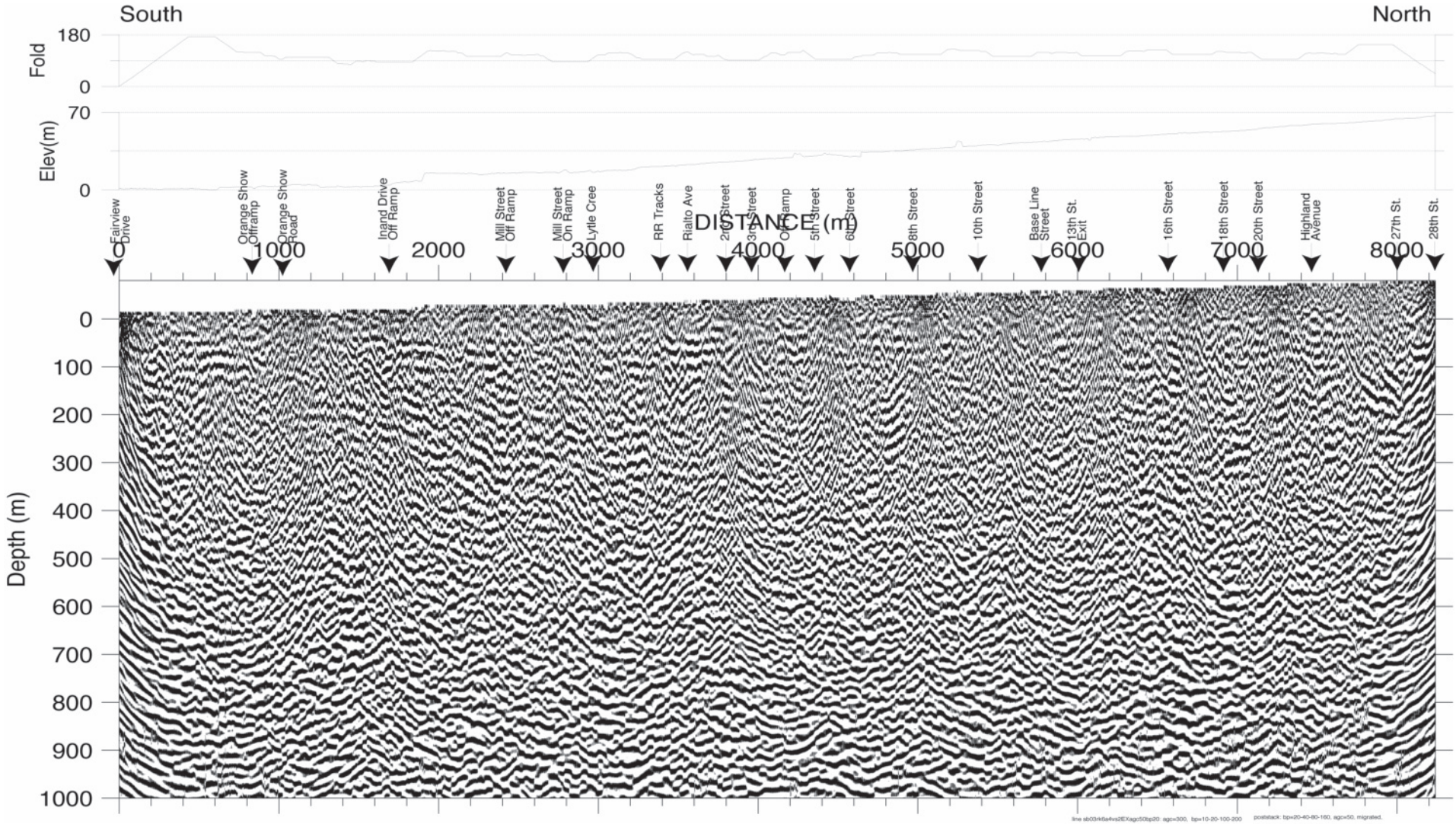
South
North
Fold
180
0
Elev(m)
70
0
Fairview Drive
Orange Show Offramp
Orange Show Road
Inand Drive Off Ramp
Mill Street Off Ramp
Mill Street On Ramp
Lytle Cree
RR Tracks
Rialto Ave
2nd Street
3rd Street
Off Ramp
5th Street
6th Street
8th Street
10th Street
Base Line Street
13th St. Exit
16th Street
18th Street
20th Street
Highland Avenue
27th St.
28th St.
DISTANCE (m)
0
1000
2000
3000
4000
5000
6000
7000
8000
Depth (m)
0
100
200
300
400
500
600
700
800
900
1000

Fig. 12c

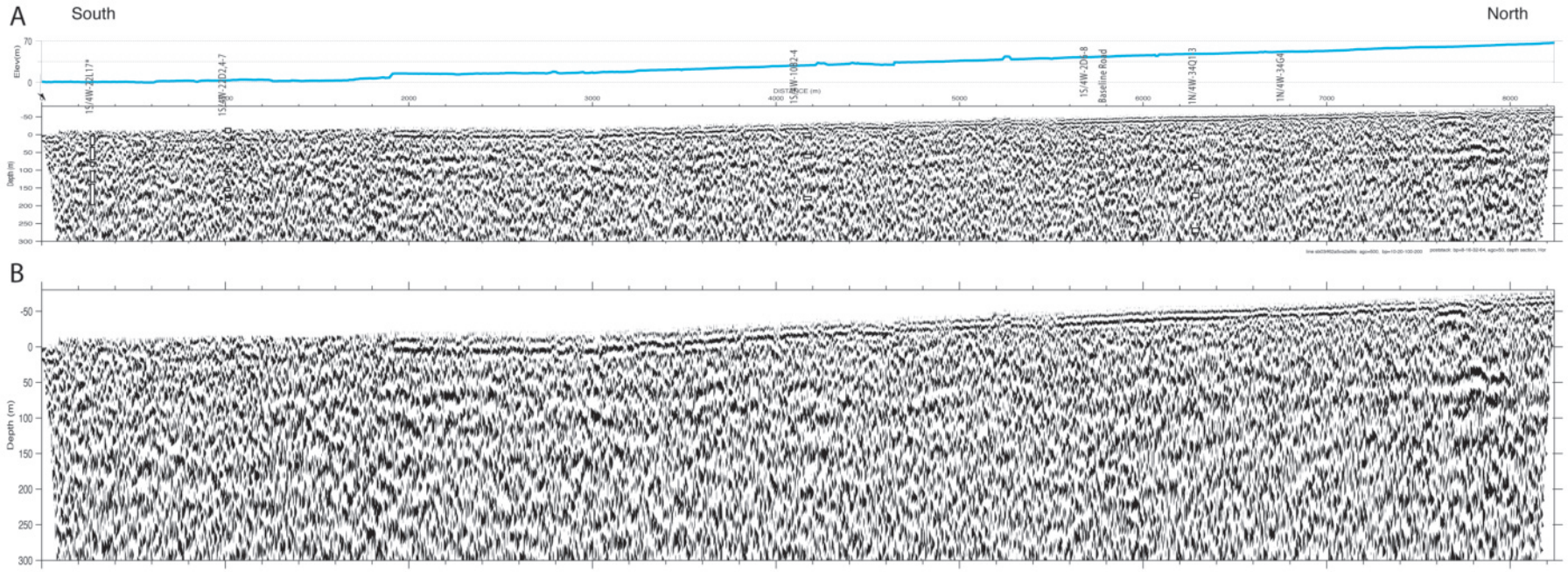

Fig. 12d

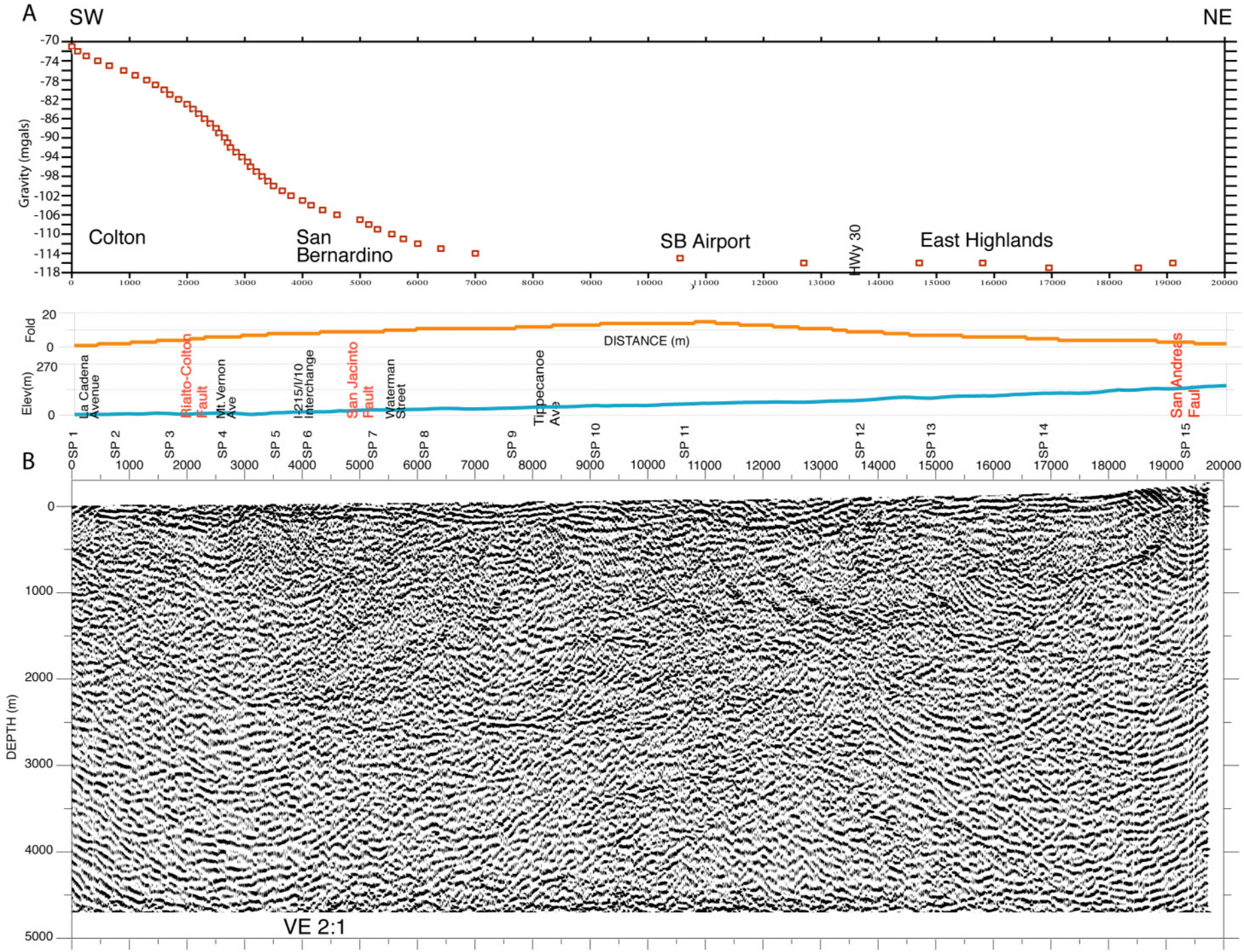
A
SW
NE
Gravity (mgals)
-70
-74
-78
-82
-86
-90
-94
-98
-102
-106
-110
-114
-118
Colton
San Bernardino
SB Airport
HWy 30
East Highlands
0
1000
2000
3000
4000
5000
6000
7000
8000
9000
10000
11000
12000
13000
14000
15000
16000
17000
18000
19000
20000
Fold
20
0
DISTANCE (m)
Elev(m)
270
0
La Cadena Avenue
Rialto-Colton Fault
Mt.Vernon Ave
I-215/I/10 Interchange
San Jacinto Fault
Waterman Street
Tippecanoe Ave
San Andreas Fault
SP 1
SP 2
SP 3
SP 4
SP 5
SP 6
SP 7
SP 8
SP 9
SP 10
SP 11
SP 12
SP 13
SP 14
SP 15
B
DEPTH (m)
0
1000
2000
3000
4000
5000
VE 2:1
line r1 k3 a3 p13v1: agc=1000, bp=1-2-10-20 mig=20,8000,30 poststack: bp=2-4-50-100, agc=1000

Fig.13

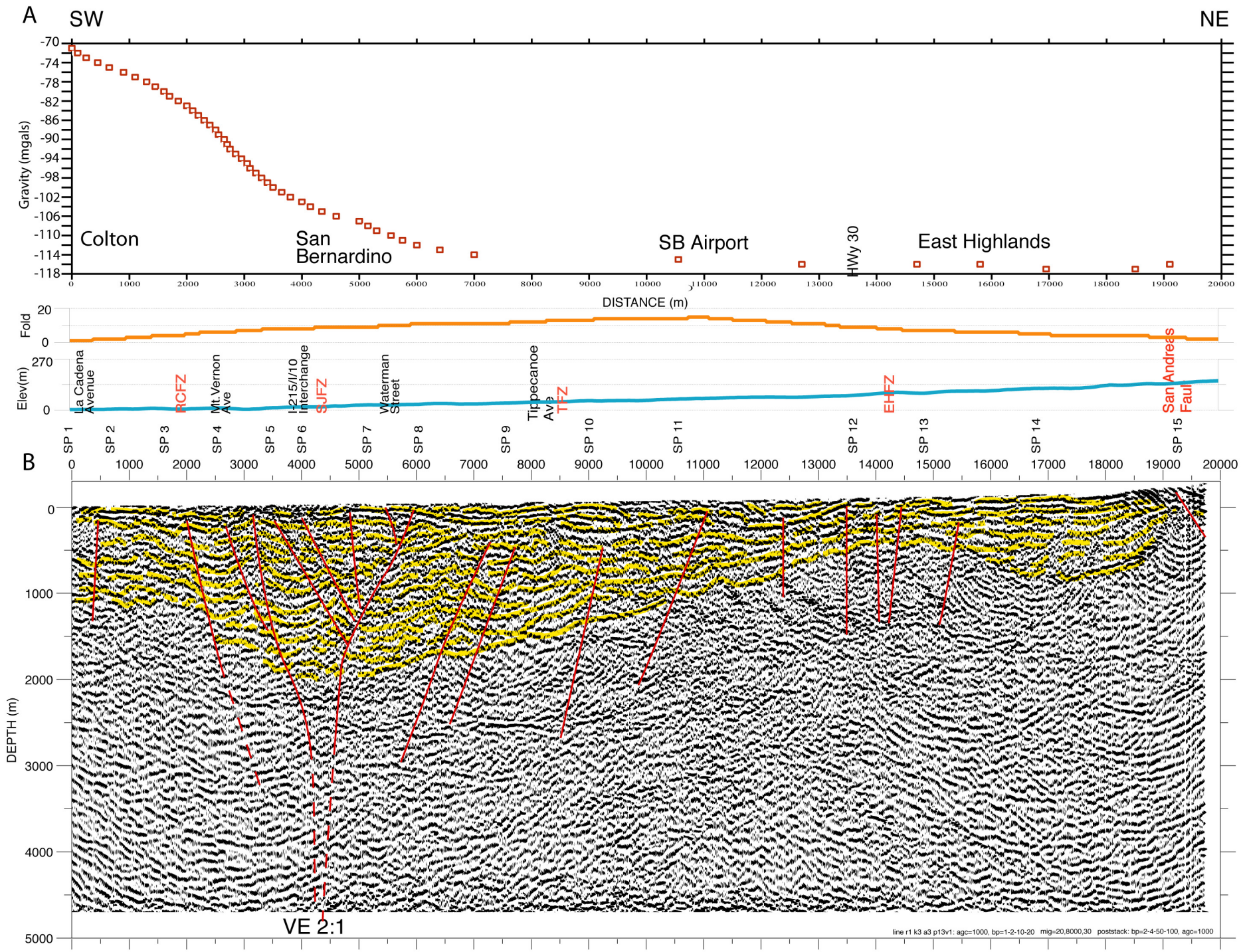
A
SW
NE
Gravity (mgals)
Colton
San Bernardino
SB Airport
HWy 30
East Highlands
DISTANCE (m)
Fold
Elev(m)
La Cadena Avenue
RCFZ
Mt.Vernon Ave
I-215/I-10 Interchange
SJFZ
Waterman Street
Tippecanoe Ave
TFZ
EHFZ
San Andreas Fault
SP 1
SP 2
SP 3
SP 4
SP 5
SP 6
SP 7
SP 8
SP 9
SP 10
SP 11
SP 12
SP 13
SP 14
SP 15
B
DEPTH (m)
VE 2:1
line r1 k3 a3 p13v1: agc=1000, bp=1-2-10-20 mig=20,8000,30 poststack: bp=2-4-50-100, agc=1000

Fig.14

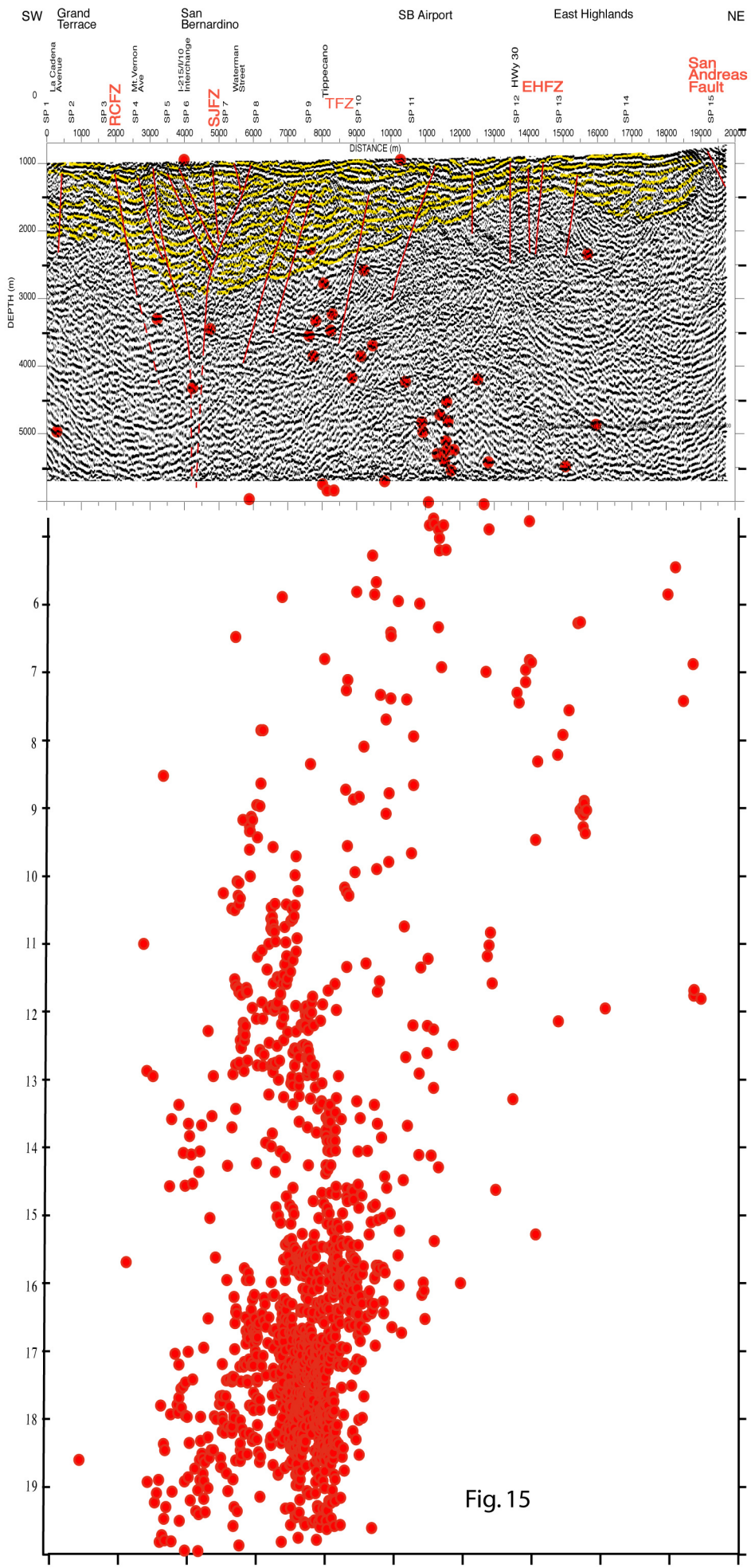
SW
Grand Terrace
San Bernardino
SB Airport
East Highlands
NE
La Cadena Avenue
Mt Vernon Ave
I-215/I-10 Interchange
Waterman Street
Tippecano
HWy 30
RCFZ
SJFZ
TFZ
EHFZ
San Andreas Fault
SP 1
SP 2
SP 3
SP 4
SP 5
SP 6
SP 7
SP 8
SP 9
SP 10
SP 11
SP 12
SP 13
SP 14
SP 15
DISTANCE (m)
DEPTH (m)
Fig. 15

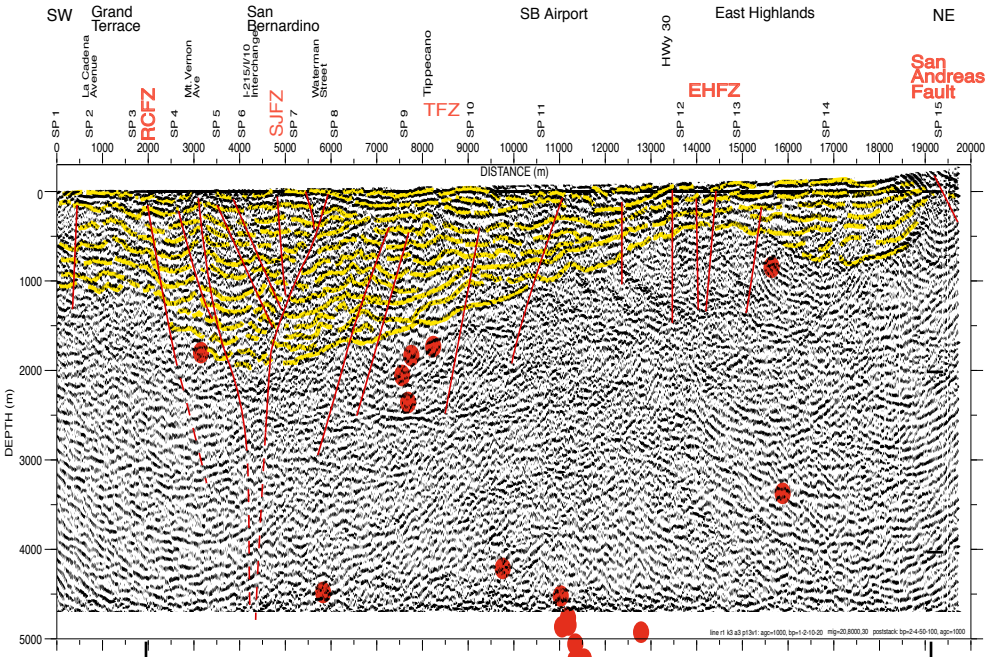
SW
Grand Terrace
San Bernardino
SB Airport
East Highlands
NE
La Cadena Avenue
Mt. Vernon Ave
I-215/I-10 Interchange
Waterman Street
Tippecano
HWy 30
RCFZ
SJFZ
TFZ
EHFZ
San Andreas Fault
SP 1
SP 2
SP 3
SP 4
SP 5
SP 6
SP 7
SP 8
SP 9
SP 10
SP 11
SP 12
SP 13
SP 14
SP 15
DISTANCE (m)
DEPTH (m)

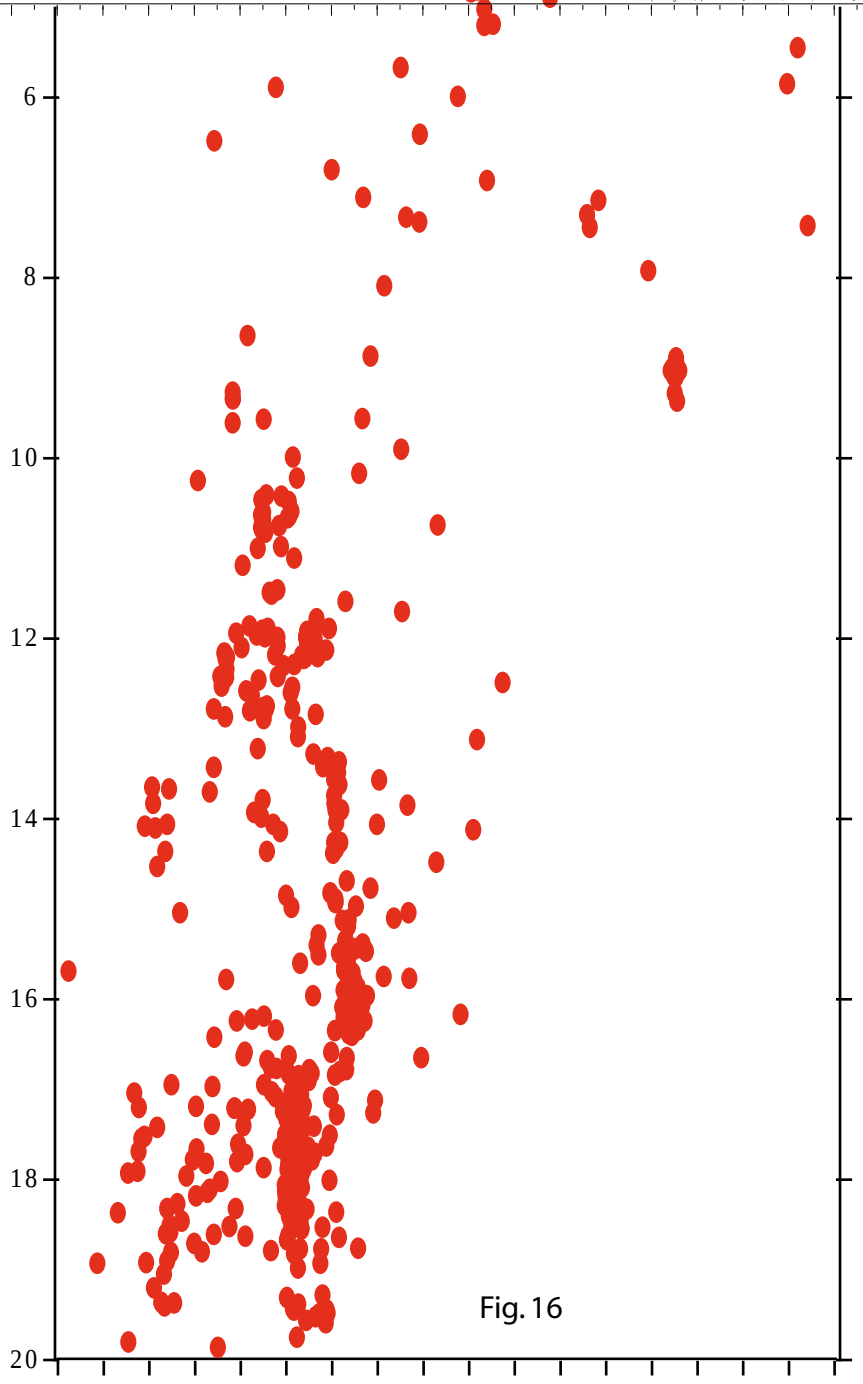

Fig. 16

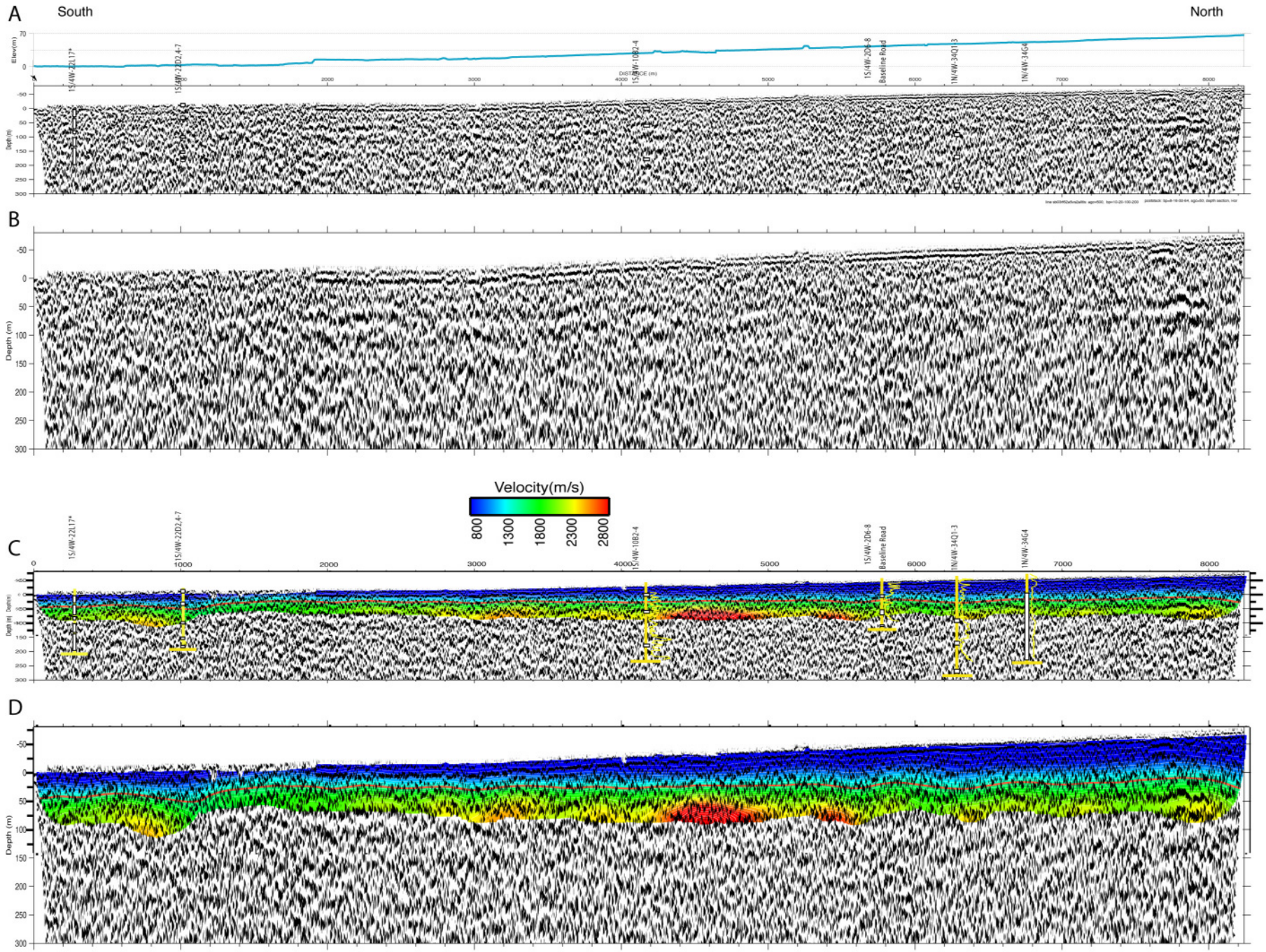
A
South
North
B
C
D
Velocity(m/s)
800
1300
1800
2300
2800
Depth (m)
Elev(m)
Baseline Road

Fig. 17

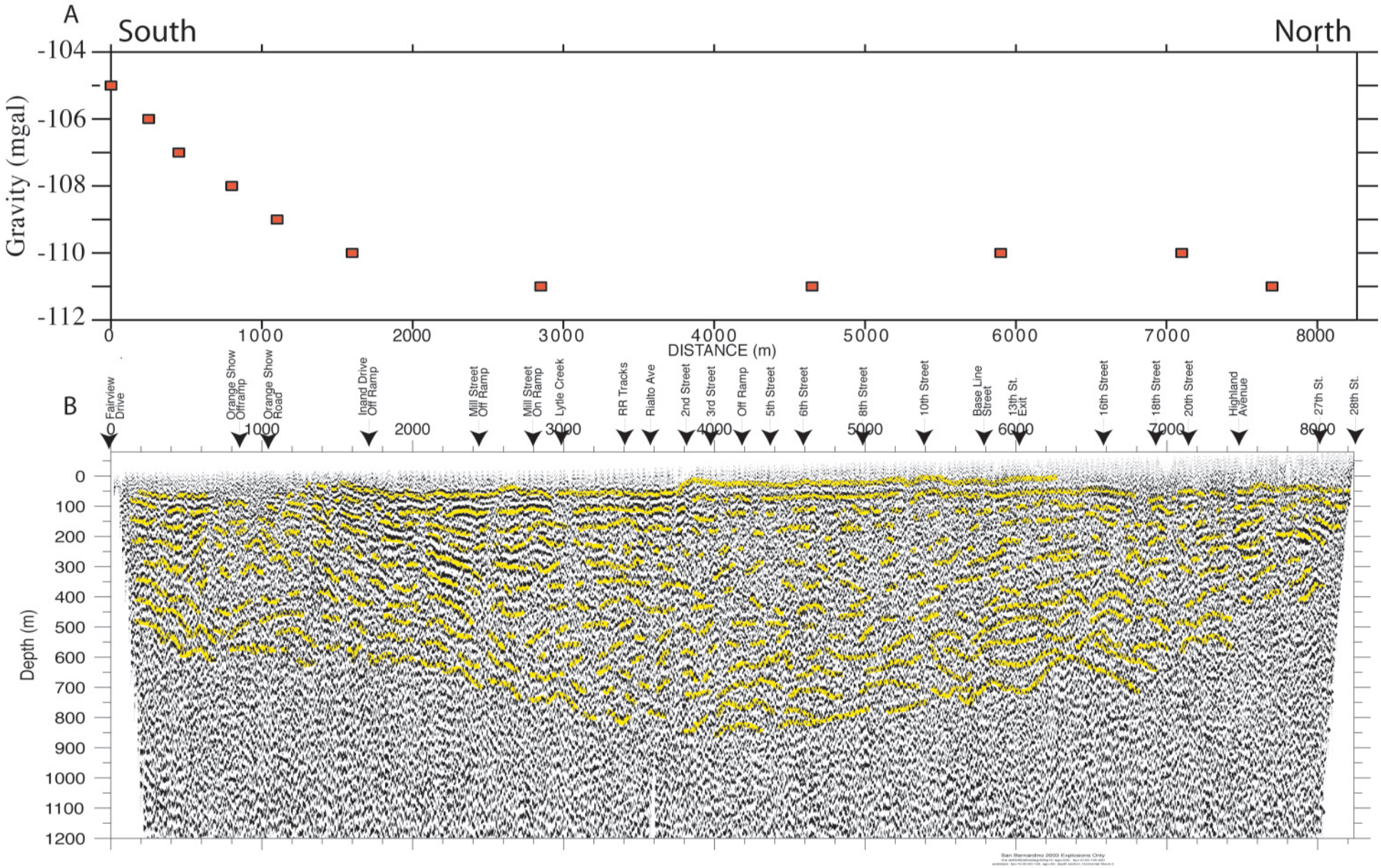
A
South
North
-104
-106
-108
-110
-112
Gravity (mgal)
0
1000
2000
3000
4000
5000
6000
7000
8000
DISTANCE (m)
B
Fairview Drive
Orange Show Offramp
Orange Show Road
Inand Drive Off Ramp
Mill Street Off Ramp
Mill Street On Ramp
Lytle Creek
RR Tracks
Rialto Ave
2nd Street
3rd Street
Off Ramp
5th Street
6th Street
8th Street
10th Street
Base Line Street
13th St. Exit
16th Street
18th Street
20th Street
Highland Avenue
27th St.
28th St.
0
1000
2000
3000
4000
5000
6000
7000
8000
Depth (m)
0
100
200
300
400
500
600
700
800
900
1000
1100
1200

Fig. 18

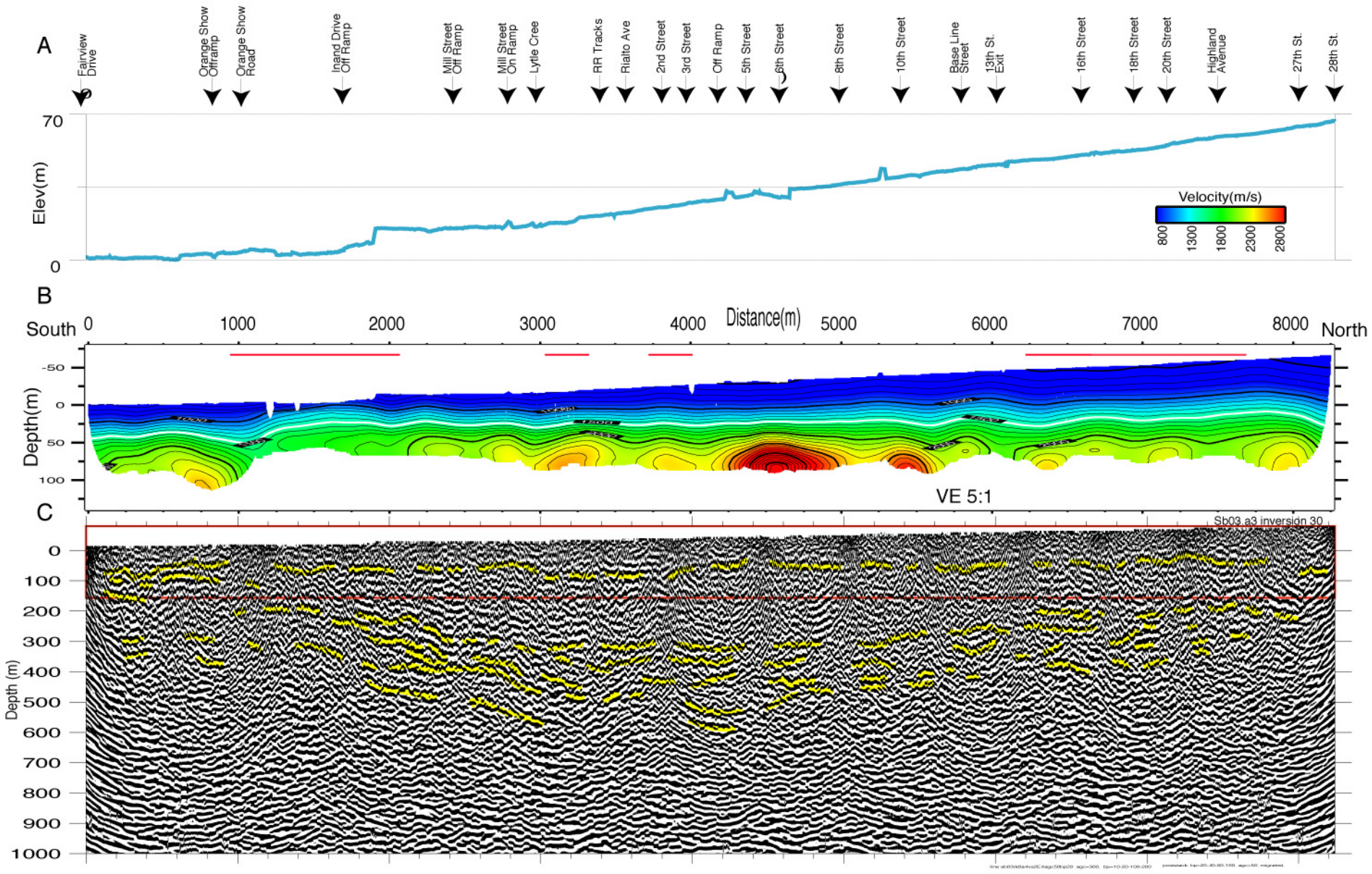
A
Fairview Drive
Orange Show Offramp
Orange Show Road
Inand Drive Off Ramp
Mill Street Off Ramp
Mill Street On Ramp
Lytle Cree
RR Tracks
Rialto Ave
2nd Street
3rd Street
Off Ramp
5th Street
6th Street
8th Street
10th Street
Base Line Street
13th St. Exit
16th Street
18th Street
20th Street
Highland Avenue
27th St.
28th St.
70
Elev(m)
0
Velocity(m/s)
800
1300
1800
2300
2800
B
South
0
1000
2000
3000
4000
Distance(m)
5000
6000
7000
8000
North
-50
0
50
100
Depth(m)
VE 5:1
C
Sb03.a3 inversion 30
0
100
200
300
400
500
600
700
800
900
1000
Depth (m)

Fig. 19

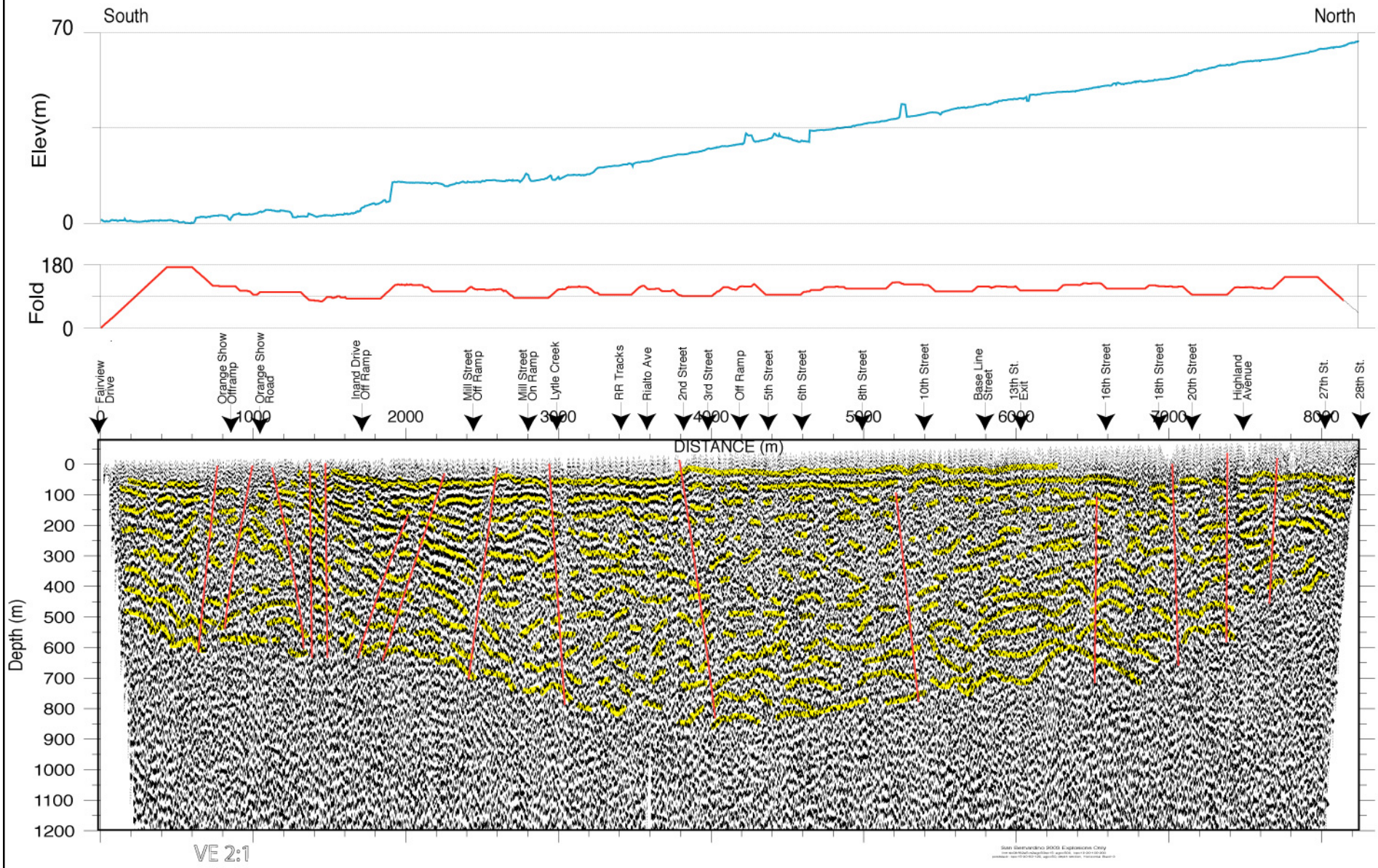
South
North
70
Elev(m)
0
180
Fold
0
Fairview Drive
Orange Show Offramp
Orange Show Road
Inand Drive Off Ramp
Mill Street Off Ramp
Mill Street On Ramp
Lytle Creek
RR Tracks
Rialto Ave
2nd Street
3rd Street
Off Ramp
5th Street
6th Street
8th Street
10th Street
Base Line Street
13th St. Exit
16th Street
18th Street
20th Street
Highland Avenue
27th St.
28th St.
0
1000
2000
3000
4000
5000
6000
7000
8000
DISTANCE (m)
Depth (m)
0
100
200
300
400
500
600
700
800
900
1000
1100
1200
VE 2:1

Fig. 20

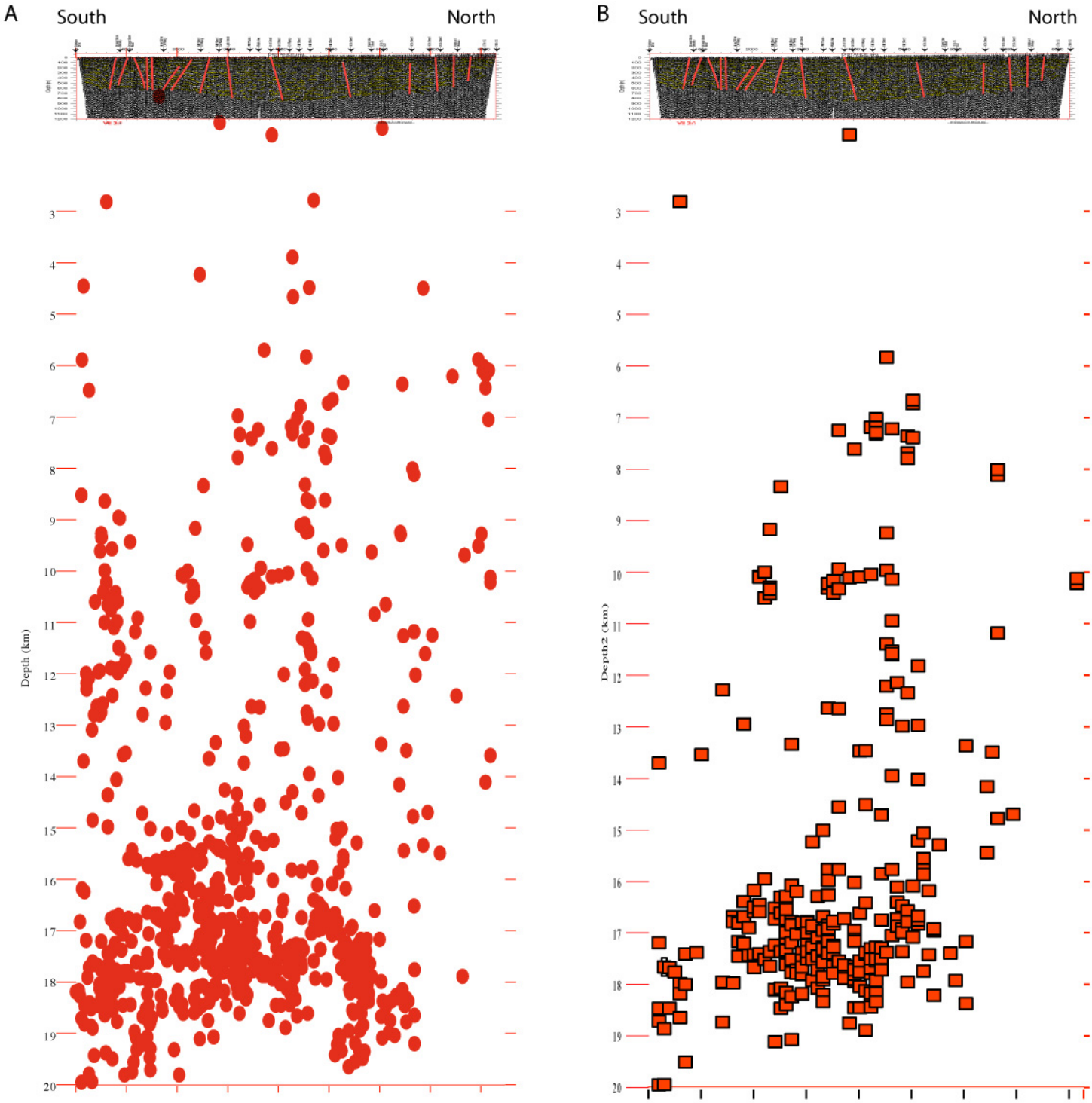
A
South
North
B
South
North
Depth (km)
Depth2 (km)
3
4
5
6
7
8
9
10
11
12
13
14
15
16
17
18
19
20

Fig. 21

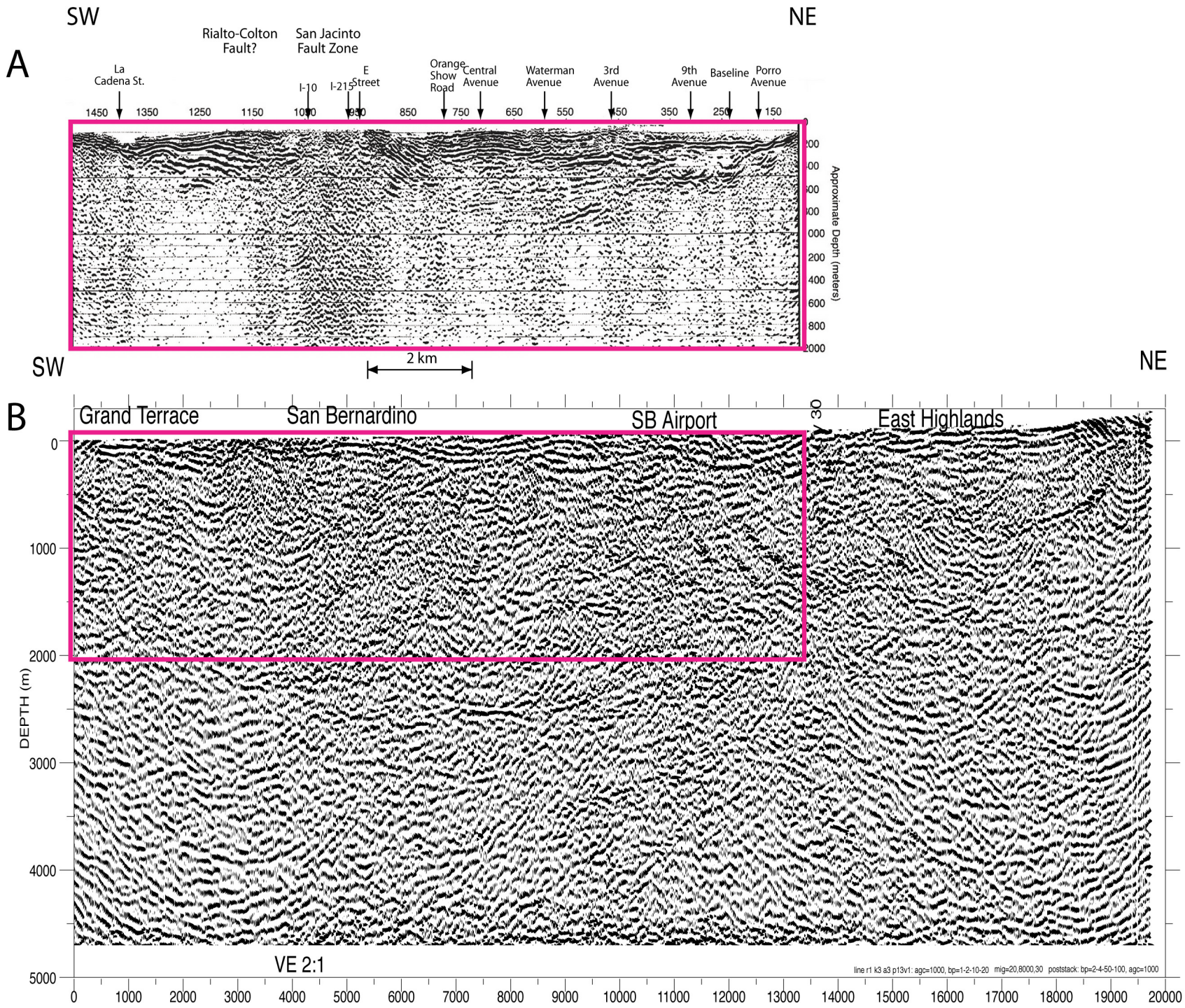
A
SW
NE
Rialto-Colton Fault?
San Jacinto Fault Zone
La Cadena St.
I-10
I-215
E Street
Orange Show Road
Central Avenue
Waterman Avenue
3rd Avenue
9th Avenue
Baseline
Porro Avenue
1450
1350
1250
1150
1050
950
850
750
650
550
450
350
250
150
Approximate Depth (meters)
2 km
SW
NE
B
Grand Terrace
San Bernardino
SB Airport
East Highlands
DEPTH (m)
0
1000
2000
3000
4000
5000
VE 2:1
0
1000
2000
3000
4000
5000
6000
7000
8000
9000
10000
11000
12000
13000
14000
15000
16000
17000
18000
19000
20000

Fig. 22

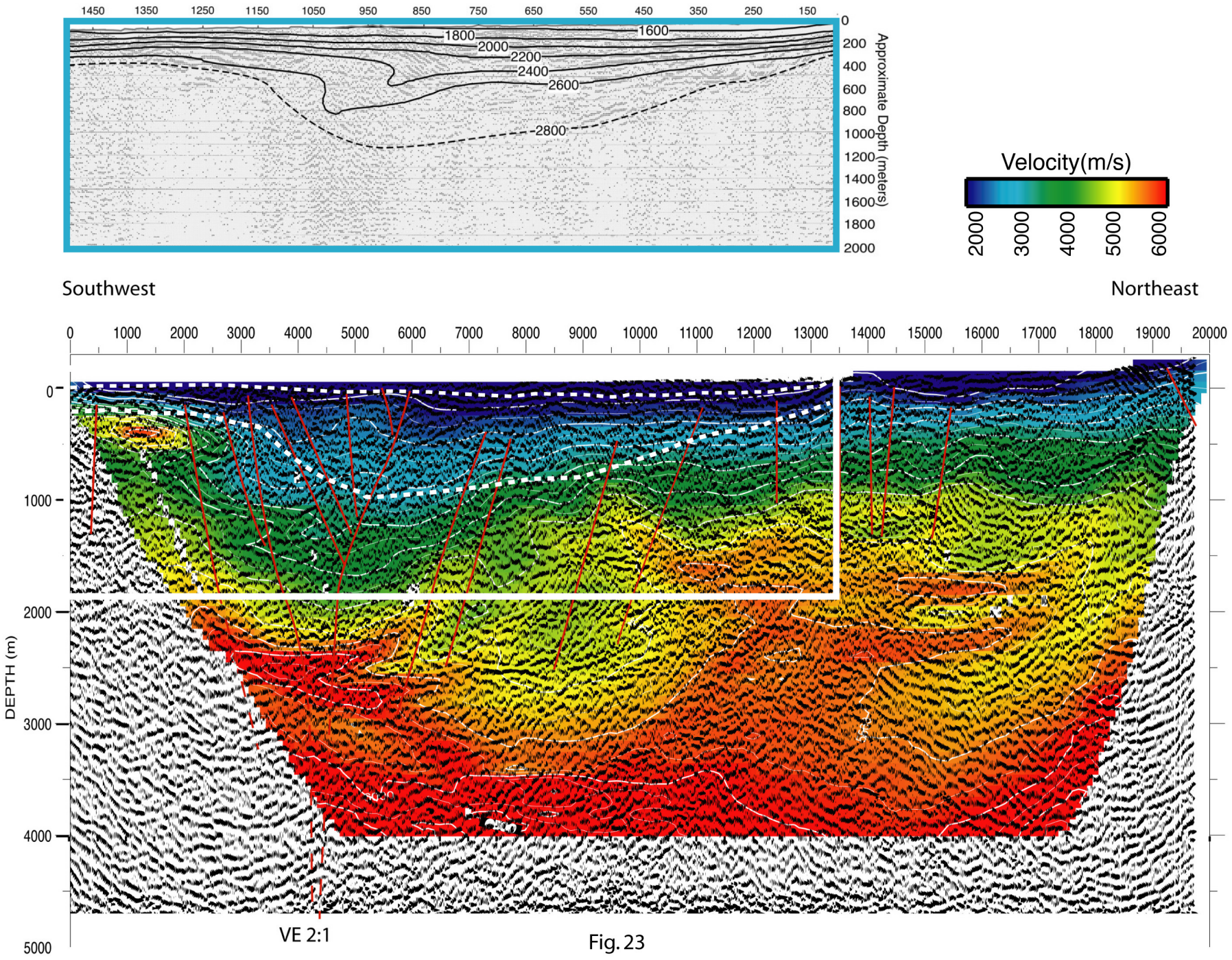
1450 1350 1250 1150 1050 950 850 750 650 550 450 350 250 150
1600
1800
2000
2200
2400
2600
2800
0 200 400 600 800 1000 1200 1400 1600 1800 2000
Approximate Depth (meters)
Velocity(m/s)
2000 3000 4000 5000 6000
Southwest
Northeast
0 1000 2000 3000 4000 5000 6000 7000 8000 9000 10000 11000 12000 13000 14000 15000 16000 17000 18000 19000 20000
0
1000
2000
3000
4000
5000
DEPTH (m)
VE 2:1

Fig. 23

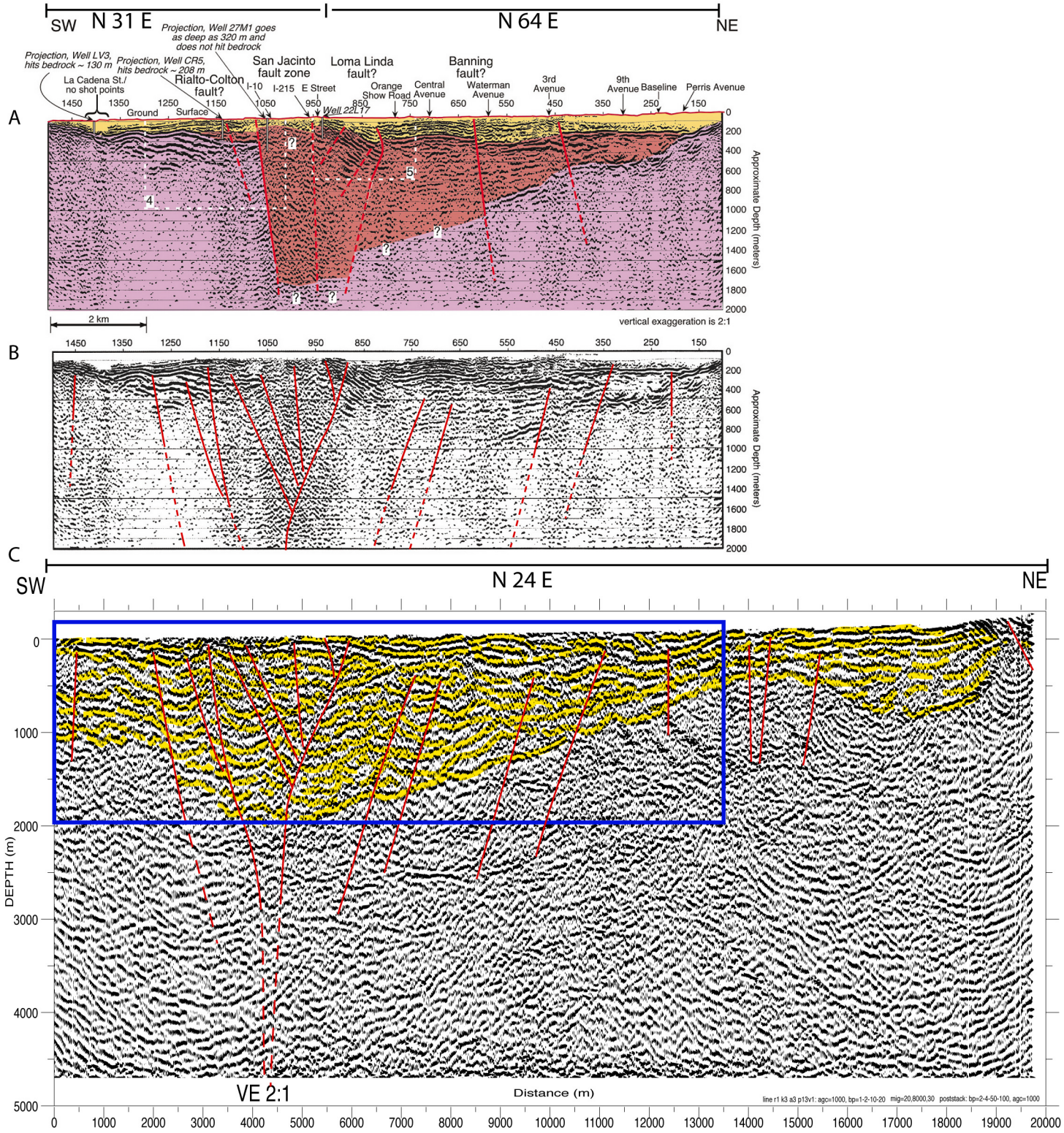
A
SW
N 31 E
N 64 E
NE
Projection, Well 27M1 goes as deep as 320 m and does not hit bedrock
Projection, Well LV3, hits bedrock ~ 130 m
Projection, Well CR5, hits bedrock ~ 208 m
La Cadena St./ no shot points
Rialto-Colton fault?
San Jacinto fault zone
Loma Linda fault?
Banning fault?
I-10
I-215
E Street
Orange Show Road
Central Avenue
Waterman Avenue
3rd Avenue
9th Avenue
Baseline
Perris Avenue
Ground Surface
Well 22L17
1450 1350 1250 1150 1050 950 850 750 650 550 450 350 250 150
0 200 400 600 800 1000 1200 1400 1600 1800 2000
Approximate Depth (meters)
2 km
vertical exaggeration is 2:1
B
C
SW
N 24 E
NE
DEPTH (m)
0 1000 2000 3000 4000 5000
VE 2:1
Distance (m)
0 1000 2000 3000 4000 5000 6000 7000 8000 9000 10000 11000 12000 13000 14000 15000 16000 17000 18000 19000 20000

Fig. 24

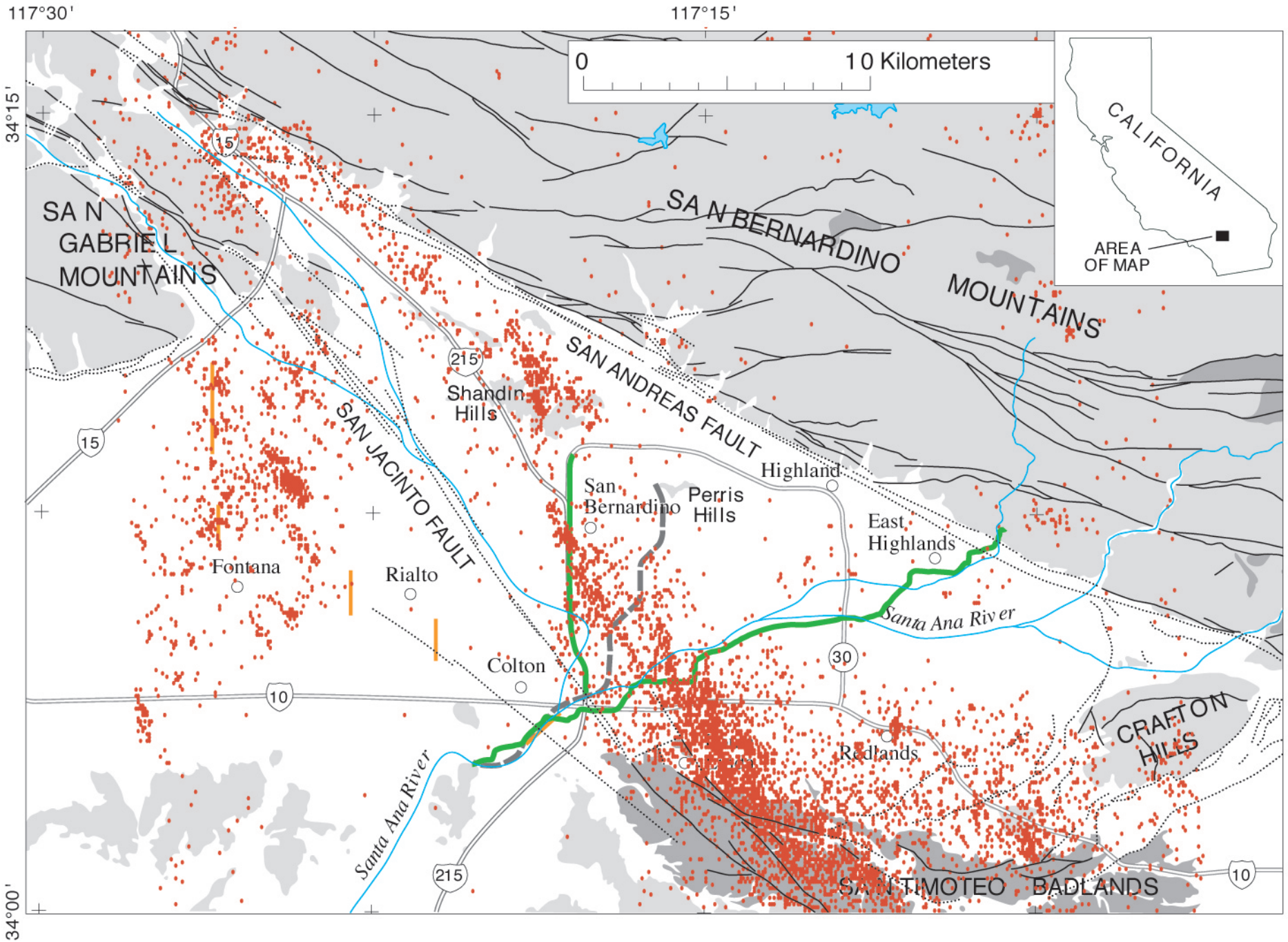
117°30'
117°15'
34°15'
34°00'
0
10 Kilometers
CALIFORNIA
AREA OF MAP
SA N GABRIE L MOUNTAINS
SA N BERNARDINO MOUNTAINS
SAN ANDREAS FAULT
SAN JACINTO FAULT
Shandin Hills
Perris Hills
San Bernardino
Highland
East Highlands
Fontana
Rialto
Colton
Redlands
Santa Ana River
Santa Ana River
CRAFTON HILLS
SAN TIMOTEO BADLANDS
15
215
10
30

Fig. 25a

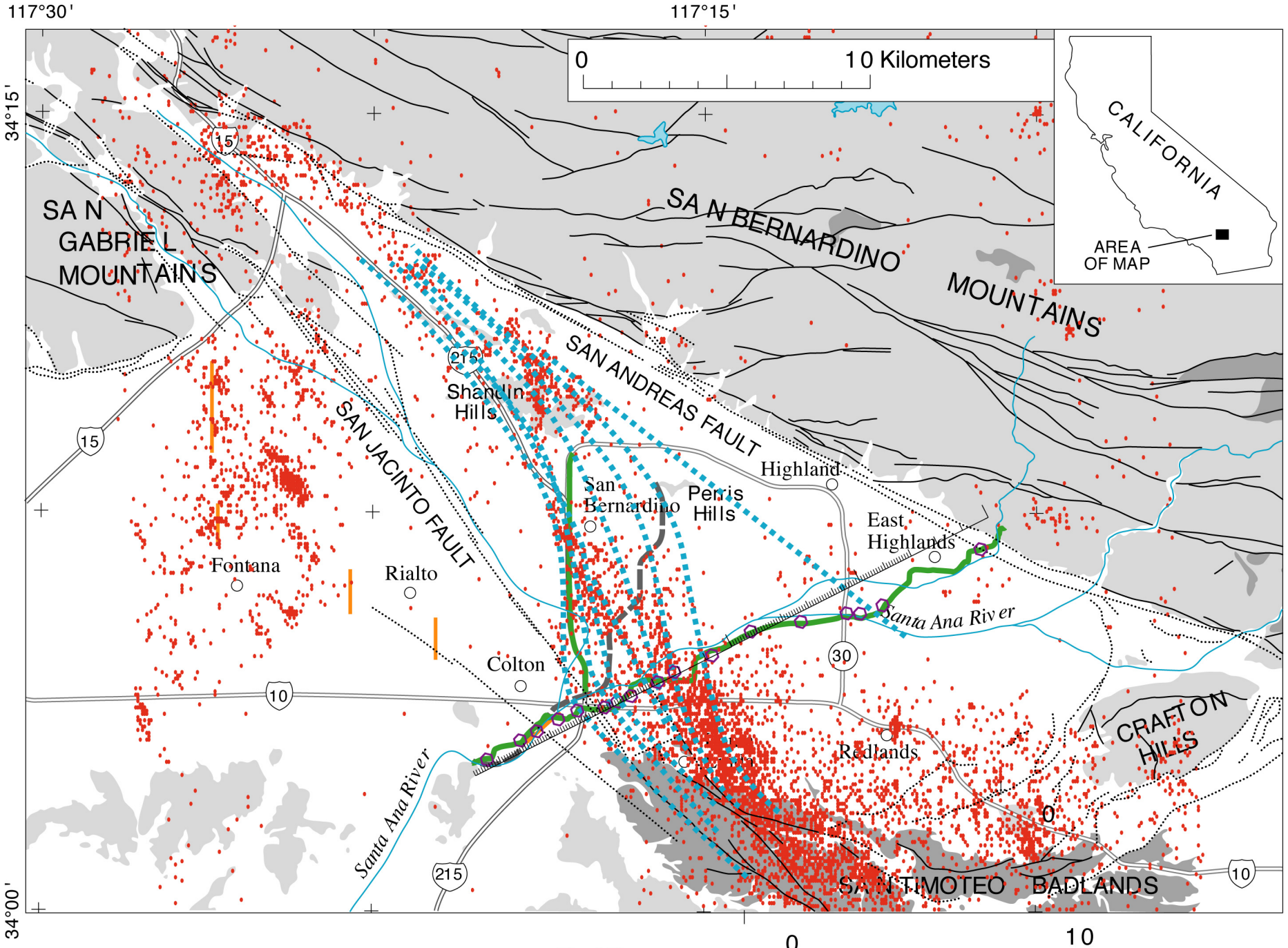
0
10
117°30'
117°15'
34°15'
34°00'
0
10 Kilometers
CALIFORNIA
AREA
OF MAP
SA N
GABRIE L
MOUNTAINS
SA N BERNARDINO
MOUNTAINS
SAN ANDREAS FAULT
SAN JACINTO FAULT
Shandin
Hills
San
Bernardino
Perris
Hills
Highland
East
Highlands
Fontana
Rialto
Colton
Redlands
Santa Ana River
Santa Ana River
CRAFTON
HILLS
SA N TIMOTEO
BADLANDS
15
215
10
30
0
10
0
10

Fig 25b

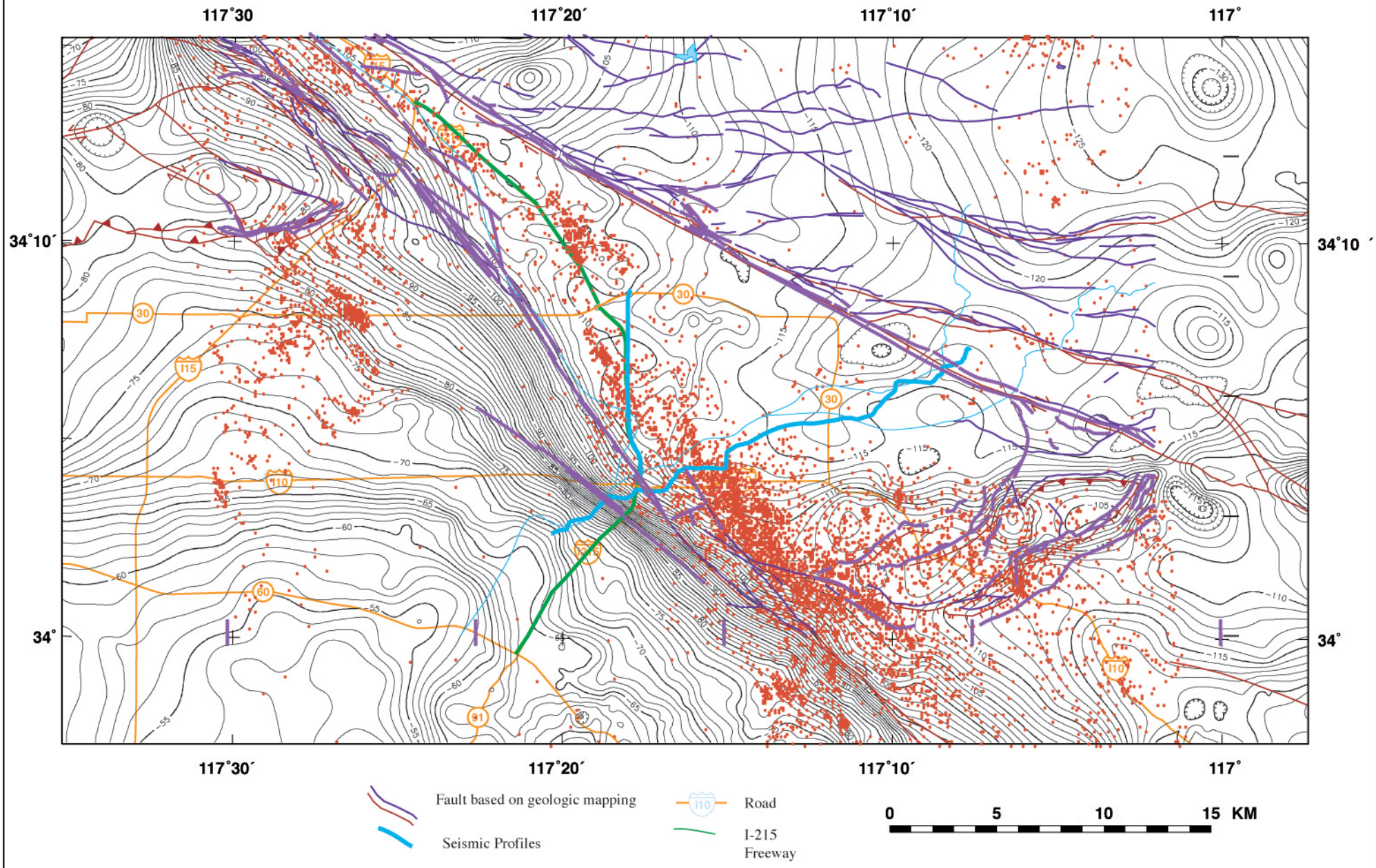
117°30
117°20´
117°10´
117°
34°10´
34°
117°30´
117°20´
117°10´
117°
Fault based on geologic mapping
Seismic Profiles
Road
I-215
Freeway
0
5
10
15 KM

Fig. 26a

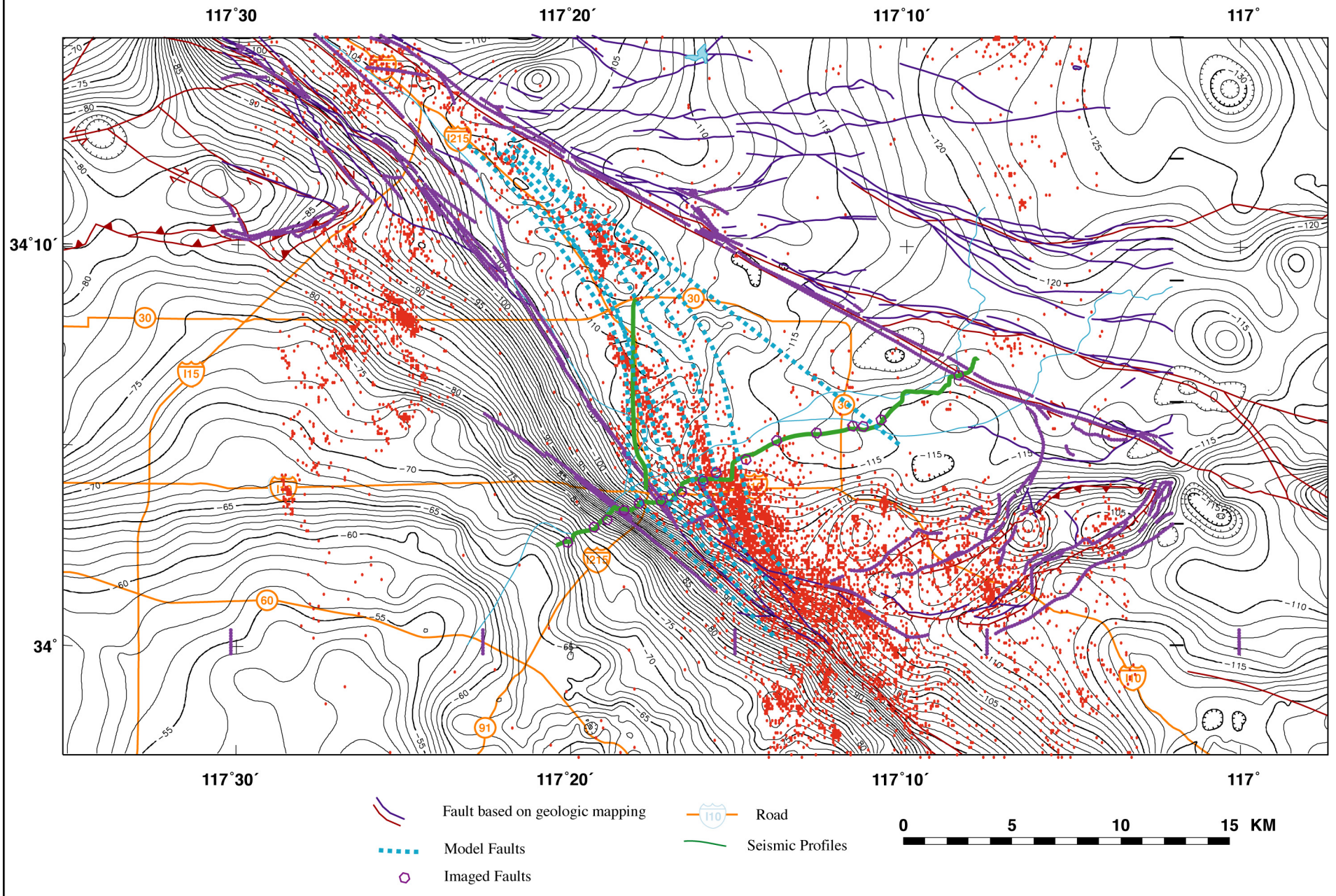
117°30
117°20´
117°10´
117°
34°10´
34°
117°30´
117°20´
117°10´
117°
Fault based on geologic mapping
Model Faults
Imaged Faults
Road
Seismic Profiles
0 5 10 15 KM

Fig. 26b

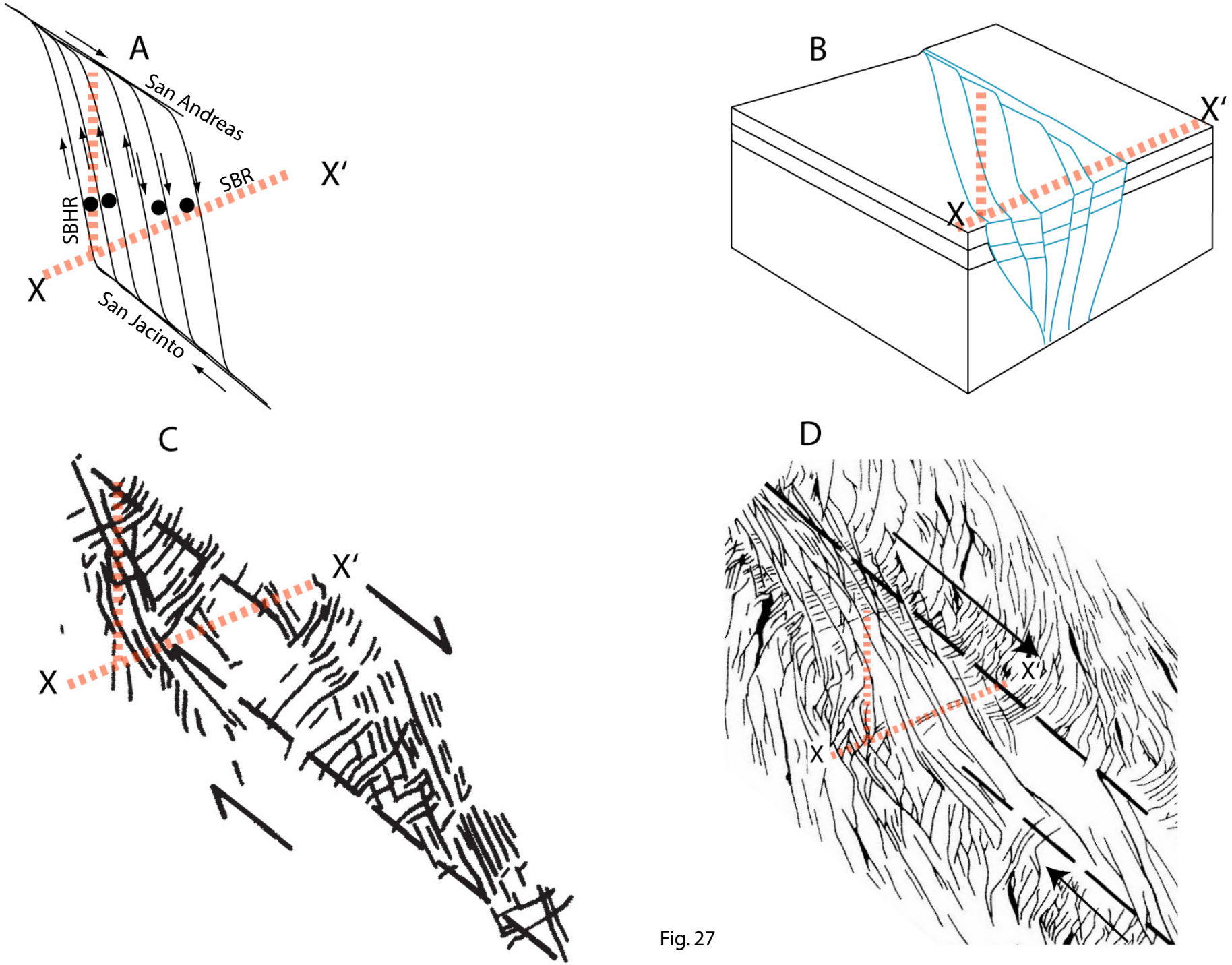

Fig. 27

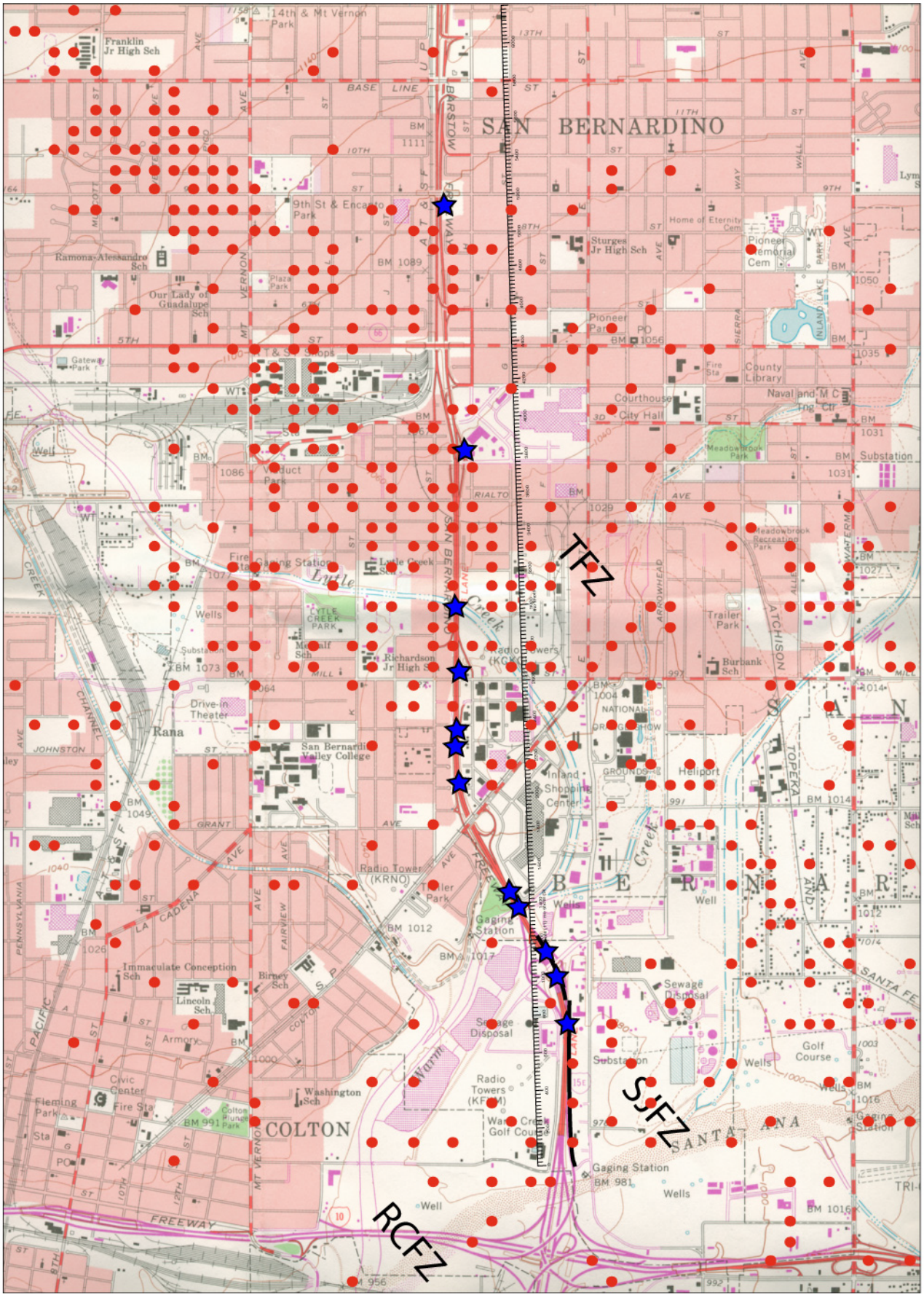
SAN BERNARDINO
COLTON
RANA
TFZ
SJFZ
RCFZ
SANTA ANA
Little Creek
Warm Creek
Franklin Jr High Sch
14th & Mt Vernon Park
9th St & Encanto Park
Ramona-Alessandro Sch
Our Lady of Guadalupe Sch
Sturges Jr High Sch
Pioneer Memorial Cem
Home of Eternity Cem
Pioneer Park
PO
County Library
Courthouse
City Hall
Naval and M C Trng Ctr
Meadowbrook Park
Substation
Gateway Park
Viaduct Park
Fire Sta
Gaging Station
Lytle Creek Sch
Lytle Creek Park
Wells
Richardson Jr High Sch
Radio Towers (KCKC)
Trailer Park
Burbank Sch
Meadowbrook Recreating Park
Drive-in Theater
San Bernardino Valley College
Inland Shopping Center
Heliport
Radio Tower (KRNO)
Immaculate Conception Sch
Lincoln Sch
Birney Sch
Armory
Civic Center
Fleming Park
Colton Plunge Park
Washington Sch
Radio Towers (KFMJ)
Golf Course
Sewage Disposal
Substation
Gaging Station
Well
FREEWAY

Fig. 28a

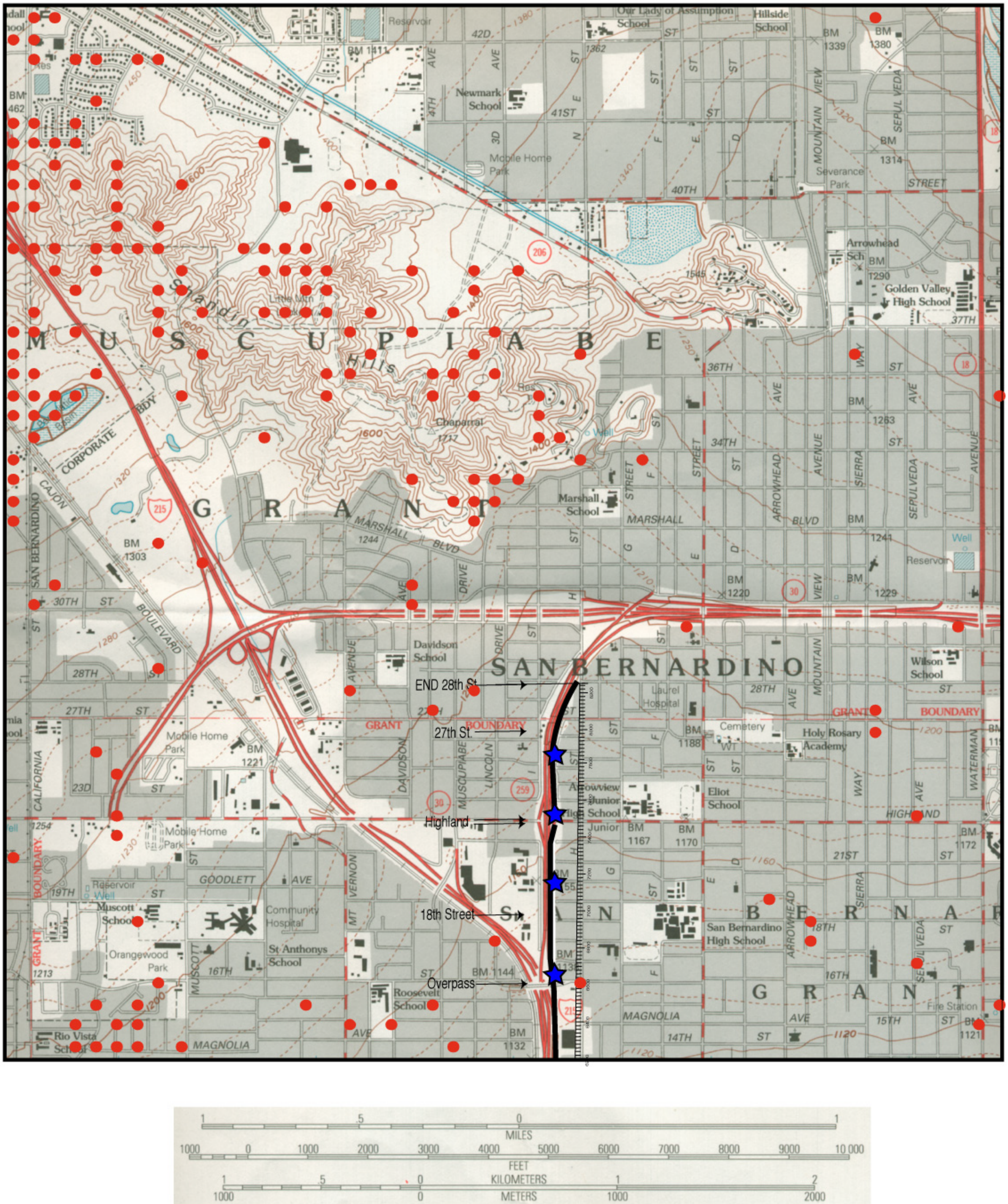
END 28th St
27th St.
Highland
18th Street
Overpass
SAN BERNARDINO
MUSCUPIABE
GRANT
MILES
FEET
KILOMETERS
METERS

Fig. 28b

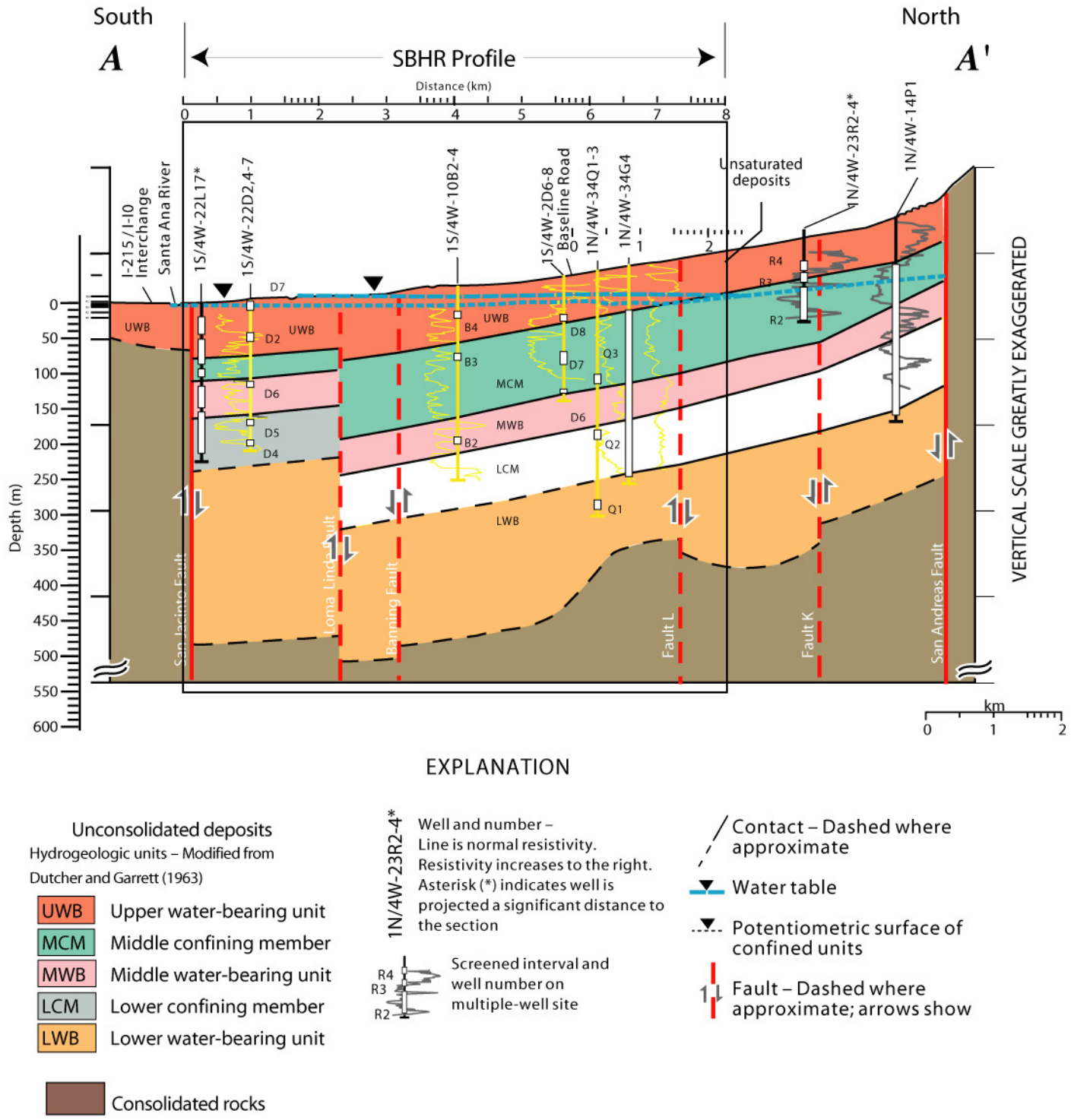
South
A
SBHR Profile
North
A'
Distance (km)
0 1 2 3 4 5 6 7 8
I-215 / I-10 Interchange
Santa Ana River
1S/4W-22L17*
1S/4W-22D2,4-7
1S/4W-10B2-4
1S/4W-2D6-8 Baseline Road
1N/4W-34Q1-3
1N/4W-34G4
Unsaturated deposits
1N/4W-23R2-4*
1N/4W-14P1
Depth (m)
0 50 100 150 200 250 300 350 400 450 500 550 600
UWB
MCM
MWB
LCM
LWB
D7 D2 D6 D5 D4 D8 B4 B3 B2 Q3 Q2 Q1 R4 R3 R2
San Jacinto Fault
Loma Linda Fault
Banning Fault
Fault L
Fault K
San Andreas Fault
VERTICAL SCALE GREATLY EXAGGERATED
km
0 1 2
EXPLANATION
Unconsolidated deposits
Hydrogeologic units – Modified from Dutcher and Garrett (1963)
UWB Upper water-bearing unit
MCM Middle confining member
MWB Middle water-bearing unit
LCM Lower confining member
LWB Lower water-bearing unit
Consolidated rocks
1N/4W-23R2-4*
Well and number – Line is normal resistivity. Resistivity increases to the right. Asterisk (*) indicates well is projected a significant distance to the section
R4 R3 R2
Screened interval and well number on multiple-well site
Contact – Dashed where approximate
Water table
Potentiometric surface of confined units
Fault – Dashed where approximate; arrows show

Fig. 29a

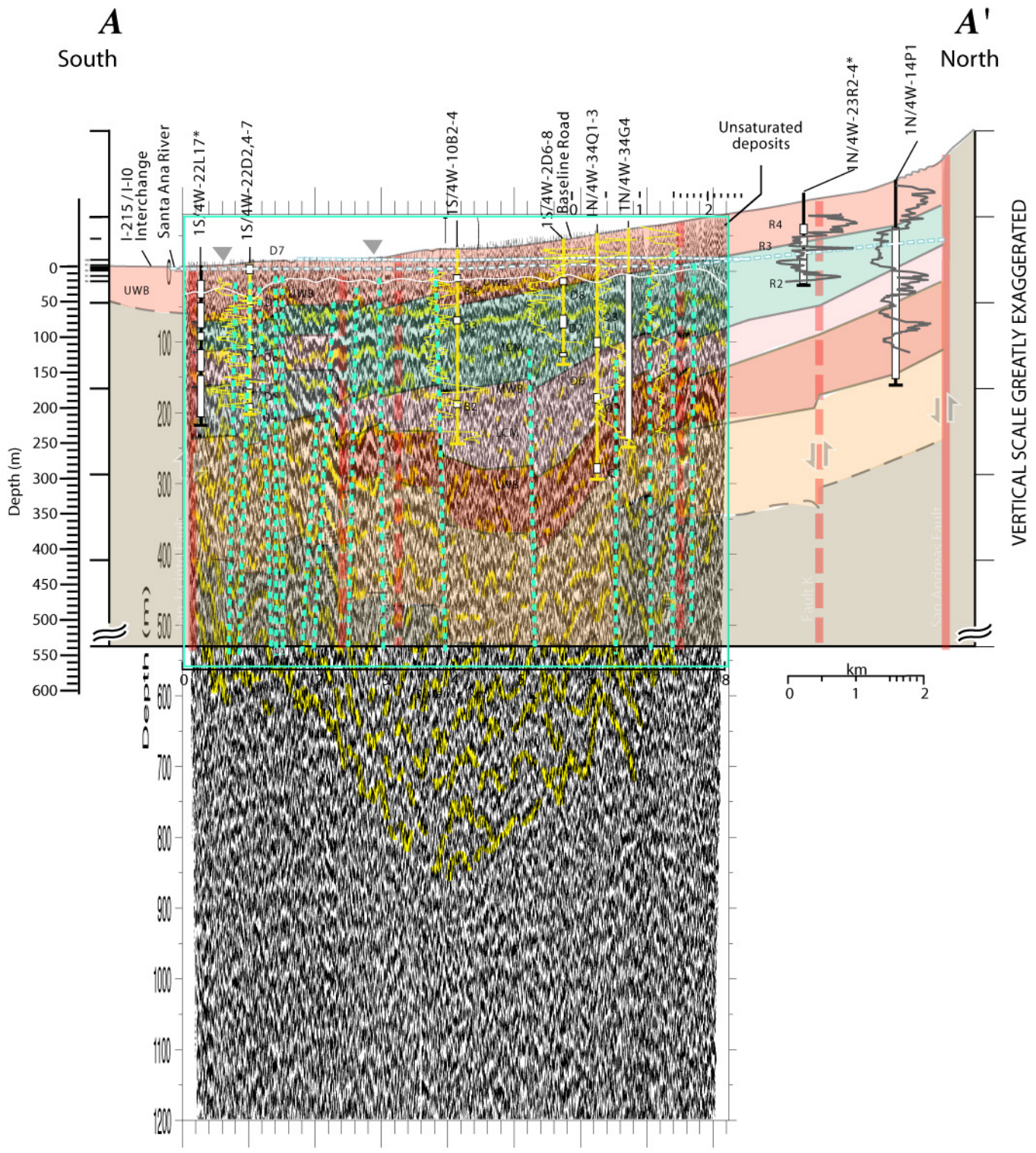
A
South
A'
North
I-215/I-10 Interchange
Santa Ana River
1S/4W-22L17*
1S/4W-22D2,4-7
1S/4W-10B2-4
1S/4W-2D6-8 Baseline Road
1N/4W-34Q1-3
1N/4W-34G4
Unsaturated deposits
1N/4W-23R2-4*
1N/4W-14P1
UWB
LWB
LCU
D7
D8
R4
R3
R2
Depth (m)
Depth (cm)
km
VERTICAL SCALE GREATLY EXAGGERATED

Fig. 29b